

DESIGN AND CONTROL OF X5 UNMANNED AERIAL ROBOT

A THESIS SUBMITTED TO  
THE GRADUATE SCHOOL OF NATURAL AND APPLIED SCIENCES  
OF  
MIDDLE EAST TECHNICAL UNIVERSITY

BY

MEHRAN EBADOLLAHI NOUDEH

IN PARTIAL FULFILLMENT OF THE REQUIREMENTS  
FOR  
THE DEGREE OF MASTER OF SCIENCE  
IN  
ELECTRICAL AND ELECTRONICS ENGINEERING

SEPTEMBER 2015



Approval of the thesis:

**DESIGN AND CONTROL OF X5 UNMANNED AERIAL ROBOT**

submitted by **MEHRAN EBADOLLAHI NOUDEH** in partial fulfillment of the requirements for the degree of **Master of Science in Electrical and Electronics Engineering Department, Middle East Technical University** by,

Prof. Dr. Gülbin Dural Ünver  
Dean, Graduate School of **Natural and Applied Sciences**

\_\_\_\_\_

Prof. Dr. Gönül Turhan Sayan  
Head of Department, **Electrical and Electronics Engineering**

\_\_\_\_\_

Prof. Dr. M. Kemal Leblebicioğlu  
Supervisor, **Electrical and Electronics Eng. Dept., METU**

\_\_\_\_\_

**Examining Committee Members:**

Prof. Dr. Çağatay Candan  
Electrical and Electronics Engineering, METU

\_\_\_\_\_

Prof. Dr. M. Kemal Leblebicioğlu  
Electrical and Electronics Engineering, METU

\_\_\_\_\_

Assoc. Prof. Dr. İlkey Ulusoy  
Electrical and Electronics Engineering, METU

\_\_\_\_\_

Assoc. Prof. Dr. Funda Kurtuluş  
Aerospace Engineering Department, METU

\_\_\_\_\_

Assist. Prof. Dr. Yakup Özkazanç  
Electrical and Electronics Eng., Hacettepe University

\_\_\_\_\_

**Date:**

\_\_\_\_\_

**I hereby declare that all information in this document has been obtained and presented in accordance with academic rules and ethical conduct. I also declare that, as required by these rules and conduct, I have fully cited and referenced all material and results that are not original to this work.**

Name, Last Name: MEHRAN EBADOLLAHI NOUDEH

Signature :



# ABSTRACT

## DESIGN AND CONTROL OF X5 UNMANNED AERIAL ROBOT

Noudeh, Mehran Ebadollahi

M.S., Department of Electrical and Electronics Engineering

Supervisor : Prof. Dr. M. Kemal Leblebicioğlu

September 2015, 118 pages

This thesis presents a mathematical model and an autopilot of a new type Unmanned Aerial Robot (UAR) named X5 with a focus on Vertical Take-off and Landing (VTOL) systems. Physically, it consists of a large propeller to carry the main payload, and four small propellers for controlling the attitude. It presents a nonlinear 6 degrees of freedom (DOF) model of X5 based on Newton-Euler method for simulation and control. The mathematical model introduced in this work includes the rotor dynamics and detailed aerodynamic effects.

The autopilot of X5 requires special attention because of unsymmetrical action of the big propeller in the yaw plane. Three different autopilots have been developed and simulated based on the simplified mathematical model of X5. Proportional Derivative (PD) controller is the first technique developed for altitude, attitude and position control. The second controller designed is based on Proportional Integral Derivative (PID) controller. The third one is based on Lyapunov control theory. The performances of controllers have been evaluated and compared with simulation based experiments. Furthermore, all the relevant hardware components have been modeled which enable us to perform hardware-in-the-loop experiments.

In the final part of this study, the suggested aerial robot, i.e., X5, has been designed physically and it is being constructed to perform real life experiments.

Keywords: X5 Aerial Robot, UAR, VTOL, Mathematical Modeling, Autopilot, PID Controller

# ÖZ

## X5 İNSANSIZ HAVA ROBOTUNUN TASARIMI VE KONTROLÜ

Noudeh, Mehran Ebadollahi

Yüksek Lisans, Elektrik ve Elektronik Mühendisliği Bölümü

Tez Yöneticisi : Prof. Dr. M. Kemal Leblebicioğlu

Eylül 2015 , 118 sayfa

Bu tez, X5 adı verilen, insansız bir hava robotunun, dikey iniş-kalkış vurgusu yapılarak ortaya çıkarılan matematiksel modeli ve otopilot tasarımı hakkındadır. Fiziksel olarak, X5, asıl yükü taşıma amacı olan büyük bir pervane ve açısız kontrolü sağlamak amacı taşıyan dört küçük pervaneden oluşmaktadır. X5 için elde edilen doğrusal olmayan 6 serbestlik dereceli matematiksel model, Newton-Euler yaklaşımı ile benzetim ve kontrol çalışmalarında kullanılmıştır. Matematiksel model, aynı zamanda, rotor dinamiği ve detaylı aerodinamik etkileri de kapsamaktadır.

Büyük pervanenin yalpa düzlemine getirdiği simetrik olmayan etkilerden dolayı, X5'in otopilot tasarımı özel bir çalışma gerektirir. X5'in basitleştirilmiş matematiksel modeli kullanılarak, benzetim çalışmalarında kullanılmak üzere, üç farklı otopilot geliştirilmiştir. Yükseklik, açısız ve durum kontrolü için ilk geliştirilen otopilot, oransal-türev kontrolcüsüdür (PD). İkinci geliştirilen otopilot, oransal-integral-türev tabanlıdır (PID). Son olarak, Lyapunov teorisine dayanan otopilot geliştirilmiştir. Otopilotların performansları, benzetim çalışmaları kullanılarak ortaya çıkarılmış ve karşılaştırılmıştır. İlave olarak, kullanılan önemli donanım bileşenlerinin modelleri elde edilmiş ve donanım tabanlı benzetim çalışmalarında kullanılmıştır.

Bu çalışmanın son parçası olarak, X5 robotunun fiziksel tasarımı yapılmış ve gerçek hayat deneyleri için inşasına başlanmıştır.

Anahtar Kelimeler: X5 Hava Robotu, UAR, VTOL, Matematiksel Modelleme, Otopilot, PID Kontrolcüsü, Lyapunov Teorisi ile Kontrol

*To my dear family  
and  
my dear Sonnur*

## ACKNOWLEDGMENTS

I would like to sincerely thank to my supervisor, Prof. Dr. M.Kemal Leblebicioğlu for his constant support, encouragement and patience at all levels of this study. Without his kind instructions and guidance, this research could not have been completed. Thanks for giving me the chance to work with you.

This research work has been supported in part by TÜBİTAK (The Scientific and Technological Research Council of Turkey) through the projects 110E192 & 114E149. These supports are gratefully acknowledged.

My deepest gratitude is to my family. My father, who taught me perseverance and gave me courage, is with me always in spirit. My mother, provided me with the emotional strength and faith to endure this trial. My brother and my sister, whose endless support, encouragement strengthened me to complete this endeavor.

I am also thankful to my brother-in-law, and sister-in-law who have always wished for my success.

Last but not least, I dedicate this thesis to my fiancé Sonnur, without your support and encouragement, I would not be here today. Thank you for always believing in me and pushing me forward. Your smile makes me the happiest man and your love fulfills me.

## TABLE OF CONTENTS

ABSTRACT . . . . .	v
ÖZ . . . . .	vii
ACKNOWLEDGMENTS . . . . .	x
TABLE OF CONTENTS . . . . .	xi
LIST OF TABLES . . . . .	xv
LIST OF FIGURES . . . . .	xvii
LIST OF ABBREVIATIONS . . . . .	xxii
CHAPTERS	
1 INTRODUCTION . . . . .	1
1.1 Motivation . . . . .	1
1.2 Literature Review . . . . .	1
1.2.1 Brief History of UAV's . . . . .	1
1.2.2 UAV Classifications . . . . .	4
1.2.3 Comparison of Candidate VTOL Configurations . . . . .	7
1.2.3.1 Coaxial Configuration . . . . .	7
1.2.3.2 X4-Quadrotor Configuration . . . . .	9

	1.2.3.3	Y4-Quadrotor Configuration . . . . .	11
	1.2.3.4	X5-Multirotor Configuration . . . . .	13
	1.2.4	Contributions of This Study . . . . .	15
	1.2.5	Thesis Outline . . . . .	16
2		MATHEMATICAL MODELLING OF X5 AERIAL ROBOT . . . . .	17
	2.1	Introduction . . . . .	17
	2.2	Modelling with Newton-Euler Method . . . . .	17
	2.2.1	Kinematic Model of X5 . . . . .	18
	2.2.2	Aerodynamic Forces and Moments Acting on X5 . . . . .	19
	2.2.3	General Forces and Moments of X5 . . . . .	22
	2.2.4	Equations of Motion . . . . .	24
	2.2.5	Rotor Dynamics . . . . .	24
3		HARDWARE DESIGN: CONSTRUCTION OF X5 . . . . .	27
	3.1	Introduction . . . . .	27
	3.2	Sensors and Components . . . . .	28
	3.2.1	Inertial Measurement Unit . . . . .	28
	3.2.2	RPM Measurement . . . . .	29
	3.2.3	Voltage and Current Measurement . . . . .	30
	3.2.4	ESC . . . . .	31
	3.2.5	3DR Radio Telemetry Kit . . . . .	31
	3.2.6	Control Board . . . . .	32



3.2.7	Batteries . . . . .	34
3.2.8	Propellers . . . . .	34
3.2.9	Motors . . . . .	35
3.2.10	Motor and Propeller Testing . . . . .	36
3.2.11	Moment of Inertia . . . . .	48
3.3	Assembling X5 Multicopter . . . . .	50
4	AUTOPILOT DESIGN . . . . .	55
4.1	Introduction . . . . .	55
4.2	Modelling for Control . . . . .	55
4.3	Basic Actions . . . . .	60
4.3.1	Open-Loop Simulation . . . . .	60
4.3.2	Closed-Loop Simulation . . . . .	62
4.4	Complex Actions: Composite Controllers . . . . .	64
4.5	Control Methods . . . . .	66
4.5.1	PID Control Technique . . . . .	67
4.5.2	PD Controller Synthesis . . . . .	70
4.5.3	Control Using Lyapunov Theory . . . . .	71
5	SIMULATION RESULTS . . . . .	73
5.1	Introduction . . . . .	73
5.2	Open-Loop Simulations . . . . .	73
5.3	Closed-Loop Simulations . . . . .	74

5.3.1	PD Controller Simulations . . . . .	75
5.3.2	PID Controller Simulations . . . . .	85
5.3.3	Attitude Control Using Lyapunov Theory . . . . .	92
5.3.4	Results Discussion . . . . .	95
5.4	Some Experimental Results . . . . .	99
6	CONCLUSIONS AND FUTURE WORKS . . . . .	103
6.1	General Conclusion . . . . .	103
6.2	Future Studies . . . . .	104
	REFERENCES . . . . .	107
APPENDICES		
A	MODELLING . . . . .	113
A.1	Rotation Matrix R . . . . .	113
A.2	Mathematical Derivations . . . . .	115
A.2.1	Aerodynamic Forces and Moments . . . . .	115
A.3	Control Lyapunov Functions . . . . .	116

## LIST OF TABLES

### TABLES

Table 1.1	Altitude and Endurance Classification . . . . .	4
Table 1.2	Classification with Respect to Size and Payload . . . . .	5
Table 1.3	Aerodynamic Configurations of Common UAV . . . . .	6
Table 1.4	Flying Principles Comparison (1 = Bad, 3 = Good) . . . . .	6
Table 1.5	VTOL Concept Comparison (1 = Bad, 4 = Very good) . . . . .	7
Table 1.6	Coaxial's Main Advantages and Drawbacks . . . . .	8
Table 1.7	X4-Quadrotors' Main Advantages and Drawbacks . . . . .	10
Table 1.8	Main Advantages and Drawbacks of Y4 . . . . .	12
Table 1.9	Advantages and Drawbacks of X5-Multirotor "HoverMast-120" . . . .	13
Table 3.1	Propellers Variables . . . . .	35
Table 3.2	Motors Variables . . . . .	36
Table 3.3	Boom-Mounted Rotor's Thrust Measurement Result . . . . .	41
Table 3.4	Main Rotor's Thrust Measurement Result . . . . .	42
Table 3.5	Components of X5 and Their Position . . . . .	51
Table 4.1	Parameters of Both Small and Large Propellers . . . . .	57
Table 5.1	The Results of PD Altitude Controller . . . . .	76
Table 5.2	The Results of PD Attitude Controller . . . . .	77
Table 5.3	The Results of PD Position Controller . . . . .	80
Table 5.4	The Results of PD Trajectory Control . . . . .	80

Table 5.5	The Results of PID Altitude Controller . . . . .	85
Table 5.6	The Results of PID Attitude Controller . . . . .	85
Table 5.7	The Results of Position Control Using PID Controller . . . . .	86
Table 5.8	The Results of PID Trajectory Control . . . . .	88
Table 5.9	Gains of Control Lyapunov Function . . . . .	92

# LIST OF FIGURES

## FIGURES

Figure 1.1	First Fixed-Wing UAV Presented by US Navy in 1917 . . . . .	2
Figure 1.2	First Rotary-Wing UAV Introduced in 1963 . . . . .	2
Figure 1.3	Vertical Take-Off and Landing Surveillance System Introduced in 1976 . . . . .	3
Figure 1.4	Yamaha Rmax Unmanned Helicopter Introduced in 1987 . . . . .	3
Figure 1.5	General Classification of Aircrafts . . . . .	4
Figure 1.6	Coaxial Helicopter Configuration . . . . .	8
Figure 1.7	First Manned Quadrotor Flight in 1907 . . . . .	9
Figure 1.8	Unmanned Mini-Scale Quadrotors' Configuration . . . . .	10
Figure 1.9	Unmanned Mini-Scale Y4-Quadrotors' Configuration . . . . .	11
Figure 1.10	The HoverMast from Introduced by SkySapience Company . . . . .	13
Figure 1.11	Unmanned Mini-Scale X5 Multirotors' Configuration . . . . .	14
Figure 2.1	X5 Coordinate Frames . . . . .	18
Figure 2.2	Schematic Diagram of DC Motor . . . . .	25
Figure 3.1	Initial Design of X5 Aerial Robot Using CAD . . . . .	27
Figure 3.2	QRD1114 Line Edge Sensor and its Schematic Board . . . . .	29
Figure 3.3	Encoder Disk . . . . .	30
Figure 3.4	3DR Power Module Used as Voltage and Current Sensor . . . . .	30
Figure 3.5	EMAX 25A and 40A ESCs Used to Drive the BLDC Motors . . . . .	31
Figure 3.6	3DR Radio V2 Telemetry Kit . . . . .	32

Figure 3.7 Connection of 3DR Radio Telemetry to Control Board . . . . .	32
Figure 3.8 3DR Pixhawk Autopilot Controller Used as Main Controller of X5 . . . . .	33
Figure 3.9 Batteries . . . . .	35
Figure 3.10 Boom-Mounted and Main Rotors' Propellers . . . . .	36
Figure 3.11 Main and Boom-Mounted Motors . . . . .	37
Figure 3.12 Entire Test-Bench for BLDC Motors . . . . .	38
Figure 3.13 Generated Pulse Width Used for System Identification . . . . .	39
Figure 3.14 Result of Speed Measurement Data wrt Given Input Waveform . . . . .	39
Figure 3.15 Result of Current Measurement . . . . .	40
Figure 3.16 Result of Measured Current, Voltage, RPM, etc. . . . .	41
Figure 3.17 The Result of Current vs RPM for Boom-Mounted Rotors. . . . .	42
Figure 3.18 The Result of Current vs RPM for Main Rotor. . . . .	43
Figure 3.19 T-Motor ms2212-13 With 9x4.5 Propeller Given Pulse Width, RPM and Consumed Current According to the RPM . . . . .	44
Figure 3.20 Measurement Error Between Filtered and Unfiltered Measured RPM Data for Boom-Mounted Motor . . . . .	45
Figure 3.21 Histogram of Measurement Error of Measured RPM Data . . . . .	45
Figure 3.22 Estimation Results with Unfiltered Data for Boom Motors . . . . .	45
Figure 3.23 T-Motor MN4014-9 With 18x5.5 Propeller Given Pulse Width, RPM and Consumed Current According to the RPM . . . . .	46
Figure 3.24 Measurement Error Between Filtered and Unfiltered Measured RPM Data for Main Motor . . . . .	47
Figure 3.25 Histogram of Measurement Error of Measured RPM Data . . . . .	47
Figure 3.26 Estimation Result for Main Motor . . . . .	47
Figure 3.27 Inertia Tensor Measurement . . . . .	50
Figure 3.28 X5 Aerial Robot's Hardware Configuration . . . . .	52
Figure 3.29 X5 Unmanned Aerial Robot . . . . .	53

Figure 4.1	X5 Dynamics Diagram; Connection of Subsystems . . . . .	60
Figure 4.2	X5 Open-Loop Diagram . . . . .	61
Figure 4.3	Altitude Controller Block Diagram . . . . .	63
Figure 4.4	Attitude and Heading Controller Block Diagram . . . . .	64
Figure 4.5	Hover Controller Block Diagram . . . . .	64
Figure 4.6	Closed-Loop Controller Block Diagram (Complete System) . . . .	66
Figure 4.7	Proportional-Integral-Derivative (PID) Controller Block Diagram .	67
Figure 4.8	Proportional-Derivative (PD) Controller Block Diagram . . . . .	70
Figure 5.1	Open-Loop Simulation of X5 With Desired Inputs for System to Stay in Hover Position . . . . .	74
Figure 5.2	The Result of Open-Loop Simulation in z-Axis With 2m Height as an Initial Condition . . . . .	74
Figure 5.3	The Overall Closed-Loop Simulation of X5 in MATLAB/Simulink	75
Figure 5.4	Altitude Controller Result in Desired 2m Height Using PD Con- troller . . . . .	76
Figure 5.5	Result of Altitude Controller With Zero Initial Condition, 2m Height as Desired Altitude and Added Second Order Filter to the Desired Signal .	76
Figure 5.6	The Result of Roll, Pitch and Yaw Angles Using the PD Controller. The Desired Value For Roll and Pitch Was $\pi/8$ in 3rd sec and 5th sec, Respectively and $\pi/4$ in the 7th sec For the Yaw Angle . . . . .	77
Figure 5.7	The Result of Roll, Pitch and Yaw Angles Using the PD Controller wrt the Initial Conditions and Disturbance . . . . .	78
Figure 5.8	The Result of Roll, Pitch and Yaw Angles Using PD Controller . .	79
Figure 5.9	Cascade PD Controller Block Diagram for y-Axis Position Control	79
Figure 5.10	Cascade PD Controller Block Diagram For x-Axis Position Control	80
Figure 5.11	The Result of Roll, Pitch, Yaw Angles and x, y, z Position Using PD Controller . . . . .	81
Figure 5.12	The Autopilot Response to 1st Trajectory Using PD Controller . . .	82
Figure 5.13	The Autopilot Response to 1st Trajectory Using PD Controller . .	83

Figure 5.14 1st Trajectory Response Under PD Controller . . . . .	84
Figure 5.15 2nd Trajectory Response Under PD Controller . . . . .	84
Figure 5.16 Altitude Controller Result in Desired 2m Height Using PID Controller . . . . .	85
Figure 5.17 The Result of Roll, Pitch and Yaw Angles Using the PID Controller. The Desired Value For Roll and Pitch Was $\pi/8$ in the 3rd sec and 5th sec, Respectively and $\pi/4$ in the 7th sec For the Yaw Angle . . . . .	86
Figure 5.18 The Result of Roll, Pitch, Yaw Angles and x, y, z Position Using PID Controller . . . . .	87
Figure 5.19 The Autopilot Response to 1st Trajectory Using PID Controller . .	89
Figure 5.20 The Autopilot Response to 1st Trajectory Using PID Controller . .	90
Figure 5.21 1st Trajectory Response Under PID Controller . . . . .	91
Figure 5.22 2nd Trajectory Response Under PID Controller . . . . .	91
Figure 5.23 Result of Altitude of X5 Under PID Controller for 2m Desired height	92
Figure 5.24 Simulation Results of the Attitude Controller Using Lyapunov Theory to Maintain Attitude Angles at Zero Without Noise . . . . .	93
Figure 5.25 Simulation Results of the Attitude Controller Using Lyapunov Theory to Maintain Attitude Angles at Zero Under Influence of the Added Noise	94
Figure 5.26 Comparison Between Results of Altitude of X5 Under PD and PID Controller for 2m Desired height . . . . .	95
Figure 5.27 Comparison Between Simulation Results of the Attitude Controllers Using PD, PID and Lyapunov controllers to Maintain Attitude Angles at Zero with 0.1 rad as an Initial Condition . . . . .	96
Figure 5.28 Comparison Between Simulation Results of the Trajectory Control Using PD and PID controllers for X, Y and Z axes . . . . .	97
Figure 5.29 Comparison Between Simulation Results of the Roll, Pitch and Yaw Angles to the Trajectory Using PD and PID controllers . . . . .	98
Figure 5.30 Comparison Between Results PD and PID Controller to the Square Trajectory Defined by Four Way-Points . . . . .	99
Figure 5.31 Response of the Controller to the Autopilot Desired Signal in Roll Angle . . . . .	100



Figure 5.32 Response of the Controller to the Autopilot Desired Signal in Pitch Angle . . . . .	100
Figure 5.33 Response of the Controller to the Autopilot Desired Signal in Yaw Angle . . . . .	100
Figure 5.34 Response of the Controller to the Autopilot Desired Signal in Roll Angle . . . . .	101
Figure 5.35 Response of the Controller to the Autopilot Desired Signal in Pitch Angle . . . . .	101
Figure 5.36 Response of the Controller to the Autopilot Desired Signal in Yaw Angle . . . . .	101
Figure A.1 Euler Angle Diagram . . . . .	113

## LIST OF ABBREVIATIONS

### SYMBOLS

$a$	lift slope
$A_b$	boom rotor's propeller disk area
$A_c$	fuselage area
$A_m$	main rotor's propeller disk area
$b$	motor viscous friction constant
$c$	propeller chord
$\overline{C_d}$	drag coefficient at 70% radial station
$C_{Hb}$	hub force coefficient of boom rotor
$C_{Hm}$	hub force coefficient of main rotor
$C_{Qb}$	drag coefficient of boom rotor
$C_{Qm}$	drag coefficient of main rotor
$C_{Rb}$	rolling moment coefficient of boom rotor
$C_{Rm}$	rolling moment coefficient of main rotor
$C_{tb}$	thrust coefficient of the boom rotor
$C_{tm}$	thrust coefficient of the main rotor
$C_x$	friction coefficient in x-axis
$C_y$	friction coefficient in y-axis
$F$	forces in body-fixed frame
$g$	gravitational acceleration
$h$	vertical distance between center of propeller to CoG
$H$	hub force
$H_{xi}$	hub force in x-axis
$H_{yi}$	hub force in y-axis
$I$	inertia matrix
$i_a$	current of motor
$I_x, I_y, I_z$	moments of inertia

$J_r$	rotor inertia
$K$	motor torque constant
$K_{Hb}$	hub factor of boom rotor
$K_{Hm}$	hub factor of main rotor
$K_{Qb}$	drag factor of boom rotor
$K_{Qm}$	drag factor of main rotor
$K_{Rb}$	rolling factor of boom rotor
$K_{Rm}$	rolling factor of main rotor
$K_{tb}$	thrust factor of boom rotor
$K_{tm}$	thrust factor of main rotor
$L$	horizontal distance between center of propeller to CoG
$L_{mot}$	inductance of rotor
$m$	overall weight of system
$n$	number of propellers
$Q$	drag moment
$r$	position of the X5 with respect to the Earth-fixed frame
$R$	rotation matrix
$R_i$	rolling moment
$R_{brad}$	boom rotor radius
$R_{mot}$	internal resistance of motor
$R_{mrad}$	main rotor radius
$R_{mx}$	rolling moment of rotors in flight in x-axis
$R_{my}$	pitching moment of rotors in flight in y-axis
$R_r$	angular rate transformation matrix
$T$	thrust force
$U$	control inputs
$x,y,z$	position in body-fixed frame
$V$	body linear speed
$\eta$	Euler-angle
$\lambda$	inflow ratio
$\mu$	rotor advance ratio
$\Omega_r$	overall residual propeller angular speed
$\Omega_b$	boom propeller angular rate
$\Omega_m$	main propeller angular rate

$\omega$	body angular rate
$\omega_b$	boom motor angular rate
$\omega_m$	main motor angular rate
$\phi$	roll angles
$\psi$	yaw angle
$\rho$	air density
$\sigma$	Solidity ratio
$\tau_m$	torque produced by rotor
$\theta$	pitch angle
$\theta_0$	pitch of incidence
$\theta_{tw}$	twist pitch
$v$	induced velocity
$\zeta_m$	motor angular rate

## **ABBREVIATIONS**

BLDC	Brush-Less Direct Current
CoG	Center of Gravity
DOF	Degree of Freedom
IMU	Inertial Measurement Unit
MAV	Micro Aerial Vehicle
MFR	Miniature Flying Robots
NED	North, East, Down standard
PD	Proportional Derivative
PID	Proportional Integral Derivation
RPM	Revolutions Per Minute
UAR	Unmanned Aerial Robot
UAV	Unmanned Aerial Vehicle
VTOL	Vertical Take-Off and Landing



# **CHAPTER 1**

## **INTRODUCTION**

### **1.1 Motivation**

It is almost a decade that the robotics communities were showing a significant interest in developing flying machines with minimum or no human interaction, commonly known as Unmanned Aerial System (UAS), to fulfill autonomous missions effectively. Some of the fields like robotic, mechanics, aerodynamics, control systems, automation and embedded electronics are related to development of these systems. The challenge of designing mini UAS which are capable of carrying heavy payloads and the lack of existing solutions was very motivating.

In this study the main focus is on the design and control of X5 Unmanned Aerial Robot (UAR). Like other multirotors, X5 aerial robot is a multivariable, highly nonlinear and underactuated system [1]. Although there are only four control input, X5 has six Degrees of Freedom (DOF) which makes it very difficult to control because of nonlinear relation between the degrees of freedom and actuators of the system [2].

### **1.2 Literature Review**

#### **1.2.1 Brief History of UAV's**

The first fixed-wing Unmanned Aerial Vehicle (Figure 1.1) manufactured in 1917 by Lawrence and Sperry and presented by US NAVY as "Aerial Torpedo", was a biplane with 270kg weight and a 40 horsepower engine made by Ford [3]. In the Aerial Tor-

pedo, for the first time they used a gyroscope to stabilize the aircraft and keep it on level and present heading. They also used a barometer in order to measure the altitude of it. Since then, capabilities of UAVs are expanding and they have been seen as a strong option to neutralize the offensive of opponents.

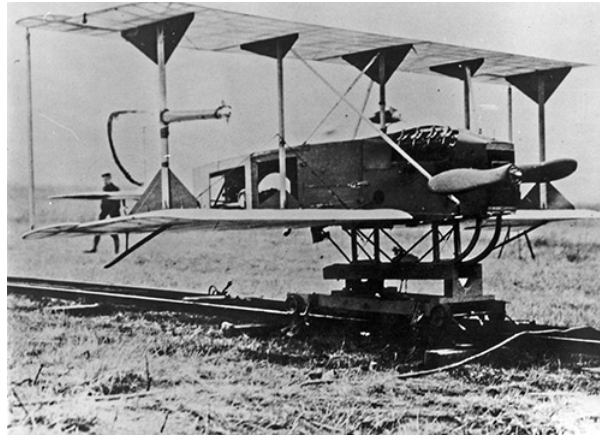


Figure 1.1: First Fixed-Wing UAV Presented by US Navy in 1917 [4]

During 1970s, the first rotary-wing UAV (see Figure 1.2) has been introduced as an anti-submarine helicopter by US Navy, known as "Gyrodyne DASH". This small rotary-wing UAV has been used as a long-range anti-submarine weapon during the Cold War. It was a major part of Fleet Rehabilitation and Modernization (FRAM) program of the US Navy [5].



Figure 1.2: First Rotary-Wing UAV Introduced in 1963 [6]

In 1976, the first remotely piloted Vertical Take-off and Landing (VTOL), known as "Westerland Wisp", was introduced by United Kingdom (See Figure 1.3). It is also



called *spy-in-the-sky* helicopter which had shorter range of operation and developed for aerial surveillance. This VTOL system could send real-time video and infra-red pictures to a portable ground control station while operating [7].



Figure 1.3: Vertical Take-Off and Landing Surveillance System Introduced in 1976 [8]

In 1990s, Yamaha motor company introduced a large-scale rotary-wing UAV called "Yamaha R-50". Later, Yamaha company improved "R-50" to "Rmax" model (See Figure 1.4), which had 20kg of payload and it was the first practical use of an Unmanned helicopter for crop dusting [9].



Figure 1.4: Yamaha Rmax Unmanned Helicopter Introduced in 1987 [10]

### 1.2.2 UAV Classifications

There are various types of UAVs and also different ways of classification. Generally, we can divide all aerial vehicles into two, Lighter Than Air (LTA) and Heavier Than Air (HTA) categories (See Diagram 1.5). This type of classification is about the flying principle and the propulsion mode.

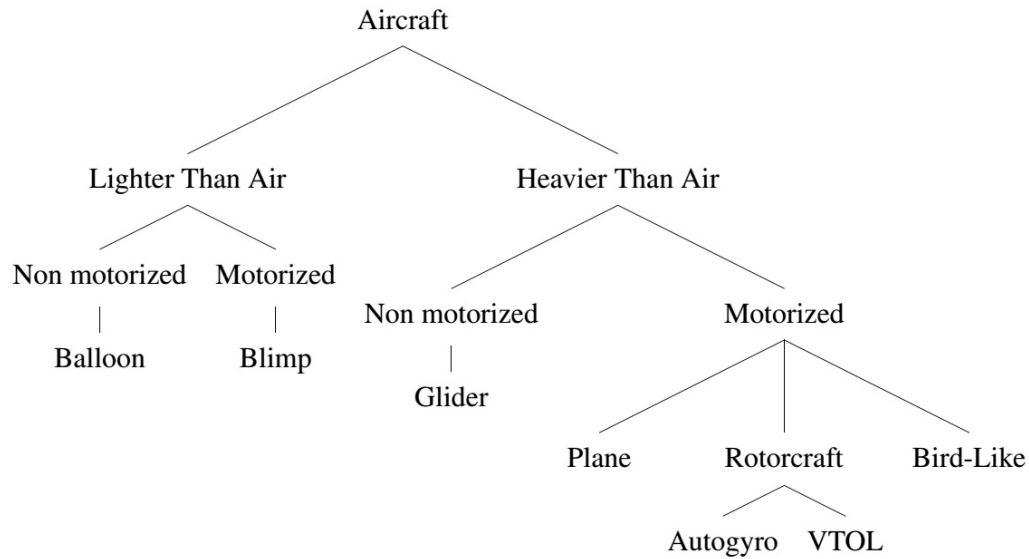


Figure 1.5: General Classification of Aircrafts [11]






In Table (1.1) we also can see another general classification with respect to the maximum reached altitude and flight endurance of each type.

Table 1.1: Altitude and Endurance Classification [3], [12]

Type of UAV	Altitude (m)	Endurance (hr.)	Main Use
High-Altitude Long-Endurance (HALE)	>15k	24+	long-range surveillance
Medium-Altitude Long-Endurance (MALE)	<15k	max 24	surveillance
Tactical UAV (TUAV)	<5k	12-18	surveillance, battle
Mini UAV (MUAV)	<9k	24-48	surveillance
Micro UAV (MAV)	<3k	2	surveillance
Nano Air Vehicle (NAV)	<1k	20min.	surveillance

Table 1.2 shows a classification of rotary-wing UAVs based on their size and payload they can carry [13].

Table 1.2: Classification with Respect to Size and Payload

Category No.	Size	Payload (kg)	Example
I	Full Scale	Significantly large	 Boeing Unmanned Little Bird [14]
II	Medium Scale	>10	 Yamaha RMAX [15]
III	Small Scale	2-10	 VARIO Benzin Trainer [16]
IV	Mini	<2	 MIT autonomous indoor quadrotor (Asc Tec) [17]
V	Micro	<100g	 the Epson micro-flying robot [18]

In order to have a better understanding of UAVs we can categories them with respect to their configurations. Table (1.3) shows four main categories of UAVs and their advantages and drawbacks.

Table 1.3: Aerodynamic Configurations of Common UAV [19], [11]

Category	Advantages	Drawbacks
Fixed-Wing Aircraft	high cruise speed, long endurance	no hovering capability
Flapping-Wing Vehicles	good maneuverability, compactness	complex mechanics, complex control
Blimps	long-endurance, low power cost	large size, weak maneuverability
Rotory-Wings UAVs	good maneuverability, VTOL, hovering	high energy consumption

In Table 1.4 we can see a more detailed comparison between different types of UAVs with respect to their flying principles [13, 11, 3]. This comparison table shows that VTOL systems like helicopters and blimps have significant advantages in low speed and stationary flight compared to the other systems. The simplicity of control and auto lifting, which are essential in the case of aerial surveillance, are the main advantages of blimps; However, the big size and weak maneuverability, which are critical in the case of protection, are the main drawbacks of blimps.

Table 1.4: Flying Principles Comparison (1 = Bad, 3 = Good) [11]

	Fixed-wing	Rotary-wing	Bird	Autogiro	Blimp
Power cost	2	1	2	2	3
Control cost	2	1	1	2	3
Payload/volume	3	2	2	2	1
Maneuverability	2	3	3	2	1
Stationary flight	1	3	2	1	3
Low speed fly	1	3	2	2	3
Vulnerability	2	2	3	2	2
VTOL	1	3	2	1	3
Endurance	2	1	2	1	3
Miniaturization	2	3	3	2	1
Indoor usage	1	3	2	1	2

Table 1.5 shows the comparison between the most recent types of VTOL configurations. One can easily notice from this table that rotary-wing aerial vehicles like Coaxial, X4-Quadrotors, Y4-Quadrotor and X5-multirotors are the most feasible choices

of VTOL systems.

Table 1.5: VTOL Concept Comparison (1 = Bad, 4 = Very good) [11]

	A	B	C	D	E	F	G	H	I	J
Power cost	2	2	2	2	1	1	1	3	3	4
Control cost	1	1	4	2	3	3	3	2	1	3
Payload/volume	2	2	4	3	3	3	4	2	1	1
Maneuverability	4	3	2	2	3	3	3	3	3	1
Mechanics simplicity	1	2	3	1	4	4	4	1	1	4
Low speed flight	4	3	4	3	4	4	4	2	2	4
High speed flight	2	4	1	2	3	3	3	3	3	1
Miniaturization	2	3	4	2	3	3	2	2	4	1
Survivability	1	3	3	1	1	1	1	2	3	3
Stationary flight	4	4	4	4	4	4	4	1	2	3
Total	24	23	32	23	33	33	33	22	24	28

A = Single rotor, B = Axial rotor, C = Coaxial rotors, D = Tandem rotors, E = X4-Quadrotor, F = Y4-Quadrotor, G = X5-multirotor, H = Bird-like, I = Insect-like, J = Blimp

### 1.2.3 Comparison of Candidate VTOL Configurations

In Table 1.5 we can easily see that not all configurations are suitable for our purpose. The coaxial, X4-quadrotor, Y4-quadrotor and X5-multirotor are the most promising candidates in the case of vertical take-off and landing systems for future unmanned aerial vehicles.

#### 1.2.3.1 Coaxial Configuration

Coaxial rotors (or Coax rotors) are a pair of rotors mounted one above the other, and they rotate in the opposite directions (contra-rotation) which removes the need for a tail rotor. Although this type of helicopters are more compact (See Figure 1.6), they got less interest compared to single rotor helicopters with tail rotor because of their complexity in swashplate mechanisms and complexity of the rotor hub. However, in the case of unmanned vehicles where the range of the action is limited, the advantages

of coaxial rotors took the attention of researchers and engineers [20].



Figure 1.6: Coaxial Helicopter Configuration [21]

In the coaxial helicopters using residual torque, because of the difference between the angular speed of two rotors, the heading of the system can be controlled simultaneously with ascending and descending rate. In the case of hover control, coaxial helicopters behave like single rotor helicopters and by simplifying the swashplate or shifting the CoG, the horizontal motion of the system can be controlled in the longitudinal and the lateral axis [22]. Table 1.6 shows the main advantages and drawbacks of the coaxial helicopters.

Table 1.6: Coaxial's Main Advantages and Drawbacks

Advantages	Drawbacks	Critical notes
Simple mechanics	Complex aerodynamics	Separation between the upper and lower rotor
Compactness	Complex mechanics	Rigid and efficient propellers

### 1.2.3.2 X4-Quadrotor Configuration

The first full-scale manned quadrotor who had a short flight in 1907 was "*Gyroplane n:01*". In this very first experiment Frenchmen Louis, Jacques Breguet and the Professor Richet built a huge X4-quadrotor (See Figure 1.7) with double propellers and no control surface [23].

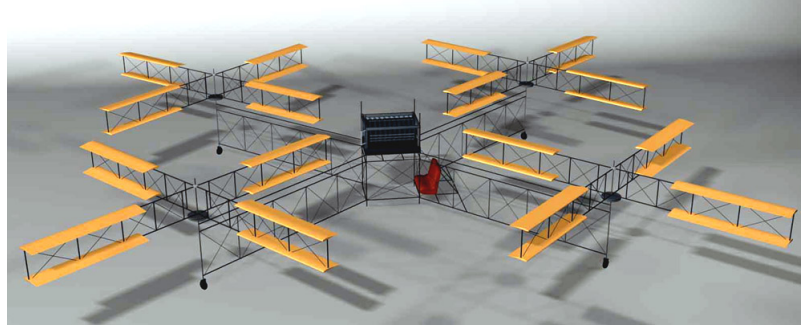


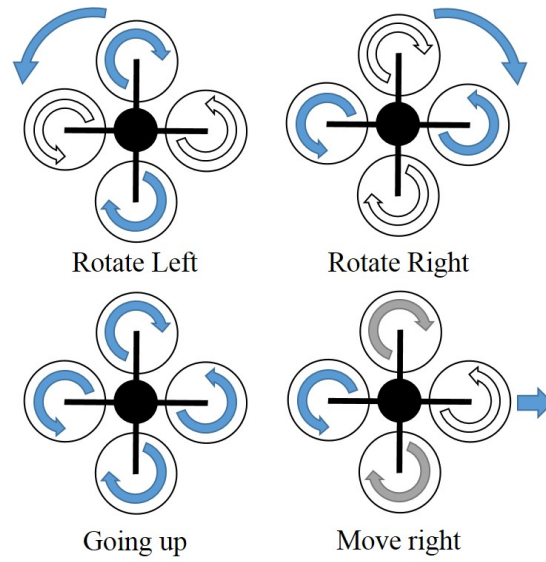
Figure 1.7: First Manned Quadrotor Flight in 1907 [24]

However, recently the quadrotors development has been limited to the unmanned flight experiments in the mini and micro-scale aerial vehicles. Nowadays, quadrotors mainly are presented as four fixed-pitch propellers in "X" (cross) configuration [25, 26, 27]. Figure 1.8a shows a mini-scale unmanned quadrotor which has two pair propellers rotating in opposite direction.

Perfectly symmetric structure and opposite rotation of propellers removes the need for tail rotor in quadrotors to control heading. By having a different angular speed between two pairs of rotors we can control the heading of the system as shown in Figure 1.8b. For climbing and descending we can increase and decrease the angular speed of four rotors at the same time. Rotation in x axis (roll) or y-axis (pitch) can be achieved by tilting the vehicle as shown in Figure 1.8b (down right figure). Although we have four actuators, X4-quadrotors is an under actuated system where degrees of freedom is more than input signals and they are dynamically highly unstable systems [29, 30]. Table 1.7 shows the main advantages and drawbacks of X4-quadrotors.



(a) Mini-scale quadrotor [28]



(b) The quadrotor Concept

Figure 1.8: Unmanned Mini-Scale Quadrotors' Configuration

Table 1.7: X4-Quadrotors' Main Advantages and Drawbacks

Advantages	Drawbacks
Simple mechanics	Large size and mass
High payload	High energy consumption
Reduced gyroscopic effects	



### 1.2.3.3 Y4-Quadrotor Configuration

A new configuration of quadrotors called "Y4 or triangular quadrotor" have been introduced by Scott Driesses and Paul E.I. Pounds from University of Queensland, Australia in 2013 [31]. The main focus in this work was about increasing the energy efficiency of quadrotors as they claimed the test-bed Y4 used 15 percent less power in flight experiments and improved the efficiency power consumption in hovering by 20 percent [32]. As we can see in Figure 1.9a, this new configuration is a combination of traditional helicopter and Y form quadrotors. They used a single large fixed-pitch rotor in the center of mass as the main rotor to provide the main thrust and three small canted rotors in order to eliminate the torque of the main rotor and to provide the control attitude of the system. Three small rotors took place around the center of mass with the same distance and there is  $120^\circ$  between each rotor.

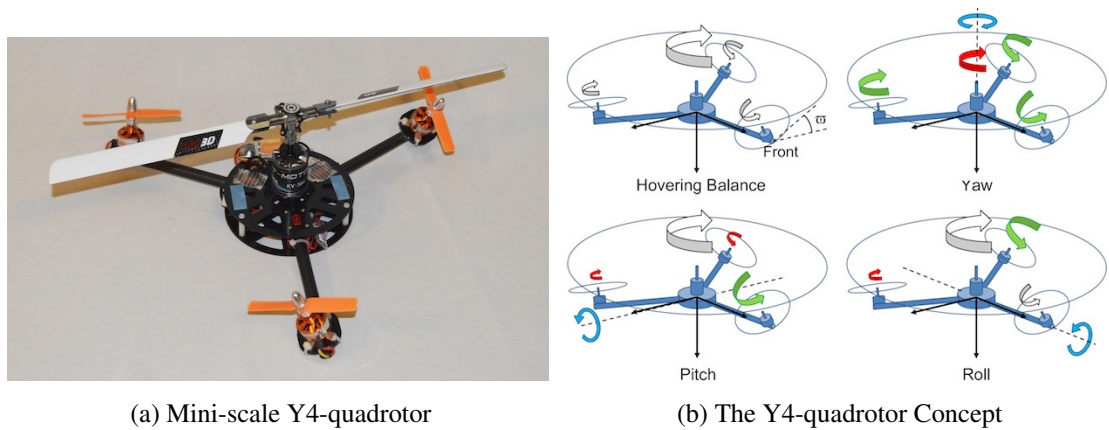


Figure 1.9: Unmanned Mini-Scale Y4-Quadrotors' Configuration [32]

All three small boom-mounted rotors of Y4 are rotate in the same direction to provide active-torque and by this provided torque we can get rid of main rotor's lateral torque. However, unlike traditional quadrotors these three rotors doesn't play significant role in producing lifting thrust. As we can see in Figure 1.9b Y4 configuration, mechanical simplicity of this rotorcraft is technically similar to X4-quadrotors' with four fixed-pitch rotors while it has one large rotor like a helicopter which delivers very big lifting surface. Table 1.8 shows the main advantages and drawbacks of triangular quadrotors.

It should be remembered that this system has good maneuverability compared to other

Table 1.8: Main Advantages and Drawbacks of Y4

<b>Advantages</b>	<b>Drawbacks</b>
High payload	Weak maneuverability
Simple mechanics	Large size and mass
Good maneuverability	High energy consumption
	Large gyroscopic effects

VTOL systems like blimps, but it stays weak compare to the traditional X4 quadrotors.

#### 1.2.3.4 X5-Multirotor Configuration

The development of a small-scale X5-multirotor configuration is first introduced by Skysapience Company called "HoverMast" in 2014 (see Figure 1.10). However, in this configuration they used two counter rotating rotors in the center of mass to provide the main thrust of system [33].



Figure 1.10: The HoverMast from Introduced by SkySapience Company [33]

The HoverMast-120 is secured by a cable which serves as a power supply and a wide-band data link which limits the altitude and range of operation to the length of cable. In this configuration using stabilized five-rotor blades, the system is able to host a large variety of payloads (for example, the HoverMast-120 is able to host 18 kg payload [34]).

Table 1.9: Advantages and Drawbacks of X5-Multirotor "HoverMast-120"

Advantages	Drawbacks
Unlimited operation time	Range of operation
Unlimited electronic power	Large size
Large payloads	Weak maneuverability
Wide-band data link	

The main focus in five-rotor platforms is mixing the energy efficiency and lift capability of a helicopter with the simplicity of the quadrotors. Unlike other VTOL aircrafts such as helicopters, quadrotors have fixed propellers, so they do not require any linkage to stabilize the rotor blade pitch, which streamline cost and simplify design. The efficiency of transferring the energy to the air by choosing suitable propellers and rotors, and choosing appropriate power sources directly affect the quality of hovering in UAV systems. These equipments also directly effect the flight time, speed and achievable payload [35]. Nevertheless, flight time, lifting power and energy consumption are the reasons that the quadrotor platforms cannot reach their full potential. Most of today's quadrotors can carry about 1 kg of additional weight and fly less than 30 minutes. However, traditional helicopters with the same size with one big rotor instead of four small ones, can lift more payloads than quadrotors with more energy efficiency. For this reason, Skycranes and Cargo helicopters have particularly larger diameter rotors or multiple rotors [36].

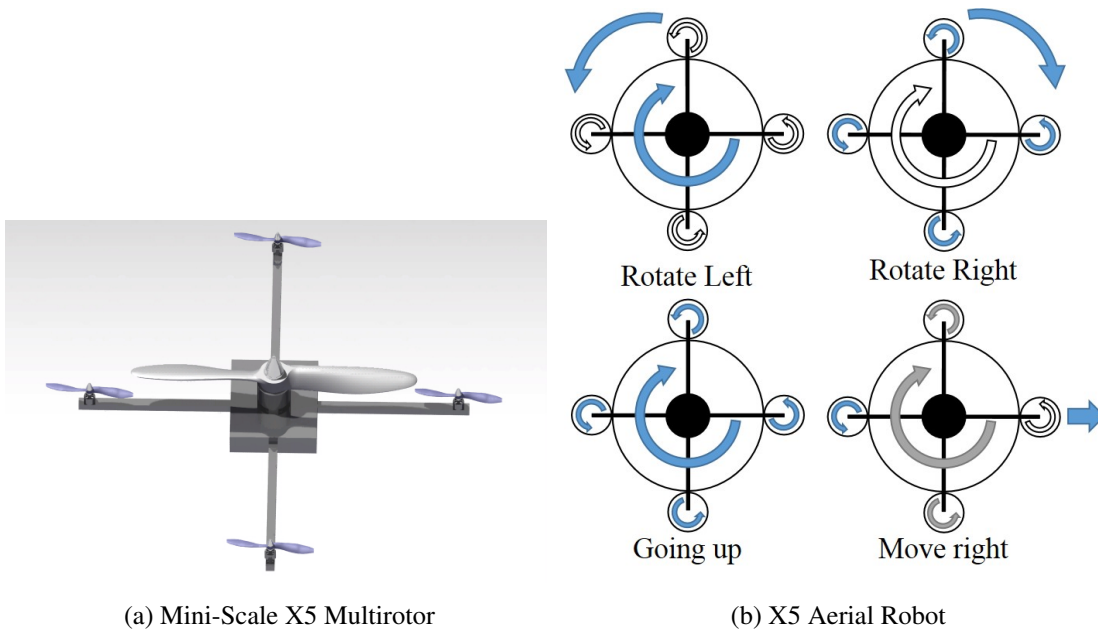


Figure 1.11: Unmanned Mini-Scale X5 Multirotors' Configuration

Increasing available energy stores requires larger and heavier aircraft, but it does not certainly mean that you can carry correspondingly larger and heavier payloads. The energy density of power sources of helicopter are better, but they are very compli-

cated and require intensive maintenance compared to traditional quadrotors which are simple and robust. Therefore, our focus in this work is on mixing the energy efficiency and lift capability of a helicopter with the simplicity of the quadrotors. This is achieved by applying a single large rotor (main rotor) at the center of the traditional quadrotors in order to provide the main lift power (See Figure 1.11a). The other four smaller rotors, which are smaller with comparison to standard quadrotors, furnish counter-torque like the tail rotor of a traditional helicopter. By applying a large central rotor above the maneuvering rotors we can maximize the size of propeller of the main rotor to provide more lift power. In addition, we can increase the attitude control bandwidth by decreasing rotational inertias of smaller rotors [37].

The control of X5 aerial robot is achieved by differential control of the thrust generated with these four smaller rotors. The large rotor provide active torque like traditional helicopters and the other four rotors feed control torques. These four smaller rotors are much like standard quadrotors (the speed of one rotor increases while the cross one is decreases and the other two rotates with same speed to provide roll or pitch motion). However, in X5 both sets of front-rear and left-right rotors turn in same direction, which is opposite to the direction of the large rotor (See Figure 1.11b).

#### 1.2.4 Contributions of This Study

This study focuses on the design and control of an unmanned X5-multirotor helicopter. The contribution of this study consists of three main topics.

- *Mathematical modeling of X5 aerial robot*: the aim is to get a suitable mathematical representation of the physical system in order to analyze the system and design the autopilot.
- *System design*: the goal is to minimize the the weight of X5 aerial system and to maximize the payload.
- *Autopilot*: the objective is to design the autopilot of the system by understanding the dynamics and applying suitable control techniques.

### **1.2.5 Thesis Outline**

The outline of this study is as follows: In Chapter 2, the modelling of X5 Aerial Robot is presented. Chapter 3 presents the hardware design and structure of X5 and also presents results of some tests. The autopilot design will be presented in Chapter 4. In this chapter PD, PID and control using Lyapunov theory will be presented. Chapter 5 deals with the simulation results of autopilot designed in the previous chapter. Finally, conclusion and future work of the topics presented previously are given in Chapter 6.

## **CHAPTER 2**

### **MATHEMATICAL MODELLING OF X5 AERIAL ROBOT**

#### **2.1 Introduction**

In this chapter, Newton-Euler method and blade element and momentum theory were used to derive the kinematics and dynamics models for the X5 multi-rotor. After deriving the kinematic model, all the aerodynamic and general forces and moments acting on the X5 will be discussed. Then, the equations of the motion of X5 will be presented as two rotational and translational subsystems. The rotor dynamics will come next. The following items are the list of assumptions for the model developed in this thesis.

- The model is symmetric and rigid.
- The propellers are rigid.
- The center of gravity is the origin of the body fixed frame.
- Thrust and drag are proportional to the square of propeller's speed.

#### **2.2 Modelling with Newton-Euler Method**

In Newton-Euler formalism, we can find a global characterization of the dynamics of a rigid body due to external forces and torques applied to the center of gravity [38] which is in body-fixed frame as shown in the following:

$$\begin{bmatrix} mI_{3 \times 3} & 0 \\ 0 & I \end{bmatrix} \begin{bmatrix} \dot{V} \\ \dot{\omega} \end{bmatrix} + \begin{bmatrix} \omega \times mV \\ \omega \times I\omega \end{bmatrix} = \begin{bmatrix} F \\ \tau \end{bmatrix} \quad (2.1)$$

### 2.2.1 Kinematic Model of X5

Before starting to discuss about the kinematic model of the X5, let us consider an Earth reference frame and a body frame as seen in Figure 2.1. In the coordinate frame (Figure 2.1) the Earth-fixed frame is shown with N, E and D (North, East, Down) axes and the body-fixed frame with  $x$ ,  $y$  and  $z$  axes [39].

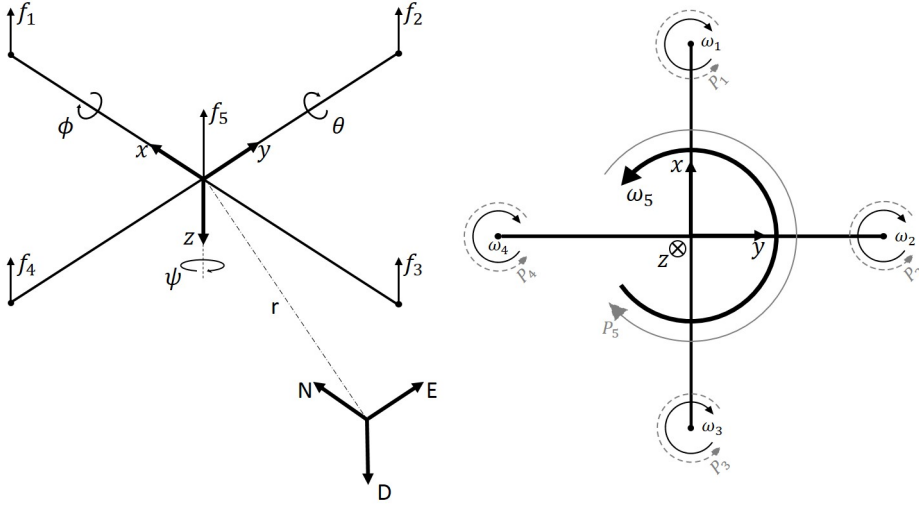


Figure 2.1: X5 Coordinate Frames

where  $r = \begin{bmatrix} x & y & z \end{bmatrix}^T$  shows the distance between inertial frame and the position of the center (center of mass) of the the body-fixed frame and roll, pitch and yaw angles ( $\phi, \theta$  and  $\psi$ ) describe the orientation of body-fixed frame. The roll angle represents the rotation of the body around  $x$  axes, in a similar way pitch and yaw angles represent the rotations around  $y$  and  $z$  axes, respectively. Using a rotation matrix  $R$  we can find the orientation of the airframe from body-fixed frame to Earth-fixed frame, where  $R \in SO3$  is derived based on the sequence of principle rotations as (see 2.2):



$$R = \begin{bmatrix} \cos\theta\cos\psi & \cos\theta\sin\psi & -\sin\theta \\ \sin\phi\sin\theta\cos\psi - \cos\phi\sin\psi & \sin\phi\sin\theta\sin\psi + \cos\theta\cos\psi & \sin\phi\cos\theta \\ \cos\phi\sin\theta\cos\psi + \sin\phi\sin\psi & \cos\phi\sin\theta\sin\psi - \sin\theta\cos\psi & \cos\phi\cos\theta \end{bmatrix} \quad (2.2)$$

Some states like X5 position and the gravitational forces are measured in the inertial frame and some of them like the thrust forces of propellers are measured in the body-fixed frame. The rotation matrix which is also known as Direction Cosine Matrix (DCM) is used as a transformation of states from one frame to the other frame.

To obtain the body-axis rates  $\omega = [p \ q \ r]^T$  and Euler-angle rates  $\dot{\eta} = [\dot{\phi} \ \dot{\theta} \ \dot{\psi}]^T$  we need to use the relationship between angular velocity of X5 and Euler angles as given in the following transformation (Equation 2.3), where  $(R^{-1} \neq R^T)$ .

$$R_r = \begin{bmatrix} 1 & 0 & -\sin\theta \\ 0 & \cos\phi & \sin\phi\cos\theta \\ 0 & -\sin\phi & \cos\phi\cos\theta \end{bmatrix} \quad (2.3)$$

Using the transformation (Equation 2.3), following results can be obtained:

$$\begin{bmatrix} p \\ q \\ r \end{bmatrix} = R_r \begin{bmatrix} \dot{\phi} \\ \dot{\theta} \\ \dot{\psi} \end{bmatrix} \quad (2.4)$$

The detailed derivation of the rotation matrix and angular rates are provided in Appendix A.1.

### 2.2.2 Aerodynamic Forces and Moments Acting on X5

By using blade element and momentum theory we can find the aerodynamic forces and moments acting on each rotor [40]. The detailed mathematical derivations of the following forces and moments which is based on [41], [42] have been provided in Appendix A.2.1

## Thrust Force

To determine the thrust force we can integrate the vertical forces (provided by four small boom rotors and the main rotor in the center) acting on the blade elements [43].

$$\begin{cases} T_i = C_{tb}\rho A_b \Omega_i^2 R_{brad}^2 & \text{where } i = 1, \dots, 4 \\ T_5 = C_{tm}\rho A_m \Omega_5^2 R_{mrad}^2 \end{cases} \quad (2.5)$$

## Hub Force

The hub force derivation is almost similar to the thrust derivation with the one difference: the horizontal forces integrated over all the blade elements can be neglected in this case due to negligible fuselage of X5.

$$\begin{cases} H_i = C_{Hb}\rho A_b \Omega_i^2 R_{brad}^2 & \text{where } i = 1, \dots, 4 \\ H_5 = C_{Hm}\rho A_m \Omega_5^2 R_{mrad}^2 \end{cases} \quad (2.6)$$

## Drag Moment

Aerodynamic forces acting on the blade elements also cause drag moment on the rotor shaft and this derivations acts on the center of the rotor. The importance of this torque is that it is used to determine the required power to keep rotor spinning.

$$\begin{cases} Q_i = C_{Qb}\rho A_b \Omega_i^2 R_{brad}^3 & \text{where } i = 1, \dots, 4 \\ Q_5 = C_{Qm}\rho A_m \Omega_5^2 R_{mrad}^3 \end{cases} \quad (2.7)$$

## Rolling Moment

The rolling moment comes from the integration over the entire rotor of the lift of each section acting at its radial position. In particular, it is created by a propeller

while moving horizontally through the air (forward flight in this case) and it is due to the fact that the advancing blade section see larger velocity component and leads to produce more lift than the retreating one. It is better to not confuse this rolling moment with the overall rolling moment mentioned in general forces and moment.

$$\begin{cases} R_i = C_{Rb}\rho A_b\Omega_i^2 R_{brad}^3 & \text{where } i = 1, \dots, 4 \\ R_5 = C_{Rm}\rho A_m\Omega_5^2 R_{mrad}^3 \end{cases} \quad (2.8)$$

The only variable parameter in the equations above is the air density. Since we have limited range of altitude in the case of the multi-rotors specially in the case of X5, we can consider it as constant and Equations (2.5 2.6 2.7 2.8) can be simplified as shown in the following [44] [45].

$$\begin{cases} T_i = K_{tb}\Omega_i^2 & \text{where } i = 1, \dots, 4 \\ T_5 = K_{tm}\Omega_5^2 \end{cases} \quad (2.9)$$

$$\begin{cases} H_i = K_{Hb}\Omega_i^2 & \text{where } i = 1, \dots, 4 \\ H_5 = K_{Hm}\Omega_5^2 \end{cases} \quad (2.10)$$

$$\begin{cases} Q_i = K_{Qb}\Omega_i^2 & \text{where } i = 1, \dots, 4 \\ Q_5 = K_{Qm}\Omega_5^2 \end{cases} \quad (2.11)$$

$$\begin{cases} R_i = K_{Rb}\Omega_i^2 & \text{where } i = 1, \dots, 4 \\ R_5 = K_{Rm}\Omega_5^2 \end{cases} \quad (2.12)$$

### 2.2.3 General Forces and Moments of X5

General forces and moments come from different physical effects which results which creates to movement of X5.

#### Forces in x Axis Direction

Total forces along  $x$  axis come from actuator actions, hub force and the friction in  $x$  axis which can be summarized in the following equations:

$$\begin{array}{ll}
 \text{actuators action} & (\cos\phi\sin\theta\cos\psi + \sin\phi\sin\psi)(\sum_{i=1}^5 T_i) \\
 \text{hub force in x axis} & - \sum_{i=1}^5 H_{xi} \\
 \text{drag} & \frac{1}{2}C_x\rho A_c\dot{x}|\dot{x}|
 \end{array} \tag{2.13}$$

#### Forces in y Axis Direction

Total forces along  $y$  axis can be calculated in the similar way of forces along  $x$  axis and comes from actuators action, hub force and the friction in  $y$  axis which can be summarized in the following equations:

$$\begin{array}{ll}
 \text{actuators action} & (\cos\phi\sin\theta\sin\psi - \sin\phi\cos\psi)(\sum_{i=1}^5 T_i) \\
 \text{hub force in y axis} & - \sum_{i=1}^5 H_{yi} \\
 \text{drag} & \frac{1}{2}C_y\rho A_c\dot{y}|\dot{y}|
 \end{array} \tag{2.14}$$

#### Forces in direction of z axis

In the case of VTOL multi-rotors without wings forces along  $z$  axis only depends on actuator actions and weight of the aerial vehicle. The following equations describe actuator actions and the total weight of X5, respectively.

$$\begin{array}{ll}
 \text{actuators action} & (\cos\phi\cos\theta)(\sum_{i=1}^5 T_i) \\
 \text{weight} & mg
 \end{array} \tag{2.15}$$

## Rolling Moments

Overall rolling moment of X5 depends on a number of effects like body gyro effect, propeller gyro effect and a number of other effects as indicated below:

body gyro effect	$\dot{\theta}\dot{\psi}(I_y - I_z)$	
propeller gyro effect	$J_r\Omega_r\dot{\theta}$	
actuators action in roll motion	$L(-T_2 + T_4)$	(2.16)
hub moment due to sideward flight	$h(\sum_{i=1}^5 H_{yi})$	
rolling moment due to forward flight	$(\sum_{i=1}^4 R_{mxi} - R_{mx5})$	

## Pitching Moments

Similar to the equations above, the overall pitching moment of X5 depends on a number of effects as mentioned below:

body gyro effect	$\dot{\phi}\dot{\psi}(I_z - I_x)$	
propeller gyro effect	$J_r\Omega_r\dot{\phi}$	
actuators action in roll motion	$L(T_1 - T_3)$	(2.17)
hub moment due to forward flight	$h(\sum_{i=1}^5 H_{xi})$	
pitching moment due to sideward flight	$(\sum_{i=1}^4 R_{myi} - R_{my5})$	

## Yawing Moments

Counter-torque unbalance plays the main rule in the overall yawing moment which is important in the case of multi-rotors as heading controller. This moment also depends on a number of other effects as mentioned below.

body gyro effect	$\dot{\phi}\dot{\theta}(I_x - I_y)$	
inertia counter-torque	$J_r\dot{\Omega}_r$	
counter-torque unbalance	$L(\sum_{i=1}^4 Q_i) - Q_5$	(2.18)
hub force unbalance in forward flight	$L(H_{x2} - H_{x4})$	
hub force unbalance in sideward flight	$L(-H_{y1} + H_{y3})$	

### 2.2.4 Equations of Motion

The complete equations of motion of X5 are derived from (2.1) and all the general forces and moments mentioned in the section 2.2.3.

$$\begin{cases}
 \ddot{x} = -\left(\frac{\cos\phi\sin\theta\cos\psi + \sin\phi\sin\psi}{m}\right) \sum_{i=1}^5 T_i - \sum_{i=1}^5 H_{xi} - \frac{1}{2}C_x A_c \rho \dot{x}|\dot{x}| \\
 \ddot{y} = -\left(\frac{\cos\phi\sin\theta\sin\psi - \sin\phi\cos\psi}{m}\right) \sum_{i=1}^5 T_i - \sum_{i=1}^5 H_{yi} - \frac{1}{2}C_y A_c \rho \dot{y}|\dot{y}| \\
 \ddot{z} = g - (\cos\phi\cos\theta) \sum_{i=1}^5 T_i \\
 \ddot{\phi} = \frac{\dot{\theta}\dot{\psi}}{I_x}(I_y - I_z) + \frac{J_r\Omega_r}{I_x}\dot{\theta} + \frac{L}{I_x}(-T_2 + T_4) - \frac{h}{I_x}(\sum_{i=1}^5 H_{yi}) + \frac{1}{I_x}(\sum_{i=1}^4 R_{mxi} - R_{mx5}) \\
 \ddot{\theta} = \frac{\dot{\phi}\dot{\psi}}{I_y}(I_z - I_x) + \frac{J_r\Omega_r}{I_y}\dot{\phi} + \frac{L}{I_y}(T_1 - T_3) - \frac{h}{I_y}(\sum_{i=1}^5 H_{xi}) + \frac{1}{I_y}(\sum_{i=1}^4 R_{myi} - R_{my5}) \\
 \ddot{\psi} = \frac{\dot{\phi}\dot{\theta}}{I_z}(I_x - I_y) + \frac{J_r\Omega_r}{I_z}\dot{\psi} + \frac{1}{I_z}(\sum_{i=1}^4 Q_i - Q_5) + \frac{L}{I_z}(H_{x2} - H_{x4}) + \frac{L}{I_z}(-H_{y1} + H_{y3})
 \end{cases} \quad (2.19)$$

### 2.2.5 Rotor Dynamics

For multi-rotor UAV's we need a type of motors which provide more torque and small friction. Therefore, Brush-Less Direct Current (BLDC) motor, which satisfies the requirements are used as both boom and main motor. Both types are assumed to be non-gearred rotors and coupling between the rotors and the propellers are rigid. In Figure 2.2 we can see a schematic of a BLDC motor.

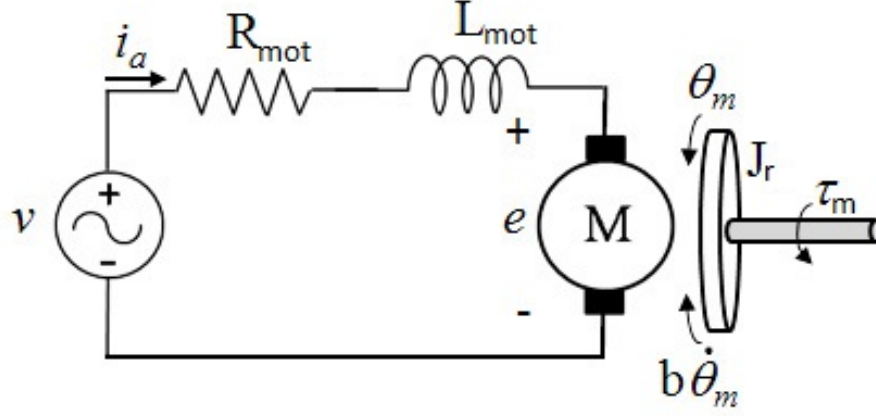


Figure 2.2: Schematic Diagram of DC Motor

Using Newton's second law and Kirchhoff's voltage law we can derive the following equations.

$$J_r \dot{\zeta}_m + b \zeta_m = K i_a \quad (2.20)$$

$$L_{mot} \frac{di_a}{dt} + R_{mot} i_a = u - K \zeta_m \quad (2.21)$$

where  $\zeta_m := \dot{\theta}_m$ ,  $\dot{\zeta}_m := \ddot{\theta}_m$ ,  $K$  represent the the motor torque constant and the back emf constant which are equal according to SI unit for DC motors and  $b \zeta_m$  is the torque generated by the propellers as mentioned in Equations 2.11 The inductance in small BLDC motors is very low and can be neglected and Equation 2.21 may be simplified as,

$$i_a = -\frac{K}{R_{mot}} \zeta_m + \frac{1}{R_{mot}} u \quad (2.22)$$

Substituting the Equations 2.22 and 2.20 we get,

$$J_r \dot{\zeta}_m = -\left(\frac{K^2}{R_{mot}} + b\right) \zeta_m + \frac{K}{R_{mot}} u \quad (2.23)$$

Equation (2.23) can be rewritten in linearized form around an operating point  $\dot{\zeta}_0$  as

follows,

$$\dot{\zeta}_m = -A\zeta_m + Bu \quad (2.24)$$

where

$$A = \left( \frac{K^2}{J_r R_{mot}} + b \right), \quad B = \left( \frac{K}{J_r R_{mot}} \right)$$

Using Matlab Identification Toolbox we can approximate the rotor dynamics in Chapter 3 and the final expression is given as [11].

$$G(s) = \frac{\text{Actual rotor speed}}{\text{Speed set-point}} \quad (2.25)$$



## CHAPTER 3

### HARDWARE DESIGN: CONSTRUCTION OF X5

#### 3.1 Introduction

The main concept of this chapter is to build a prototype model for testing the control strategies. The main goal is to develop a methodology in order to achieve the optimal design which we have been working on it. In general, the focus was on small-scale vehicle able to carry heavy payloads and having simple mechanics. The initial design of X5 aerial robot was computer based design using CAD programs (See result in Figure 3.1).

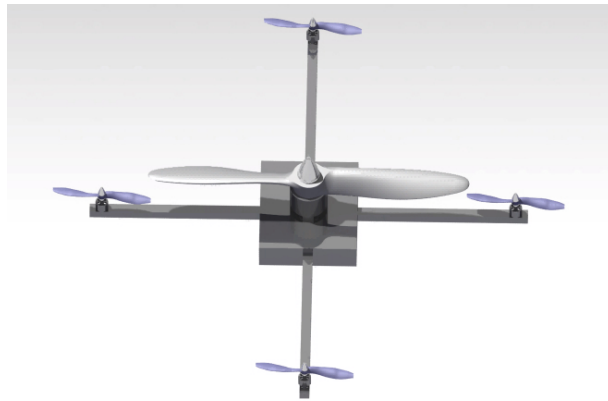


Figure 3.1: Initial Design of X5 Aerial Robot Using CAD

## 3.2 Sensors and Components

In this section all the sensors and main components of our design are described. The working principles of sensors and why we have chosen these sensors will be described in this section as well.

### 3.2.1 Inertial Measurement Unit

An Inertial Measurement Unit (IMU) is an electronic device which can measure orientation, gravitational forces and velocity of a craft using gyroscopes, magnetometers and accelerometers. IMUs are generally used to navigate any types of manned and unmanned crafts such as aircraft, rotorcraft, spacecraft including satellites and landers, watercraft and guided missiles. The IMU used in our system is the onboard unit on Pixhawk control board which includes the following sensors:

- ST Micro L3GD20H 16 bit gyroscope,
- ST Micro LSM303D 14 bit accelerometer / magnetometer,
- Invensense MPU 6000 3-axis accelerometer/gyroscope,
- MEAS MS5611 barometer.

There are several reasons for using two or more sensors with the same functions in Inertial Measurement Unit of Pixhawk control board.

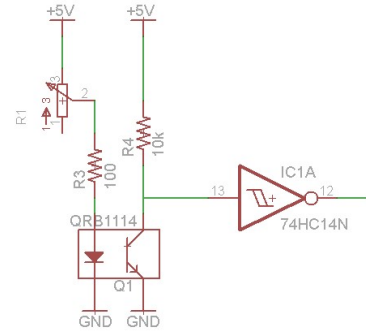
- *Safety*: if one of sensors fails, the other one can replace it.
- *Reliability*: Several values can be calculated from several sensors and a vector can decide the final output value which make it more reliable.
- *Power consumption*: The power consumption of sensors are different according to their accuracy. Using two different sensors with distinct accuracy can make a big difference on power consumption.
- *Frequency of analysis*: If frequency of a sensor interfere with an external frequency with the same value, we will get dc-offset in our measurement. Using another sensor with the same function with different frequency, we can get rid of this problem.

### 3.2.2 RPM Measurement

There exist several methods to measure the rpm of a BLDC motor. In [46], for instance, Magnussen and Kjell Eivind measured the frequency of two of the motor phases using a Hall effect sensor. In this study we used time domain analysis because it is easy to implement comparing with the other techniques. In the case of BLDC motors, the measurements of both current and speed are significantly important in order to find characteristic of the motors. To measure the speed of our brushless motors we used an opto-coupler QRD1114 (See Figure 3.2a) due to its fast response and simplicity of implementation.



(a) QRD1114 Optocoupler



(b) Schematic of the QRD1114 Board

Figure 3.2: QRD1114 Line Edge Sensor and its Schematic Board

There is one IR-LED and one photo-transistor on QRD1114 opto-coupler line edge sensors. The light emitted from the IR led is reflected from the surface of the encoder and according to the light density coming, which depends on the color of the surface, the voltage on the collector of the photo-transistor is changing: at high density it gives very low voltages (around several mV). In order to change the light density emitted from the LED, there is a potentiometer in series with the 100ohm resistor. The light density is regulated according to the distance between encoder disk and the sensor. In order to generate a digital signal which the measuring microcontroller can sense easily and to prevent unwanted fast jumps/drops on the sensor, the sensor is connected to the microcontroller via a Schmitt Trigger (74HC14) circuit. Figure 3.2b shows the schematic of the sensor board.

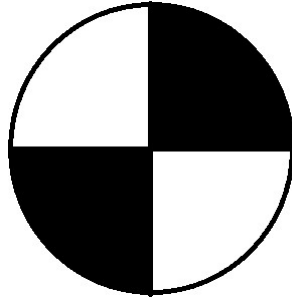


Figure 3.3: Encoder Disk

The encoder disk that we used to determine the speed of rotor has only two poles which allows the sensor to have high accuracy of measurement even in very high speeds. Figure 3.3 shows the simple encoder disk we used.

### 3.2.3 Voltage and Current Measurement

We used a battery as power supply for the entire system such as motors, data link, RC receiver and controller board and in order to measure the remaining power of the battery we have to use a power module to monitor the status of the battery. Figure 3.4 shows the 3DR power module which is commonly used for multirotors. The maximum input voltage it can handle is 18V (up to 4S Lipo battery) which we have used as power supply in our design and a maximum of 90Amps as an input current which is more than what we need. This PM provides 5.37V and 2.25Amp continuously, which reduces the chance of intentional or unintentional drops in voltage and current (brown-out).

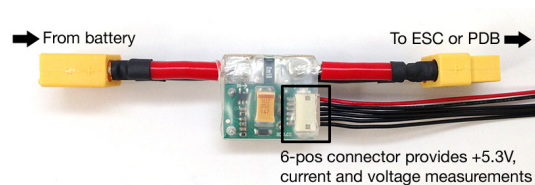


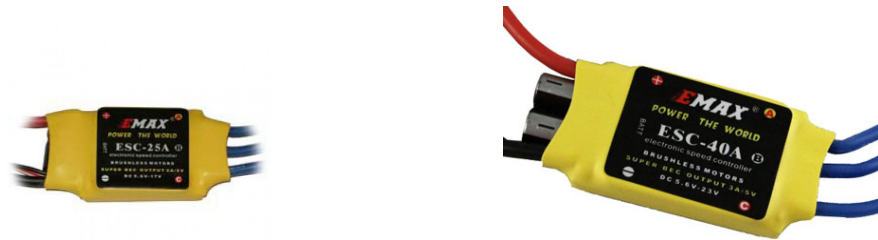
Figure 3.4: 3DR Power Module Used as Voltage and Current Sensor

Another reason of choosing this PM is that it allows us to monitor the battery's voltage and current and triggering RTL (return to launch) mode when the voltage of the battery becomes lower than 3.7V per cell or the total power consumed approaches the

battery's capacity which depends on what one set as initial setting for ones system.

### 3.2.4 ESC

An Electronic Speed Control (ESC) is an electronic circuit used to change the speed of electric motors. The ESCs most often used to generate three-phase electric power with low voltage source of energy to drive brushless motors by sending a sequence of signals for rotation. Most of the ESCs have a Battery Eliminator Circuit (BEC) module which is usually a linear or a switched mode regulator used to regulate the voltage for the receiver. Figures 3.5a and 3.5b show the 25A and 40A DC brushless ESCs used for boom-mounted rotors and main rotor, respectively.



(a) ESC Used for Boom Mounted Motors

(b) ESC Used for Main Motor

Figure 3.5: EMAX 25A and 40A ESCs Used to Drive the BLDC Motors

The nominal PWM signal frequency they can receive is 50Hz; however, they can receive signals up to 100Hz and even some ESCs which are specifically used for T-Motors can receive update frequency in 400+Hz. The low response time and high update frequency were the reasons to chose EMAX electronic speed controllers.

### 3.2.5 3DR Radio Telemetry Kit

The 3DR radio telemetry is a transceiver used to make a connection between main control board implemented on multirotor and ground control station. The reasons of choosing 3DR radio telemetry are that it is small, light weight and cheap. It is also available in both 915Mhz and 433Mhz models and works well in 300m range which can be extended to several kilometers by using a patch antenna on the ground control

station. Figure 3.6a shows both types of 3DR radio and Figure 3.6b shows the description of 3DR radio's pins [47].

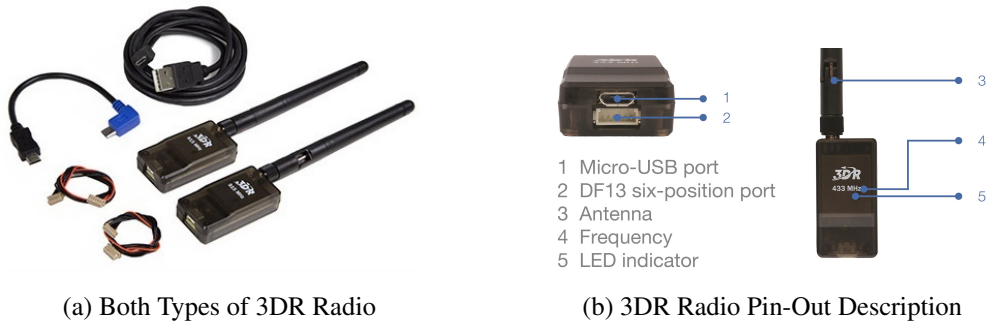


Figure 3.6: 3DR Radio V2 Telemetry Kit

This radio telemetry designed to work well with MAVlink communication protocol and uses open source firmware. Figure 3.7 shows how to connect the 3DR radio telemetry to main control board.

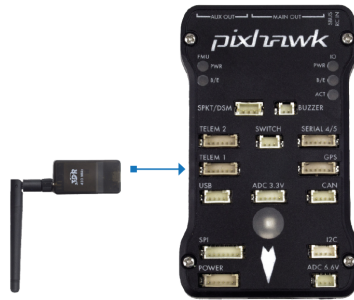


Figure 3.7: Connection of 3DR Radio Telemetry to Control Board

### 3.2.6 Control Board

Pixhawk or PX4 have been chosen to use as main control board to run the data processing and control system. This autopilot hardware is a combination of Flight Management Unit (FMU) and Input/Output Module (IO) in a single package [48]. Figure 3.8 explains all the pins of PX4 autopilot. PX4 is an independent and open source project with the objective of understanding and providing a highly reliable autopilot to the academic, hobby and industrial communities at low costs and high availability.

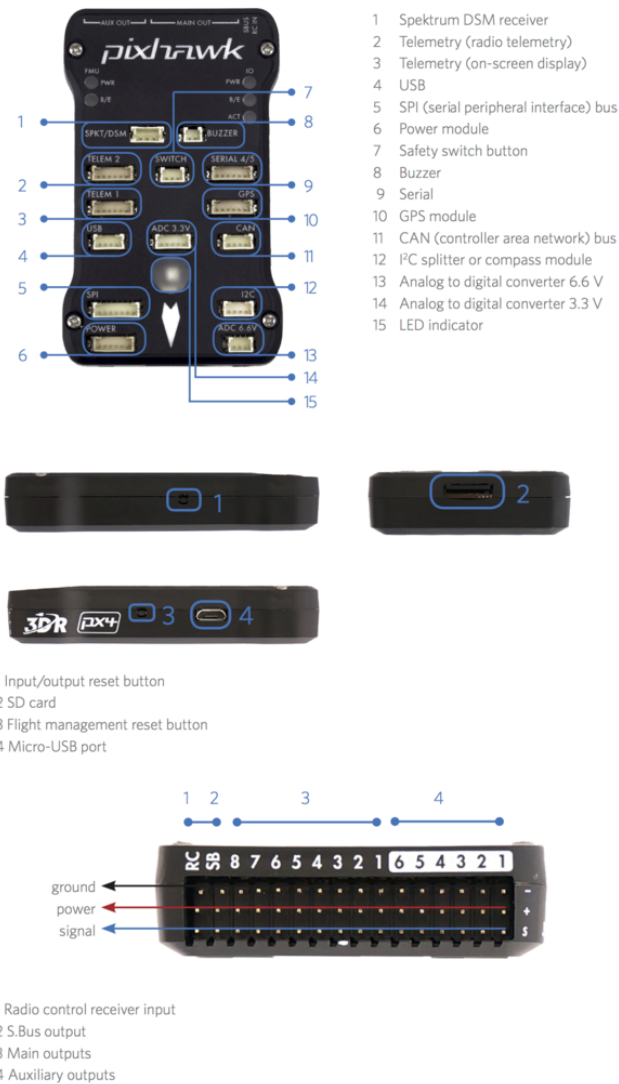


Figure 3.8: 3DR Pixhawk Autopilot Controller Used as Main Controller of X5

PX4 is a complete software and hardware platform that can run several autopilot applications like PX4 flight stick and APM. This autopilot module has a real-time operating system (RTOS) that can provide a Portable Operating System Interface (POSIX)-style environment (Not to be confused with Unix, Unix-like or Linux). More details about chosen autopilot hardware is as follows:

- **Processor:**
- 32bit STM32F427 Cortex M4 core with Floating Point Unit (FPU),
- 168 MHz,
- 256 KB RAM,

- 2 MB Flash,
- 32 bit STM32F103 failsafe co-processor.
- **Interfaces:**
  - 5x UART (serial ports), one high-power capable, 2x with HW flow control,
  - 2x CAN (one with internal 3.3V transceiver, one on expansion connector),
  - Spektrum DSM / DSM2 / DSM-X® Satellite compatible input,
  - Futaba S.BUS® compatible input and output,
  - PPM sum signal input,
  - RSSI (PWM or voltage) input,
  - I2C,
  - SPI,
  - 3.3 and 6.6V ADC inputs,
  - Internal microUSB port and external microUSB port extension.

### 3.2.7 Batteries

One of the major components of this project is batteries. The battery is the heaviest component among all components implemented in X5. Also, remaining power in the battery directly influences the flight duration. Figure 3.9a shows a four cell lithium polymer (Li-Po) battery which yields 14.8 volts and 10000 mAh to drive entire the system. This battery can feed 350 amperes continuously and can peak up to 700 amperes. Figure 3.9b also shows another Li-Po battery with three cells and 5000 mAh used in test-bench for BLDC motors. it can feed continuously 225 amperes and peak up to 450 amperes.

### 3.2.8 Propellers

The propellers were chosen based on the description of the motors and performance of them with respect to applied voltage and overall lift power we expected from each motor according to our design. After choosing some appropriate propellers for each motor, the final decision was made based on experimental tests of propellers. we





(a) 4s 10000mah Li-Po Used as Main Power Supply

(b) 3S 5000mAh Li-Po Battery Used as Test Bench Power Supply

Figure 3.9: Batteries

have chosen 9x4.5 three-blade propeller for boom-mounted motors and 18x5.5 T-motor style heavy duty carbon fiber propeller for the main motor. Figure 3.10 shows the chosen propellers used in prototype design. Table 3.1 shows the variables of the propellers used in main design.

Table 3.1: Propellers Variables [11] [32]

Name	Parameter	Value	Unit
<b>Boom Mounted Propeller</b>			
Mass	$m_{pb}$	12	g
Thrust coefficient	$C_{tb}$	$3.13e - 5$	$Ns^2$
Drag coefficient	$C_{Qb}$	$7.5e - 7$	$Nms^2$
Inertia	$J_{rb}$	$5e - 6$	$kgm^2$
<b>Main Propeller</b>			
Mass	$m_{pm}$	35	g
Thrust coefficient	$C_{tm}$	0.0230	$Ns^2$
Drag coefficient	$C_{Qm}$	$3.36e - 4$	$Nms^2$
Inertia	$J_{rm}$	$7e - 4$	$kg.m^2$

### 3.2.9 Motors

Both boom-mounted and main motors were chosen based on experimental tests on test-bench design and availability. These motors are BLDC motors made for model rotorcrafts. Figure 3.11a shows a T-Motor MS2212-13 which has 980 KV (980 rpm/volt) value and 160W maximum continuous power and Figure 3.11b shows a navigation series T-Motor (MN4014-9) with 400 KV (400 rpm/volt) value and 900W



(a) 9x4.5 3-Blade Propeller Used as Boom Rotor's Propeller



(b) 18x5.5 T-Motor Style Propeller Used as Main Rotor's Propeller

Figure 3.10: Boom-Mounted and Main Rotors' Propellers

maximum continuous power. In the case of BLDC motors, the lower the KV value is, the lesser the rotational speed and higher torque are. Table 3.2 shows the variables of the motors used in main design.

Table 3.2: Motors Variables [11] [32]

Name	Parameter	Value	Unit
<b>Boom Mounted Motor</b>			
Mass	$m$	57	g
Maximum power	$P_{mb}$	160	W
Internal resistance	$R_{motb}$	85	$m\Omega$
Inertia	$J_{mb}$	$4e - 7$	$kgm^2$
<b>Main Motor</b>			
Mass	$m$	150	g
Maximum power	$P_{mb}$	800	W
Inertial resistance	$R_{motm}$	67	$m\Omega$
Inertia	$J_{mm}$	$6e - 5$	$kg.m^2$

### 3.2.10 Motor and Propeller Testing

Motor and propeller tests were carried out in order to finding the characteristics of motors coupled with propeller and complete the dynamic model.



(a) 980KV BLDC T-Motor Used as Boom Motor



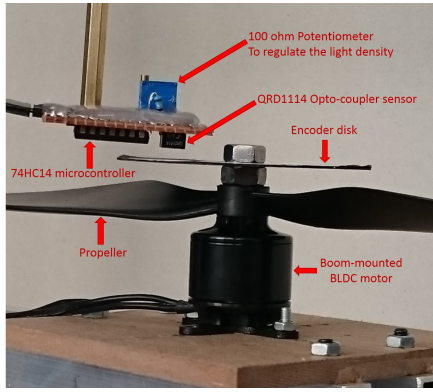
(b) 400KV BLDC T-Motor Used as Main Motor  
Placed in Center of Mass

Figure 3.11: Main and Boom-Mounted Motors

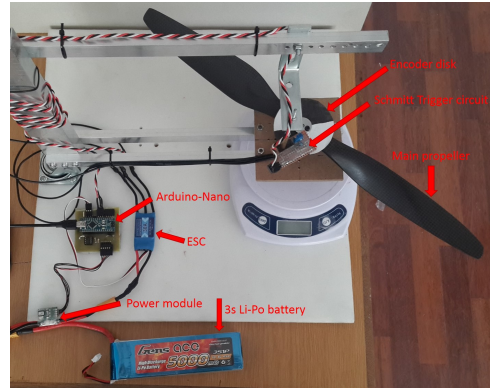
### Speed Measurement

In order to measure the speed, we first try to count the pulses in a certain amount of time. However it made the system more discretized since the number of the poles on the encoder disk we used were low (see Figure 3.3). Figure 3.12a shows the RPM measurement unit mounted near the encoder disk. Due to high speed this kind of disk was necessary. So, we measure the speed with the help of the period of the signal in which the motor completes half a tour. We took the total of the periods and the total pulse count and send the computer the mean of them which also allows us to eliminate measurement noise slightly. As the sampling period increases, measurement noise decreases.

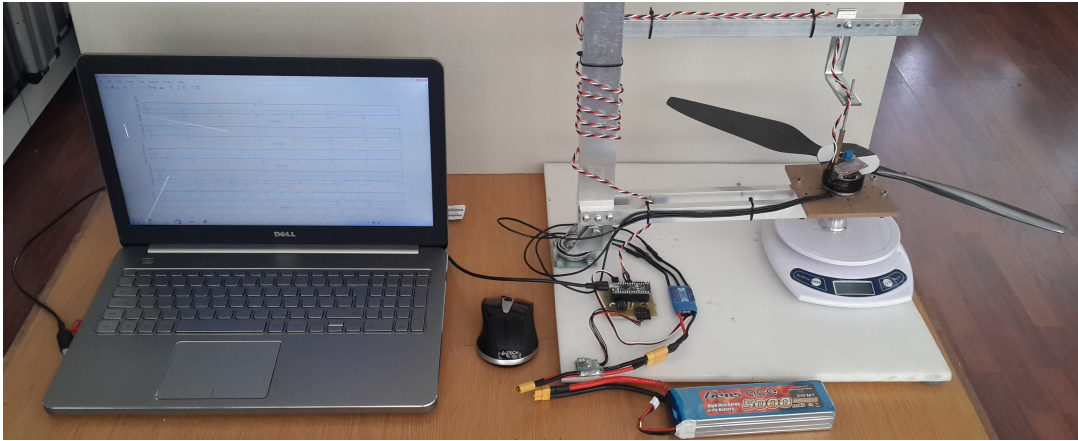
We used an Arduino-Nano board as a microcontroller (see Figure 3.12b) because it was easy to operate and allows us to implement the project faster. We have tried different microprocessors; however initialization and debugging took too much time. The sensor is connected to one of its external interrupt pins and the interrupt is triggered with the positive edge of the sensor which means the sensor is reading white color. When the positive edge comes again, it means that half a round is completed and the time between two consecutive edges is added to the total and the measurement count is increased by one. In the loop, when the sampling time is completed, the total is divided by the count and the mean is send through the serial port to the computer. This method also provides a low pass filter for us.



(a) Details of RPM measurement Unit



(b) Arduino-Nano, ESC, Power Module, etc.



(c) Test-Bench Design to Find Out the Characteristics of Motors

Figure 3.12: Entire Test-Bench for BLDC Motors

In addition to that, the microcontroller generates the input waveform. The BLDC motor is driven by the ESC (Electronic Speed Controller) and the necessary wave is a square wave of 50Hz frequency with the pulse width between one and two milliseconds. Arduino can generate this wave with the resolution of microseconds. We tried to send the desired speed from computer; however the response time of the system was low. Figure 3.13 shows the applied input waveform.

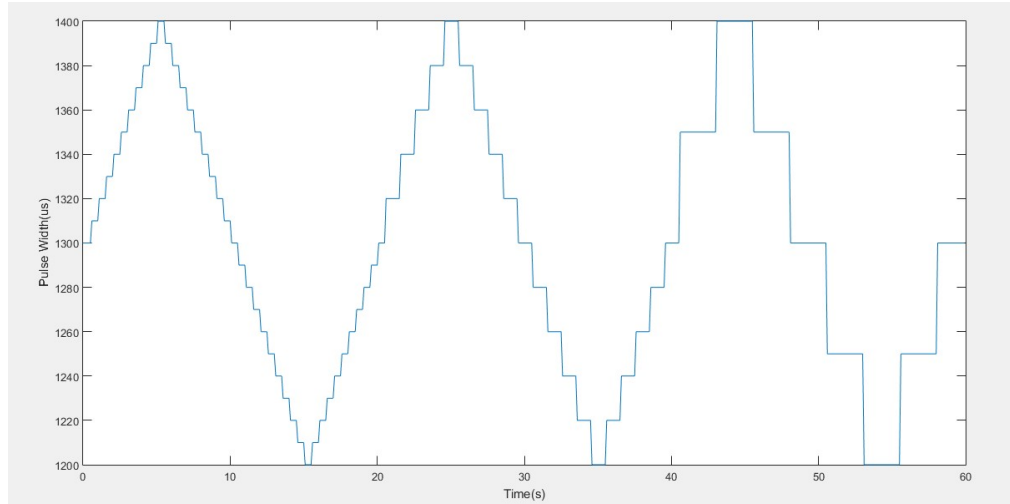


Figure 3.13: Generated Pulse Width Used for System Identification

This type of waveform is used to determine both fast and slow acceleration/deceleration. The mean is adjusted as  $1300\mu s$ . The measurements are taken by the Matlab on a computer via serial port. When the Matlab script sends the starting signal to the microprocessor, the motor is started and the measurements are conducted on the computer as packages of the voltage of the battery, the current which system draws and the RPM data. The voltage data is used not to harm the battery; if the voltage drops under a certain level, the test is terminated. The measured data is stored in the computer. Figure 3.14 shows the result of speed measurement data with respect to given input waveform.

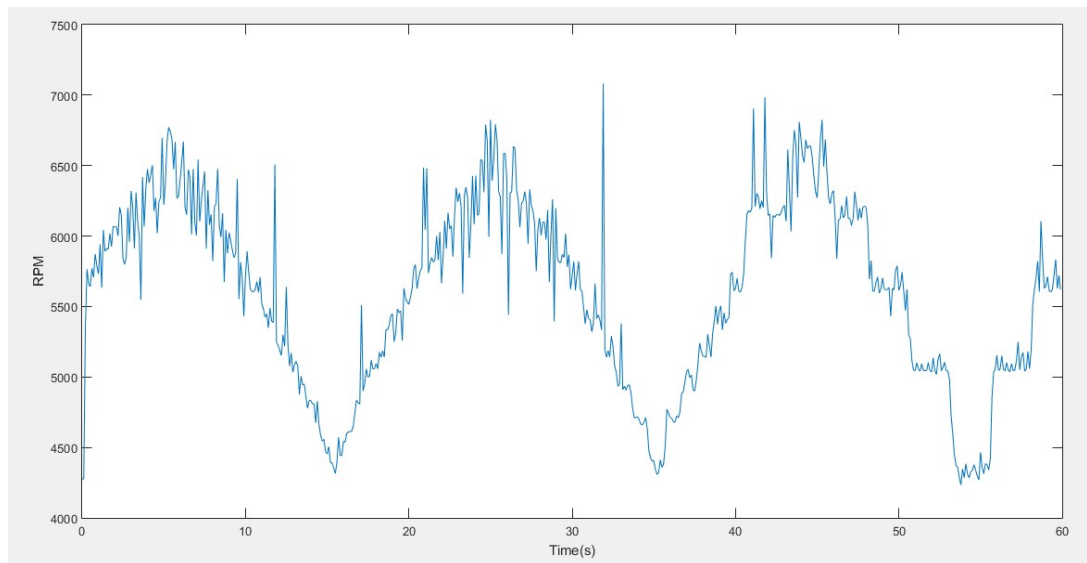


Figure 3.14: Result of Speed Measurement Data wrt Given Input Waveform

As seen in Figure 3.14, the results are little noisy and if the sampling rate is increased, the results become even more noisy. The first order 1D-median filter can be used to eliminate this noise or simply, the undesired peaks can be cleaned by the user. The calculated measurement error for both boom-mounted and main rotors are presented in the identification section.

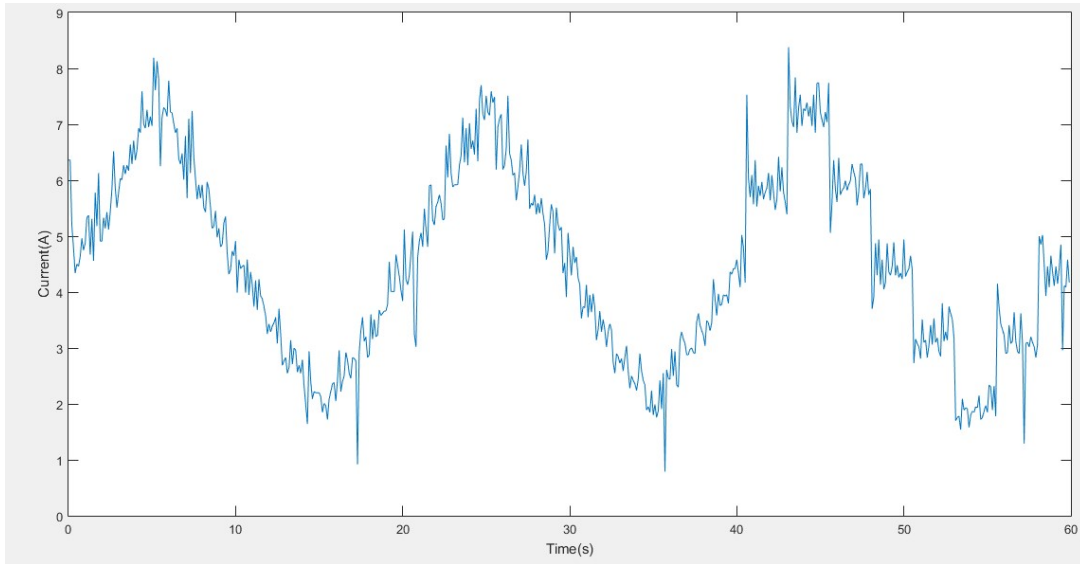


Figure 3.15: Result of Current Measurement

### Current Measurement

Another necessary parameter of the BLDC motor was the current it utilizes. The current measurement was taken with the help of the power module of the APM 2.6 which has 5.3V voltage regulator, voltage sensing opamp and the current sensor on it. The current utilized by the system is passed through a  $50m\Omega/4W$  resistor and the voltage drop on this resistor is amplified by 11 using an opamp [49]. Figure 3.15 shows the result of current measurement corresponding to the given input waveform. Figure 3.16 shows the given input waveform and measurement results of voltage, current, RPM and propeller's angular speed changes with respect to time.

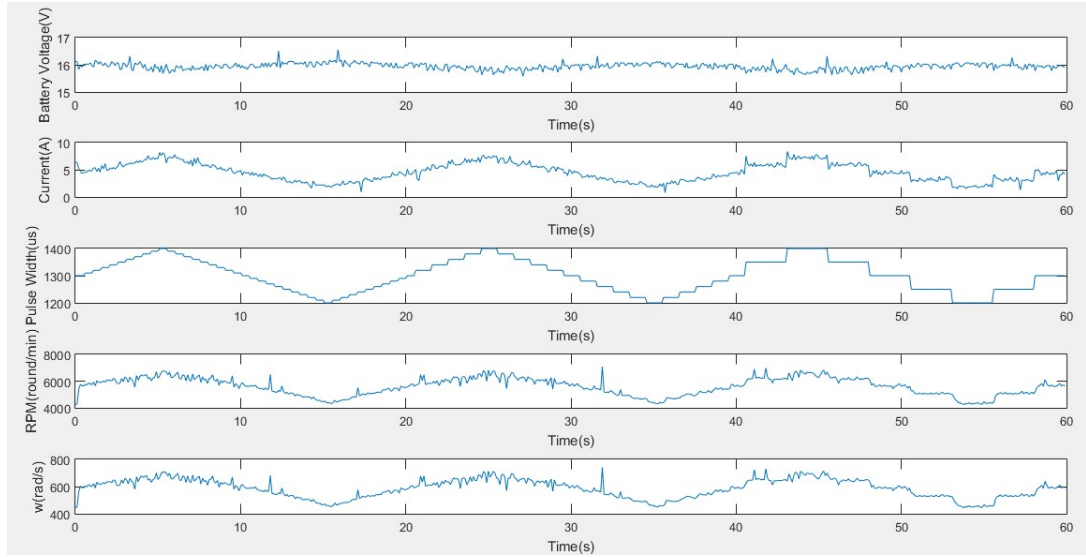


Figure 3.16: Result of Measured Current, Voltage, RPM, etc.

### Thrust Measurement

The identified motors will be used on X5 systems so the thrust of the motor-propeller system is an important parameter to perform simulations. We used electronic scales under the motor. The scale is reset before the test starts. Since we need to read the measurement from the scale, the waveform we used before was not applicable. Because of that we applied speeds from smallest to the largest. After each speed step we recorded mean of the RPM data, current, power, voltage and the weight data read from scale. Table 3.3 shows the measurements resulting from the case boom-mounted rotor coupled with 9x4.5 size propeller.

Table 3.3: Boom-Mounted Rotor's Thrust Measurement Result

PPM	RPM	Thrust (g)	Current (A)	Power (W)	Voltage (V)
1100	2100	55	0.61	7.5	12.23
1200	3650	156	1.65	20	12.21
1300	4500	237	2.70	33	12.19
1400	5350	340	4.20	50	12.15
1500	6100	445	6.00	72	12.11
1600	6800	535	7.75	92	12.04
1700	7150	580	8.95	106	11.98
1800	7800	675	10.75	127	11.90
1900	8200	750	12.85	151	11.81
2000	8200	750	12.85	151	11.81



Figure 3.17 shows the result of current versus RPM for boom-mounted rotors. The certainty of this measurement is about  $\pm 100$  rpm and for current the certainty is about  $\pm 0.05$  A.

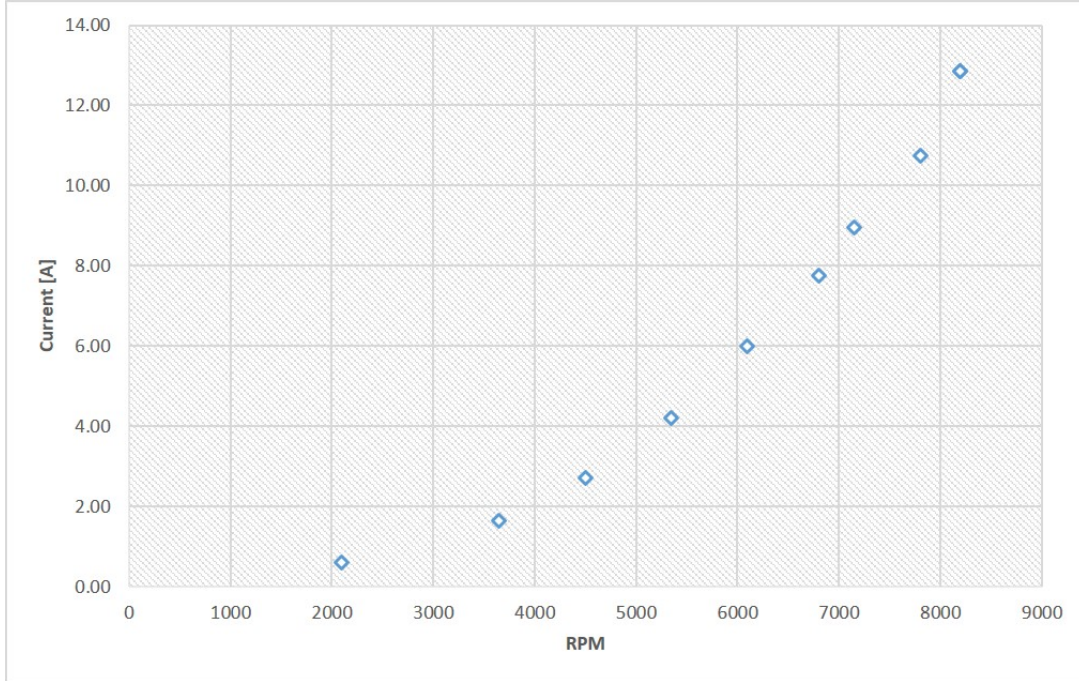


Figure 3.17: The Result of Current vs RPM for Boom-Mounted Rotors.

After measuring the thrust force of boom-mounted rotors, we replay the same test for the main rotor. Table 3.4 shows the measurements resulting from the case main rotor coupled with 18x5.5 size propeller.

Table 3.4: Main Rotor's Thrust Measurement Result

PPM	RPM	Thrust (g)	Current (A)	Power (W)	Voltage (V)
1100	1150	147	0.71	11.9	16.67
1200	2050	450	2.4	39.5	16.57
1300	2750	800	4.50	73.5	16.43
1400	3200	1150	6.97	114	16.75
1500	3600	1460	9.96	157	16.02
1600	3950	1750	12.29	195	15.83
1700	4150	1900	14.93	230	15.53
1800	4400	2040	17.26	263	15.35
1900	4558	2300	20.20	305	15.10
2000	4558	2300	20.20	305	15.10



Figure 3.18 shows the result of current versus RPM for main rotors. The certainty of this measurement is about  $\pm 100$  rpm and for current the certainty is about  $\pm 0.05$  A.

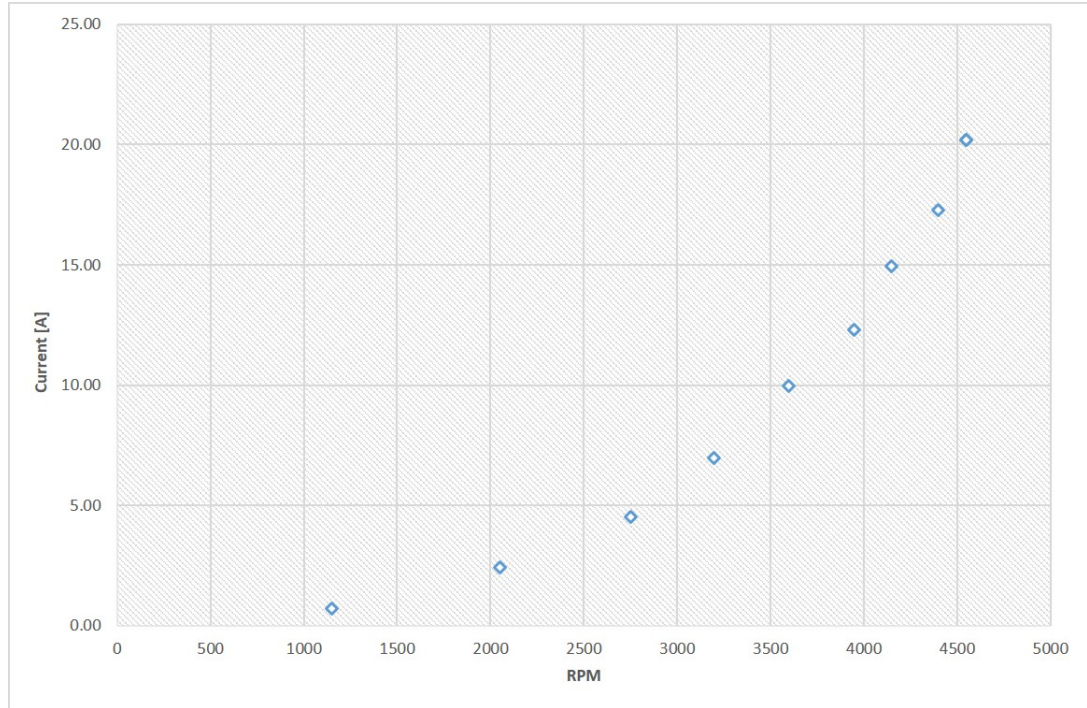


Figure 3.18: The Result of Current vs RPM for Main Rotor.

## Identification

We have taken measurements from two different types of motors with different propeller combination. The overall system can be considered by two aspects: Mechanical for the speed and the electrical for the current. The electrical side is not as important as the mechanical side for a multicopter project; however it helps to understand the system better. The overall BLDC motor system is modeled in Chapter 2. Using system identification toolbox of the Matlab to determine the overall transfer function and adding measurement results as a time domain signal to the identification toolbox, the expected pole zero number is indicated and Matlab estimates the transfer function with a certain accuracy using instrumental variable method. The instrumental method can be seen as generalizations of the Least Square (LS) method [50] which is used to estimate causal relationship when all the cases may not be delivered to the system. The overall transfer function of each tested motor includes transfer functions of motor, propeller and ESC coupled as one thruster.

## Identification Results and the Transfer Functions

First motor we tested was T-Motor MS2212-13 which has 980 KV value with 9x4.5 propeller. The measurement is given in Figure 3.19

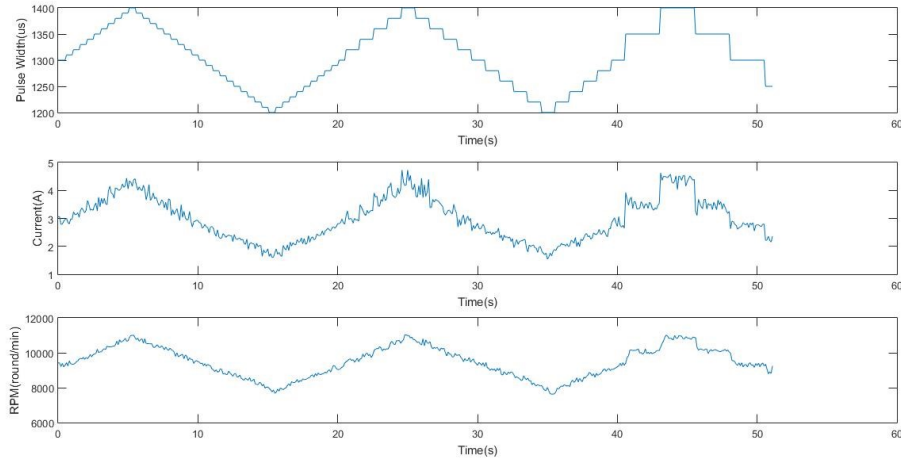


Figure 3.19: T-Motor ms2212-13 With 9x4.5 Propeller Given Pulse Width, RPM and Consumed Current According to the RPM

Since the measurements were noisy, first order median filter was applied to the rotation speed measurement of boom-mounted motor to make the results more reliable and to increase accuracy of the estimation results. Figure 3.20 shows the measurement error between the unfiltered and filtered data for boom-mounted motor and we can see the histogram of the measurement error in Figure 3.21. The histogram of the measurement error shows distribution of the error which has a mean of 1 rad/sec. Figure 3.22 shows the estimation results from the case where boom motors coupled with 9x4.5 propeller.

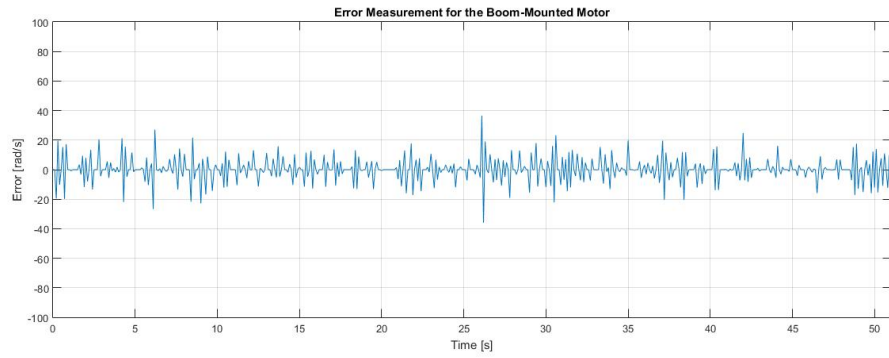


Figure 3.20: Measurement Error Between Filtered and Unfiltered Measured RPM Data for Boom-Mounted Motor

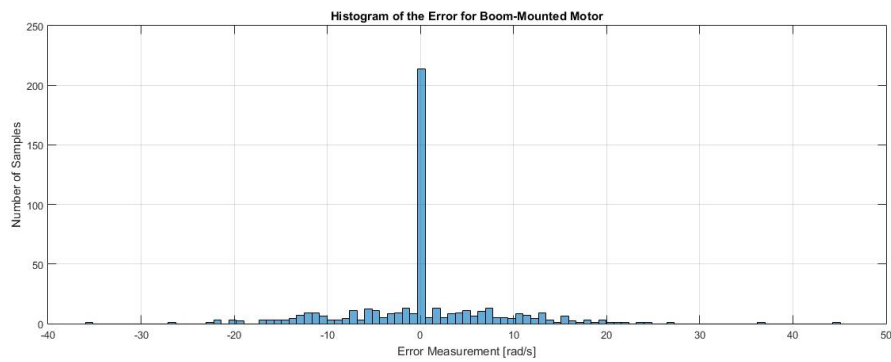


Figure 3.21: Histogram of Measurement Error of Measured RPM Data

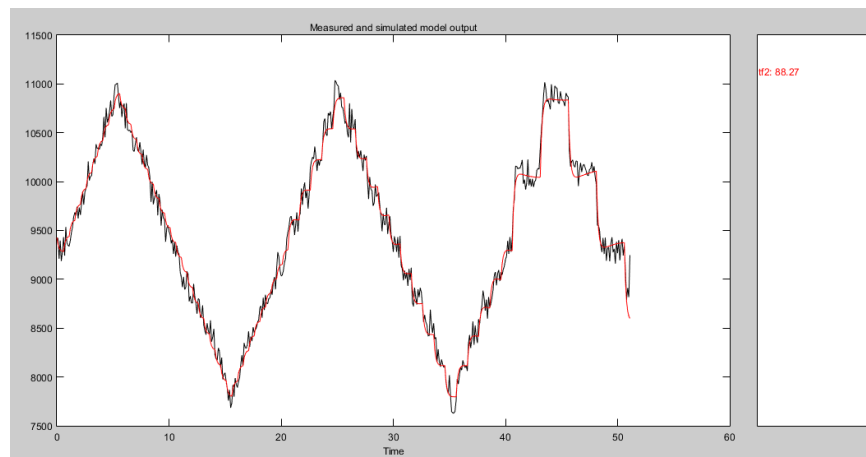


Figure 3.22: Estimation Results with Unfiltered Data for Boom Motors

The transfer function obtained for boom motors coupled with 9x4.5 inches propeller is given as:

$$G_1(S) = \frac{Y(S)}{U(S)} = \frac{108.1s^3 + 33.49s^2 + 16.28s + 0.2148}{s^4 + 6.893s^3 + 2.542s^2 + 1.011s + 0.02997} \quad (3.1)$$

where  $y(t)$  describe output which is thrust force generated by motor and  $u(t)$  described input of motors which is current.

Second motor we tested was navigation series T-Motor MN4014-9 which has 400 KV value with 18x5.5 propeller. The measurement is given in Figure 3.23.

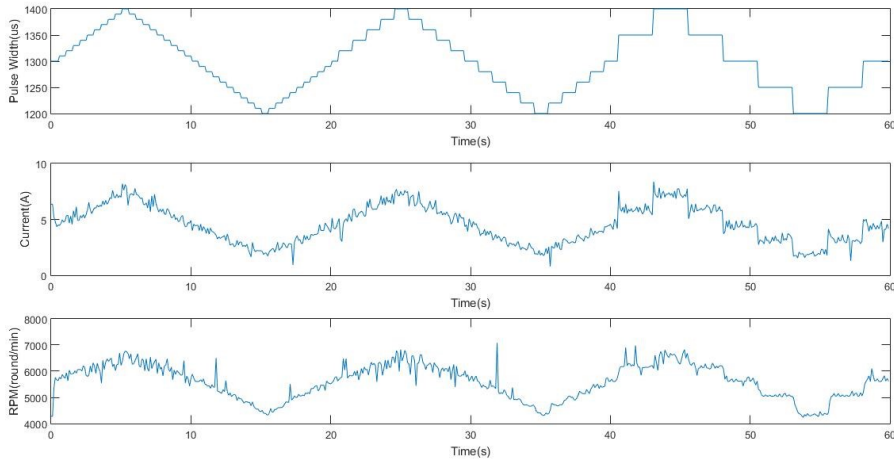


Figure 3.23: T-Motor MN4014-9 With 18x5.5 Propeller Given Pulse Width, RPM and Consumed Current According to the RPM

First order median filter was also applied to the rotation speed measurement of the main motor to make the results more reliable and to increase accuracy of the estimation results. Figure 3.24 shows the measurement error between the unfiltered and filtered data for the main motor and we can see the histogram of the measurement error in Figure 3.25. The histogram of the measurement error shows distribution of the error which has a mean of 0.2 rad/sec. Figure 3.26 shows the estimation result for the main motor coupled with 18x5.5 coupled propeller.

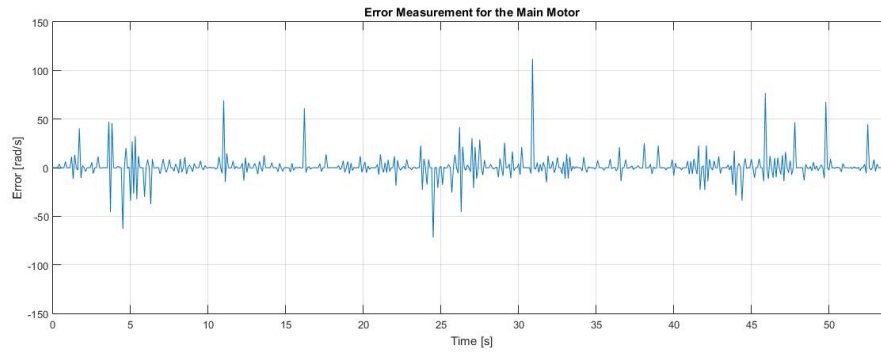


Figure 3.24: Measurement Error Between Filtered and Unfiltered Measured RPM Data for Main Motor

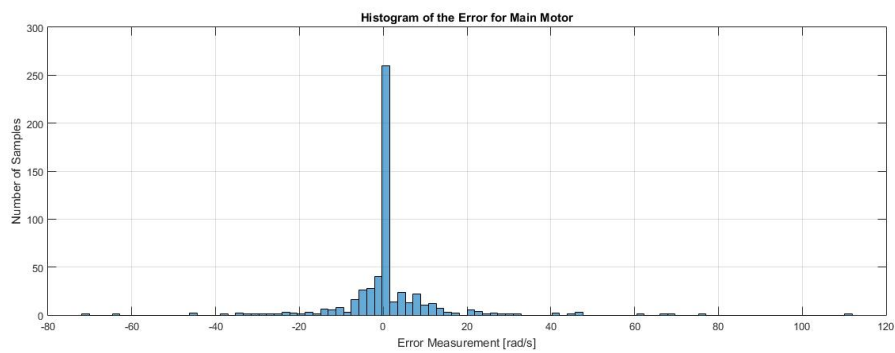


Figure 3.25: Histogram of Measurement Error of Measured RPM Data

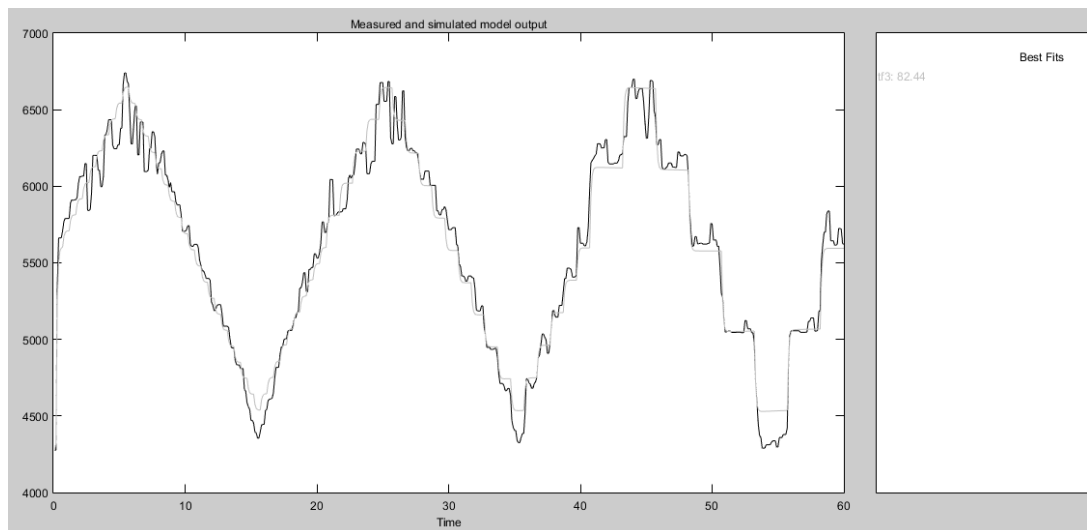


Figure 3.26: Estimation Result for Main Motor

The transfer function obtained for main motor coupled with 18x5.5 inches propeller is given as:

$$G_2(S) = \frac{Y(S)}{U(S)} = \frac{62.9s^4 + 11.23s^3 + 25.83s^2 + 4.913s + 0.3843}{s^5 + 7.038s^4 + 1.695s^3 + 3.128s^2 + 0.4734s + 0.09548} \quad (3.2)$$

where  $y(t)$  describe output which is thrust force generated by motor and  $u(t)$  described input of motors which is current.

### 3.2.11 Moment of Inertia

Inertia tensor ( $I_B$ ) or moment of inertia is defined as an object resistance to rotate when torque is applied. For simulation purposes, the inertia tensors of the components are calculated utilizing the standard prism, full cylinder, plate, and rod moment of inertia formulas at their CoG. The effect of displacements of components from CoG of the rotorcraft are taken into account using parallel axis theorem:

$$I_B = \sum_{i=1}^n (I_{B_i} + m_{B_i} [(P_i \cdot P_i) E_3 - P_i \otimes P_i]) \quad (3.3)$$

where

- $P_i$  position of each component according to  $P_{CoG}$ ,
- $m_{B_i}$  mass of each component,
- $I_{B_i}$  inertia tensor of each component,
- $i : 1..n$  index number of each component,
- $E_3$  identity matrix.

The “knife edge” [51] is utilized in measuring inertia tensor’s principals. The rotorcraft is fixed at the CoG to the free end of a pendulum rod as seen in Figure 3.27. Total pendulum system is rotated to a fixed angle, set loose to oscillate and total time of 10 oscillations is recorded. By noting the time period of oscillation, the moment of inertia for the related axis is obtained using a MATLAB function written by Ferit Çakici [52] as:

$$I_{tot} = \begin{bmatrix} I_x & 0 & 0 \\ 0 & I_y & 0 \\ 0 & 0 & I_z \end{bmatrix} = m_{tot}r \left( \frac{g}{4\pi^2} \begin{bmatrix} t_x^2 \\ t_y^2 \\ t_z^2 \end{bmatrix} - r \right) \quad (3.4)$$

where

$I_{tot}$	total inertia tensor,
$I_x, I_y, I_z$	principles of inertia tensor,
$r$	length of the pendulum rod,
$t_x, t_y, t_z$	average time period of oscillation.

Resultant inertia tensor of the aircraft is found by subtracting  $I_{rod}$  from  $I_{tot}$ , using parallel axis theorem. The product of inertia terms are assumed to be negligible due to symmetrical structure of the aircraft and the overall moment of inertia of X5 obtained as follows:

$$I_{tot} = \begin{bmatrix} I_x & 0 & 0 \\ 0 & I_y & 0 \\ 0 & 0 & I_z \end{bmatrix} = \begin{bmatrix} 0.0520 & 0 & 0 \\ 0 & 0.0530 & 0 \\ 0 & 0 & 0.0947 \end{bmatrix} \quad (3.5)$$

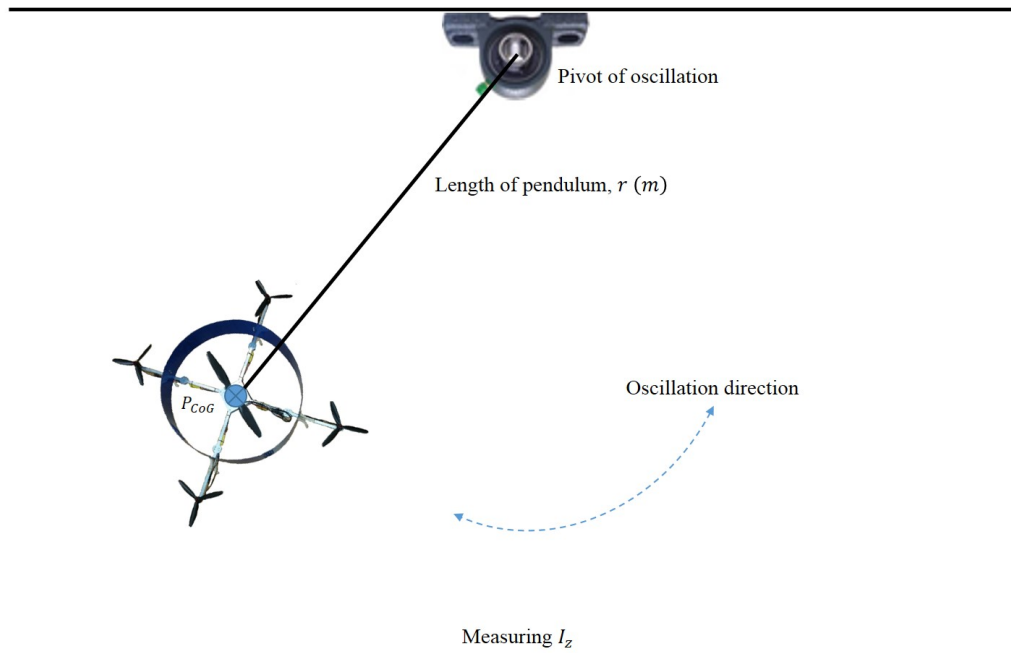


Figure 3.27: Inertia Tensor Measurement

### 3.3 Assembling X5 Multirotor

In order to install all the components to the platform, the mass of each component and the position of them should be defined. Table 3.5 shows the masses and locations of each component according to the center of gravity of X5.



Table 3.5: Components of X5 and Their Position

<b>Name</b>	<b>Mass (g)</b>	<b>Position According to CoG</b>
Body, aluminium	710	[0 0 0]
Boom-mounted motor no:1	57	[49 0 - 4]
Boom-mounted motor no:2	57	[0 49 - 4]
Boom-mounted motor no:3	57	[-49 0 - 4]
Boom-mounted motor no:4	57	[0 - 49 - 4]
Main motor	150	[0 0 - 5]
ESC 4in1 for small rotors	68.8	[0 0 - 3]
ESC for main rotor	49	[0 0 - 3]
Propeller for small rotor no:1	12	[49 0 - 6]
Propeller for small rotor no:2	12	[0 0 - 6]
Propeller for small rotor no:3	12	[-49 0 - 6]
Propeller for small rotor no:4	12	[0 - 49 - 6]
Propeller for main rotor	34	[0 0 - 6]
Main controller, pixhawk	38	[0 0 0]
GPS/Magnetometer	17	[0 0 - 32]
Power module	25	[0 0 0]
Telemetry modem	32	[3 3 0]
RC receiver	15	[3 - 3 0]
Cables and conecctions	315	[0 0 0]
Battery	980	[0 0 3]
<b>Total</b>	<b>2709.8</b>	

Figure 3.28 shows the overall connections between four boom-mounted motors, GPS, RC receiver, radio telemetry and etc. and Figure 3.29 shows the completed construction of X5.

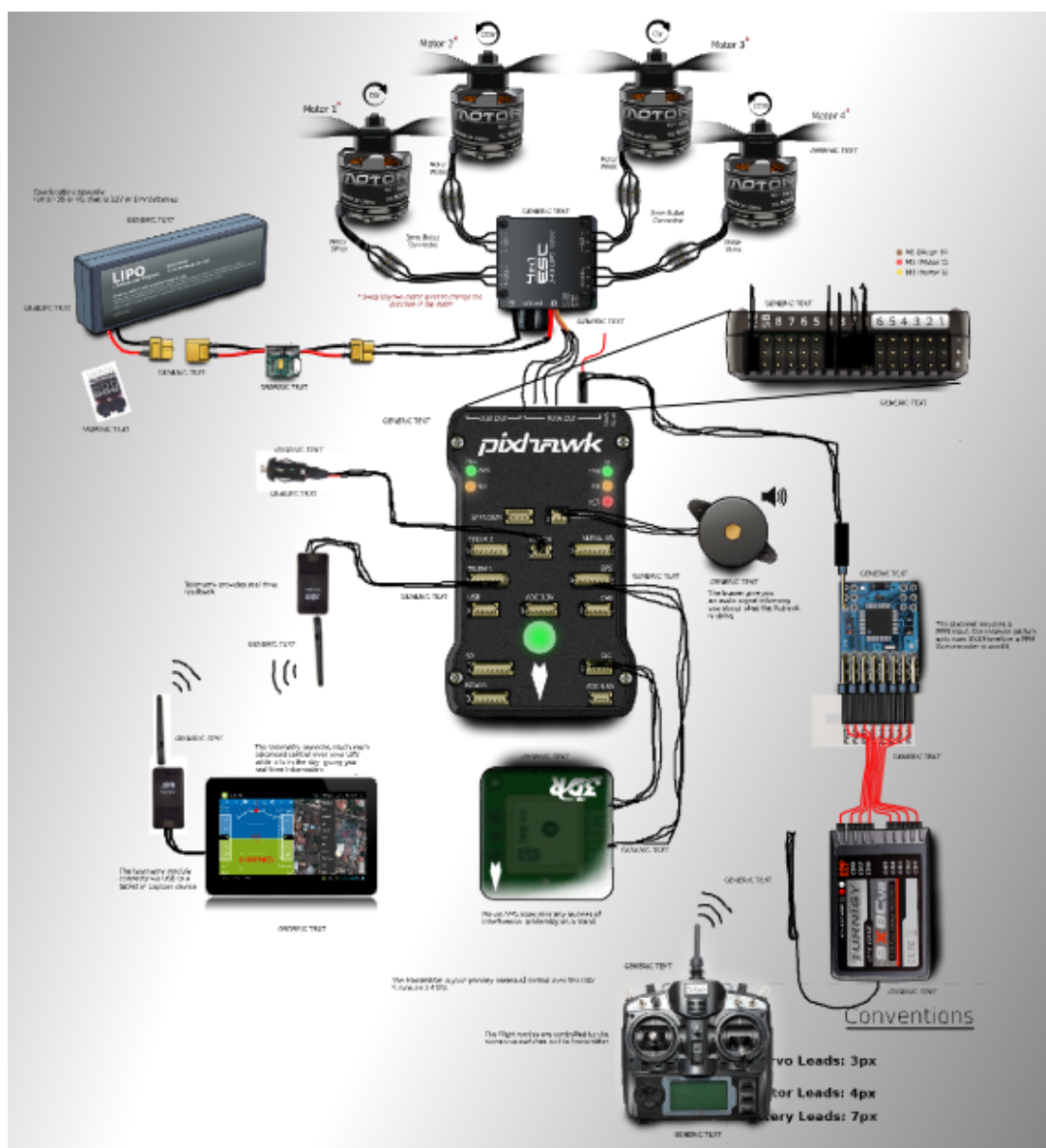


Figure 3.28: X5 Aerial Robot’s Hardware Configuration [53]

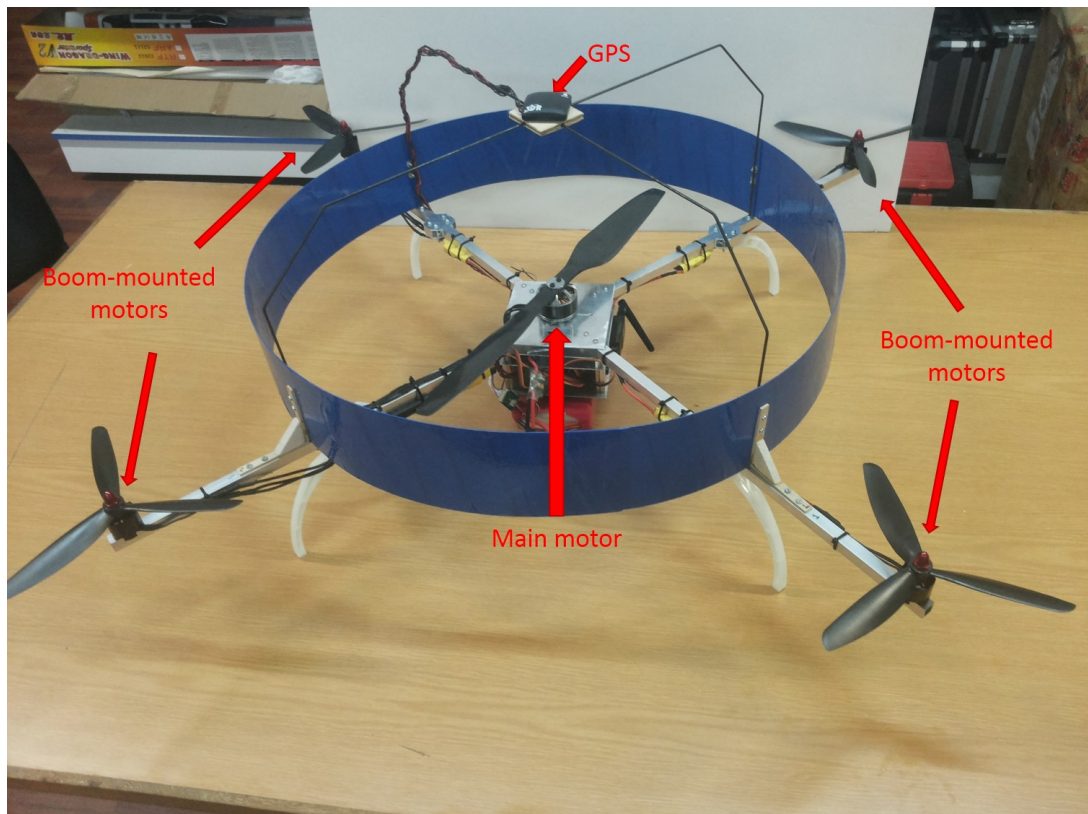


Figure 3.29: X5 Unmanned Aerial Robot



## CHAPTER 4

### AUTOPILOT DESIGN

#### 4.1 Introduction

The concept of this chapter is to modify the mathematical modeling of X5 which has been shown in Equation 2.19 for control and explain the control actions. After designing our complete control structure we will evaluate several control techniques. The simulation results of each controller will be presented in Chapter 5.

#### 4.2 Modelling for Control

The mathematical model shown in Equation 2.19 describes the differential equations of the system which can be simplified since thrust and drag coefficients in Equations 2.9 through 2.12 are assumed constant in hover situation and rolling moments and hub forces are neglected. Thus, the system model can be written in state-space representation as  $\dot{X} = f(X, U)$  where  $X$  is defined as the state vector and  $U$  is defined as the input vector.

##### The State Vector

The state vector of X5 seen in Equation 4.1 defines the position, angular and linear velocity of X5 aerial robot.

$$X = \begin{bmatrix} \phi & \dot{\phi} & \theta & \dot{\theta} & \psi & \dot{\psi} & z & \dot{z} & x & \dot{x} & y & \dot{y} \end{bmatrix}^T \quad (4.1)$$

$$\begin{aligned}
x_1 &= \phi & x_7 &= z \\
x_2 &= \dot{\phi} & x_8 &= \dot{z} \\
x_3 &= \theta & x_9 &= x \\
x_4 &= \dot{\theta} & x_{10} &= \dot{x} \\
x_5 &= \psi & x_{11} &= y \\
x_6 &= \dot{\psi} & x_{12} &= \dot{y}
\end{aligned} \tag{4.2}$$

### The Input Vector

The input vector of our system has four components and is defines as follows,

$$U = \begin{bmatrix} U_1 & U_2 & U_3 & U_4 \end{bmatrix} \tag{4.3}$$

where

$$U_1 = K_{tb}(\Omega_1^2 + \Omega_2^2 + \Omega_3^2 + \Omega_4^2) + K_{tm}(\Omega_5^2) \tag{4.4}$$

$$U_2 = K_{tb}(-\Omega_2^2 + \Omega_4^2) \tag{4.5}$$

$$U_2 = K_{tb}(\Omega_1^2 - \Omega_3^2) \tag{4.6}$$

$$U_1 = K_{Qb}(\Omega_1^2 + \Omega_2^2 + \Omega_3^2 + \Omega_4^2) - K_{Qm}(\Omega_5^2) \tag{4.7}$$

Using Equations 4.4 through 4.7 we can mix controller/actuator matrix as,

$$\begin{bmatrix} U_1 \\ U_2 \\ U_3 \\ U_4 \end{bmatrix} = \begin{bmatrix} K_{tb} & K_{tb} & K_{tb} & K_{tb} & K_{tm} \\ 0 & -K_{tb} & 0 & K_{tb} & 0 \\ K_{tb} & 0 & -K_{tb} & 0 & 0 \\ K_{Qb} & K_{Qb} & K_{Qb} & K_{Qb} & -K_{Qm} \end{bmatrix} \begin{bmatrix} \Omega_1^2 \\ \Omega_2^2 \\ \Omega_3^2 \\ \Omega_4^2 \\ \Omega_5^2 \end{bmatrix} \tag{4.8}$$

where  $K_{tb}$ ,  $K_{tm}$ ,  $K_{Qb}$  and  $K_{Qm}$  as shown in Equations 2.9 through 2.12 and are defined as follows:

$$\begin{cases} K_{tb} = C_{tb}\rho A_b R_{brad}^2 \\ K_{tm} = C_{tm}\rho A_m R_{mrad}^2 \\ K_{Qb} = C_{Qb}\rho A_b R_{brad}^3 \\ K_{Qm} = C_{Qm}\rho A_m R_{mrad}^3 \end{cases} \quad (4.9)$$

The only variable parameter in these equations is air density and since the range of altitude is limited in the case of X5, the air density have been chosen as of constant value (see Table 4.1) and the mix controller/actuator matrix can be obtained numerically as shown in Equation 4.10.

Table 4.1: Parameters of Both Small and Large Propellers [32]

Name	Parameter	Value	Unit
Thrust coefficient of small propeller	$C_{tb}$	0.0302	$Ns^2$
Drag coefficient of small propeller	$C_{Qb}$	$3.62e - 4$	$Nms^2$
Thrust coefficient of large propeller	$C_{tm}$	0.0230	$Ns^2$
Drag coefficient of large propeller	$C_{Qm}$	$3.36e - 4$	$Nms^2$
Air density	$\rho$	1.2922	$kg.m^{-3}$
Radius of small propeller	$R_{brad}$	0.1143	m
Radius of large propeller	$R_{mrad}$	0.2286	m
Disk area for small propeller	$A_b$	0.04104	$m^2$
Disk area for large propeller	$A_m$	0.16417	$m^2$

$$\begin{bmatrix} U_1 \\ U_2 \\ U_3 \\ U_4 \end{bmatrix} = \begin{bmatrix} 2.09e - 5 & 2.09e - 5 & 2.09e - 5 & 2.09e - 5 & 0.255e - 3 \\ 0 & -2.09e - 5 & 0 & 2.09e - 5 & 0 \\ 2.09e - 5 & 0 & -2.09e - 5 & 0 & 0 \\ 2.87e - 8 & 2.87e - 8 & 2.87e - 8 & 2.87e - 8 & -1.065e - 7 \end{bmatrix} \begin{bmatrix} \Omega_1^2 \\ \Omega_2^2 \\ \Omega_3^2 \\ \Omega_4^2 \\ \Omega_5^2 \end{bmatrix} \quad (4.10)$$

The control input  $U_1$  obtain all the force we need to move upward and is responsible

for altitude and its rate of change  $(x_7, x_8)$ .  $U_2$  is responsible for roll and its rate of change  $(x_1, x_2)$  by getting the thrust difference between second and forth rotors while  $U_3$  gets the thrust difference of first and third rotor and is responsible for pitch and its rate of change  $(x_3, x_4)$ . The last control input  $U_4$  which is responsible for yaw and its rate  $(x_5, x_6)$  obtained by the torque difference between four boom rotors rotating counterclockwise and the main rotor rotating clockwise.

The control input  $U_1$  generate the desired altitude while  $U_2$  generate desired roll angle,  $U_3$  generate desired pitch angle and  $U_4$  generate desired heading.

Since we have five actuators and four components as input vector, it is possible to get more than one attitude response from system for the same input signal. However, to stay in hover situation the solution becomes unique since for stationary flight beside staying in the desired altitude, we need to keep the roll, pitch and yaw angles at zero degree. For staying in the hover position, angular rate of four boom-mounted rotors should be same to avoid change in the roll and pitch angles as seen in Equations 4.17 through 4.21. This constraint is also valid for yaw angle because in the case of X5 aerial robot we can not eliminate the torque of main large rotor with only two of four boom-mounted rotors. For example, for an input signal  $U = [9.8 \ 0 \ 0 \ 0]^T$  we have unique angular rate for both boom-mounted and main rotors of X5 as follows:

$$\begin{aligned}\Omega_1 = \Omega_2 = \Omega_3 = \Omega_4 &= \sqrt{2.74e4} \\ \Omega_5 &= \sqrt{2.94e4}\end{aligned}\tag{4.11}$$

However, if we do not have any constraint in case of position and attitude of the system, means the roll, pitch and yaw angles and also the altitude of the system can freely move or rotate towards any direction, it is possible to have more than one combination between the actuators while the input signal stays the same. For instance, both combinations of rotors angular rates shown in Equations 4.12 and 4.13 can be generated by the same input signal  $U = [9.81 \ 0 \ 0 \ 0]^T$ .



$$\begin{aligned}
\Omega_1 &= \Omega_3 = \sqrt{1.74e4} \\
\Omega_2 &= \Omega_4 = \sqrt{3.74e4} \\
\Omega_5 &= \sqrt{2.94e4}
\end{aligned} \tag{4.12}$$

$$\begin{aligned}
\Omega_1 &= \Omega_3 = \sqrt{3.74e4} \\
\Omega_2 &= \Omega_4 = \sqrt{1.74e4} \\
\Omega_5 &= \sqrt{2.94e4}
\end{aligned} \tag{4.13}$$

### State-Space Model

After simplification of Equation 2.19 and using Equations 4.1 and 4.3 we can obtain:

$$\dot{X} = f(X, U) = \begin{bmatrix} \dot{\phi} \\ \frac{\dot{\theta}\dot{\psi}(I_y - I_z)}{I_x} + \frac{J_r \Omega_r \dot{\theta}}{I_x} + \frac{L}{I_x} U_2 \\ \dot{\theta} \\ \frac{\dot{\phi}\dot{\psi}(I_z - I_x)}{I_y} + \frac{J_r \Omega_r \dot{\theta}}{I_y} + \frac{L}{I_y} U_3 \\ \dot{\psi} \\ \frac{\dot{\phi}\dot{\theta}(I_x - I_y)}{I_z} + \frac{1}{I_z} U_4 \\ \dot{z} \\ g - \frac{(\cos\phi\cos\theta)}{m} U_1 \\ \dot{x} \\ -\frac{(\cos\phi\sin\theta\cos\psi + \sin\phi\sin\psi)}{m} U_1 \\ \dot{y} \\ -\frac{(\cos\phi\sin\theta\sin\psi - \sin\phi\cos\psi)}{m} U_1 \end{bmatrix} \tag{4.14}$$

### 4.3 Basic Actions

Before taking any action in designing the autopilot it is worthwhile to mention that to simplify the implementation of system dynamics of X5 we can divide the dynamics (4.14) into two subsystems, rotations and translations subsystems. Using rotational equations of motion in the body frame we can have time-independent inertia matrix and angles and their time derivations are independent from translation components; however, the translations depend on the roll, pitch and yaw angles (Figure 4.1).

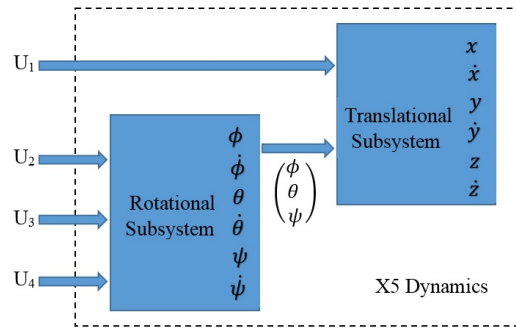


Figure 4.1: X5 Dynamics Diagram; Connection of Subsystems

Basic actions of the autopilot design includes open-loop simulation and controller design.

#### 4.3.1 Open-Loop Simulation

Using the simplified mathematical model of X5 Equation 4.14 we can implement the open-loop simulation in Simulink/Matlab as shown in the following diagram shown in Figure 4.2 in order to verify the mathematical model. The main rotor's parameters were taken from Y4 project [32] and the boom rotor's parameters were taken from a quadrotor based on OS4 hardware [11] ( $\Omega_{1-4}$  are the boom rotors and  $\Omega_5$  is the main rotor).

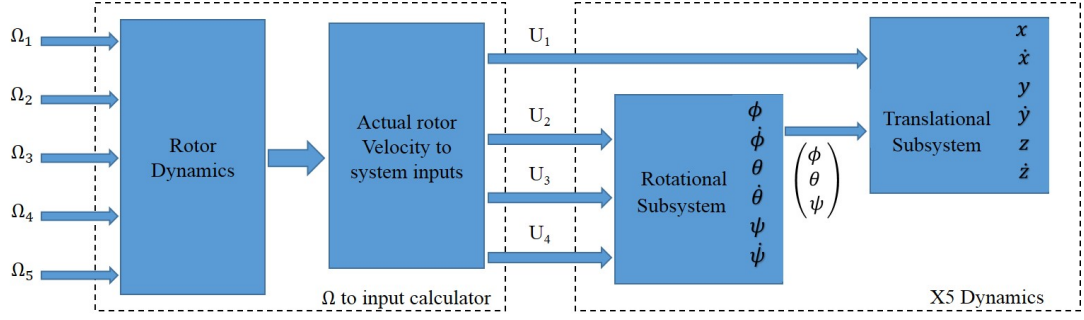


Figure 4.2: X5 Open-Loop Diagram

Calculating rotor speeds for X5 in order to stay in hover is not as simple as the other VTOLs, especially for multi-rotors. For example, the rotor speed required for quadrotors to hover can be calculated easily by Equation 4.15. The simplicity of quadrotors in hover is because of their symmetric structures, position of rotors and their rotation direction.

$$\begin{aligned} mg &= 4F_i & \text{where } i &= 1, \dots, 4 \\ mg &= 4(K_{tb}\Omega_i^2) \end{aligned} \quad (4.15)$$

Since two rotors in the quadrotors rotate clockwise and the other two rotate counterclockwise and all the rotors have the same distance from the center of mass, they provide the same force and torque if they rotate in the same speed. Thus there will no change in the heading and the only thing we need to stay at hover is to feed the angular velocities  $\Omega_1$  through  $\Omega_4$  as Equation 4.16 to keep all the states in Equation 4.1 at zero as desired.

$$\Omega_i = \sqrt{\frac{mg}{4K_{tb}}} \quad (4.16)$$

By increasing the speed of rotors above the hover value, only altitude of the quadrotors will change. We will also have the respective motion in roll, pitch and yaw angles by changing the angular velocity of the rotors; However, these changes actually are small and we can say the other state variables including roll, pitch, yaw and their derivatives will remain the same.

Unlike the quadrotors, hovering with X5 depends on 5 rotors. Four rotors have the

same symmetric structure, i.e., they have the same distance with the center of gravity. However, they all rotate in the same direction which is the opposite of the main rotor's rotating direction. The main rotor is bigger than the boom rotors, which means it can provide much bigger thrust force and lateral torque. Thus, not only we need to manage the speed of these five rotors to stay in hover position we also have to make the rotational torque equal to zero which is responsible for the heading of X5.

Assume  $\Omega_1^2 = \Omega_2^2 = \Omega_3^2 = \Omega_4^2$ , we have the following

$$mg = 4K_{tb}\Omega_1^2 + K_{tm}\Omega_5^2 \quad (4.17)$$

$$0 = 4K_{Qb}\Omega_1^2 - K_{Qm}\Omega_5^2 \quad (4.18)$$

By solving these two equations we will have

$$\Omega_1 = \Omega_2 = \Omega_3 = \Omega_4 = \sqrt{\frac{\xi}{4}K_{Qm}} \quad (4.19)$$

$$\Omega_5 = \sqrt{\xi K_{Qb}} \quad (4.20)$$

where

$$\xi = \frac{mg}{K_{Qb}K_{tm} + K_{tb}K_{Qm}} \quad (4.21)$$

" $\Omega$  to input calculator" block includes the "rotor dynamics" subsystem in order to map the desired velocity of rotors to the actual ones by using the rotors transfer function and another subsystem in which we map the actual rotor velocities to the system input as seen in Figure 4.2.

### 4.3.2 Closed-Loop Simulation

After using the open-loop simulation to verify the mathematical model of X5, we can get through the simple actions including altitude, heading and attitude controllers in close-loop simulation.

## Altitude Controller

The difference between desired altitude  $z_d$  and actual altitude of system  $z$  produces the altitude error signal  $z_e$ . The altitude controller takes the error signal  $z_e$  as an input and generates a control signal ( $U_1$ ) which is responsible for the altitude of X5 as seen in Figure 4.3.

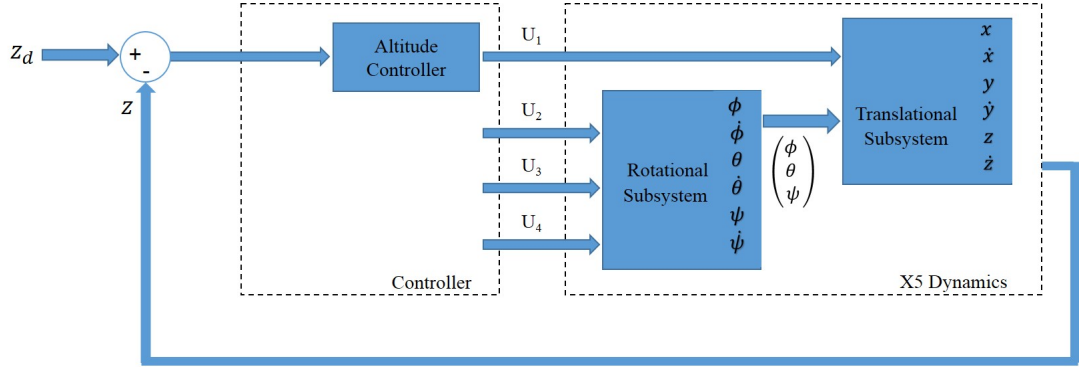


Figure 4.3: Altitude Controller Block Diagram

## Attitude and Heading Controller

The attitude controller (Figure 4.4) takes the error of roll and pitch angles by subtracting their desired value with their actual values measured by IMU and produces control signals  $U_2$  and  $U_3$  to control the attitude of system in roll and pitch angles, respectively.

The reason that we provide separate controller for heading (yaw angle) and attitude (roll and pitch angles) is behind the existence of the main rotor. Yaw controller can not be controlled similar to the case of the altitude controller. The heading controller takes the error signal of yaw angle  $e_\psi$ , which is the difference between desired angle and actual angle coming from rotational subsystem as an outer-loop controller, and a feedback from the error of ascent rate of X5 as an inner-loop controller generates a control signal ( $U_4$ ) which is responsible for heading of X5 as seen in Figure 4.4.

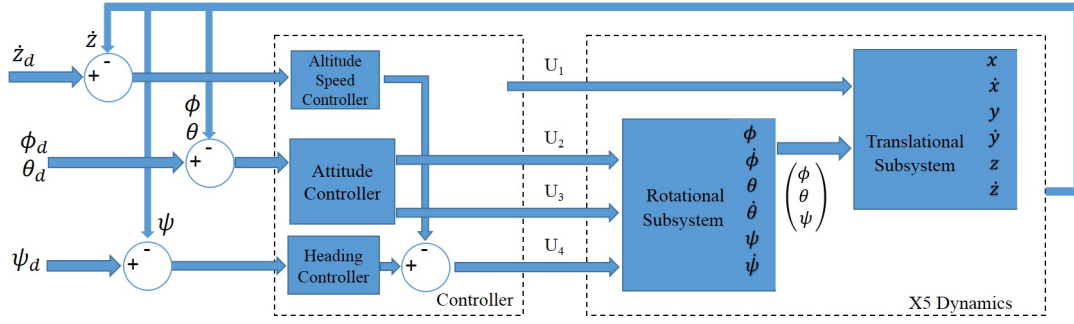


Figure 4.4: Attitude and Heading Controller Block Diagram

#### 4.4 Complex Actions: Composite Controllers

Unlike the basic actions like altitude controller, complex actions cannot be directly controlled by using one of control signals ( $U_1, \dots, U_4$ ). In this section we are going to explain hover, position and speed autopilot as composite controllers of X5.

##### Hover Controller

In designing a composite controller, say hover controller, attitude, heading and altitude controllers utilized as the basic parts of the composite controller. As we can see in Figure (4.5) the ascent rate controller is used as an inner loop to control the heading of the system while the outer loop controls the error of heading angle.

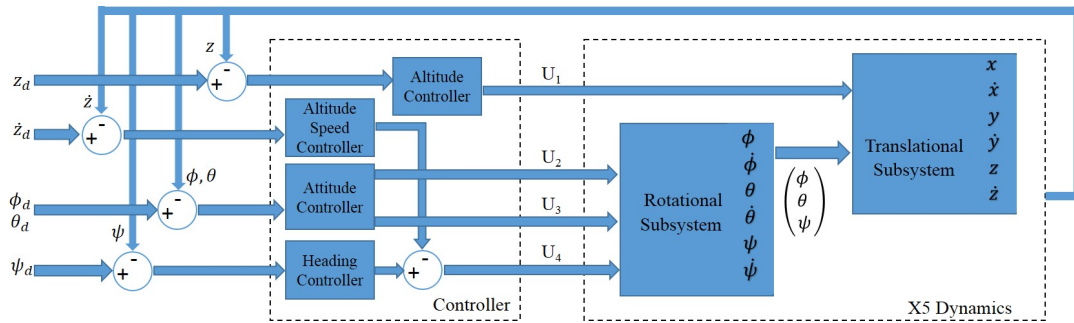


Figure 4.5: Hover Controller Block Diagram

## Position Controller

Since  $x$  and  $y$  positions can not be directly controlled using control inputs ( $U_1, \dots, U_4$ ), we should control  $x$  and  $y$  position through roll and pitch angles. Position controller takes the error of  $x$  and  $y$  position which is difference between the desired  $x$  and  $y$  and the actual  $x$  and  $y$  position of X5 from translational subsystem and produces the desired roll and pitch angles [54] . Using the following equations derived from translational subsystem we can calculate the desired value for roll and pitch angles as,

$$\ddot{x} = -\frac{U_1}{m}(\cos\phi_d \sin\theta_d \cos\psi + \sin\phi_d \sin\psi) \quad (4.22)$$

$$\ddot{y} = -\frac{U_1}{m}(\cos\phi_d \sin\theta_d \sin\psi - \sin\phi_d \cos\psi) \quad (4.23)$$

Since we operate X5 around hover (small values for roll and pitch angles), the following assumptions can be made,

$$\phi_d := \sin\phi_d$$

$$\theta_d := \sin\theta_d$$

$$\cos\phi_d = \cos\theta_d = 1$$

then we can simplify the Equations 4.22 and 4.23 to obtain,

$$\begin{bmatrix} -\sin\psi & -\cos\psi \\ \cos\psi & -\sin\psi \end{bmatrix} \begin{bmatrix} \phi_d \\ \theta_d \end{bmatrix} = \frac{m}{U_1} \begin{bmatrix} \ddot{x}_d \\ \ddot{y}_d \end{bmatrix} \quad (4.24)$$

which can be rewritten as follows, to get the desired values for roll and pitch angles.

$$\begin{aligned}
\begin{bmatrix} \phi_d \\ \theta_d \end{bmatrix} &= \frac{m}{U_1} \begin{bmatrix} -\sin\psi & -\cos\psi \\ \cos\psi & -\sin\psi \end{bmatrix}^{-1} \begin{bmatrix} \ddot{x}_d \\ \ddot{y}_d \end{bmatrix} \\
&= \frac{m}{U_1} \begin{bmatrix} -\sin\psi \ddot{x}_d + \cos\psi \ddot{y}_d \\ -\cos\psi \ddot{x}_d - \sin\psi \ddot{y}_d \end{bmatrix}
\end{aligned} \tag{4.25}$$

In order to fulfill the assumption of small values for roll and pitch angles the desired roll and pitch angles should be confined in -0.5 and 0.5 radians.

The complete controller structure of X5 aerial robot includes altitude, position and attitude controllers as shown in Figure 4.6. This structure can be used for any type of linear or nonlinear control algorithms.

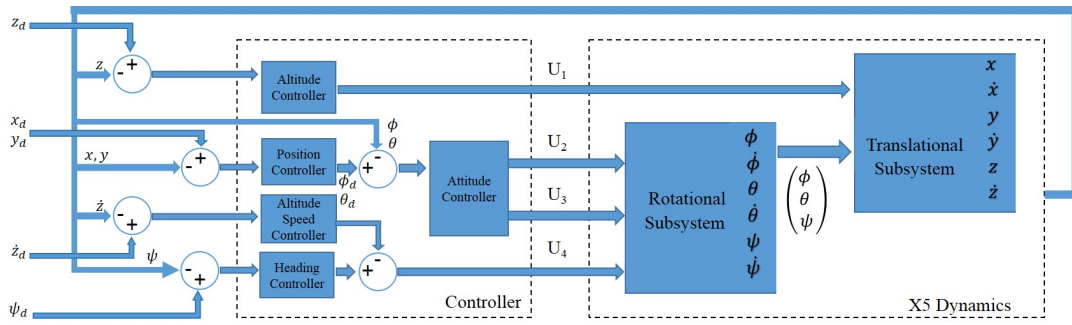


Figure 4.6: Closed-Loop Controller Block Diagram (Complete System)

## 4.5 Control Methods

As we mentioned before, the control structure shown in Figure 4.6 can contain any type of linear or nonlinear control algorithms. In this section we will present a utilization of a classic PID controller and control using Lyapunov control theory as different kinds of linear and nonlinear controllers.

It is worthwhile to mention that all the control signals produced by different types of controllers are the desired signals and they are used as inputs to the rotor dynamic. The rotor dynamics subsystem takes the desired control input signals and map them to desired rotor speeds and apply them to the rotor's transfer function which generates



the actual rotor speed. Using actual rotor speed and mapping (see Equation 4.8) we get the actual control input signals for our system.

#### 4.5.1 PID Control Technique

After verifying the mathematical model of our system and its open-loop simulation, the first control technique developed in this thesis is Proportional-Integral-Derivative (PID) control technique. The block diagram of a PID controller is shown in Figure 4.7.

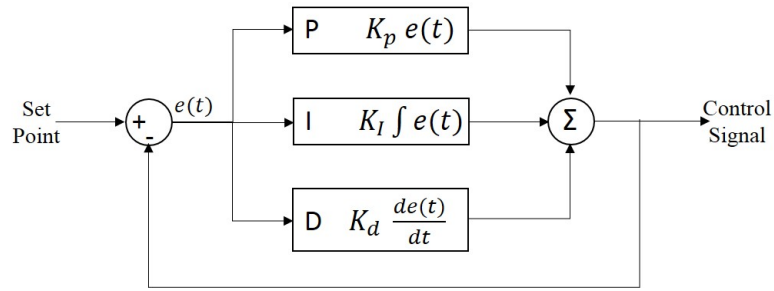


Figure 4.7: Proportional-Integral-Derivative (PID) Controller Block Diagram

#### Altitude Control

To control the altitude of X5 we only have to control the  $U_1$  signal which is responsible about the motion of the system in  $z$ -axis (up and downward) as follows.

$$U_1 = K_p(z - z_d) + K_d(\dot{z} - \dot{z}_d) + K_i \int (z - z_d) dt \quad (4.26)$$

where  $K_p$ ,  $K_i$  and  $K_d$  are the gains of PID controller and  $z_d$  and  $\dot{z}_d$  are the desired altitude and desired rate of change of altitude, respectively.

#### Attitude Control

We separated the dynamical model of X5 shown in Equation 4.14 to the angular rotations subsystem and linear translations subsystem and we are going to use the rotational subsystem in the following,

$$\begin{cases} \ddot{\phi} = \frac{I_y - I_z}{I_x} \dot{\theta} \dot{\psi} - \frac{J_r \Omega_r}{I_x} \dot{\theta} + \tau_x \\ \ddot{\theta} = \frac{I_z - I_x}{I_y} \dot{\phi} \dot{\psi} - \frac{J_r \Omega_r}{I_y} \dot{\phi} + \frac{1}{I_y} \tau_y \\ \ddot{\psi} = \frac{I_x - I_y}{I_z} + \frac{1}{I_z} \tau_z \end{cases}$$

In the equation above, there exists two gyroscopic effect in each rolling, pitching and yawing moments as mentioned in explanations associated with Equations (2.16, 2.17, 2.18). These gyroscopic effects are negligible in our system when compare with the main motors actions, especially if the system is operated in near hover situations. In these cases, these gyroscopic effects are neglected in order to make the design of multiple PID controllers possible [55]. The resultant model is simplified to the following:

$$\begin{cases} \ddot{\phi} = \frac{L}{I_x} U_2 \\ \ddot{\theta} = \frac{L}{I_y} U_3 \\ \ddot{\psi} = \frac{1}{I_z} U_4 \end{cases} \quad (4.27)$$

When the rotor's linearized dynamics are included in the model as observed in Equation 2.24, the Equation 4.27 takes the following form in the Laplace domain.

$$\begin{cases} \phi(s) = \frac{B^2 L}{s^2 (s+A)^2 I_x} U_2 \\ \theta(s) = \frac{B^2 L}{s^2 (s+A)^2 I_y} U_3 \\ \psi(s) = \frac{B^2}{s^2 (s+A)^2 I_z} U_4 \end{cases} \quad (4.28)$$

## Heading Control

The heading of X5 does not only depend on the four small rotors since the main rotor have a significant role in both overall thrust force and yawing moment. Four small boom rotors provide sufficient moment in the opposite direction of main rotor's moment to keep the heading in desired angle. Since these four small rotors have fixed position in the upward direction, they also generate thrust force added to the thrust force of the main rotor. The input signal  $U_4$  which is responsible for heading of the system has been calculated as:

$$U_4 = K_p(\psi_d - \psi) + K_d(\dot{\psi}_d - \dot{\psi}) + K_i \int (\psi_d - \psi) dt \quad (4.29)$$

## Position Control

The position controller was obtained after developing stable controllers for both altitude and attitude of system. In order to control the position of X5 we have to calculate  $\ddot{x}_d$  and  $\ddot{y}_d$  which are the desired accelerations for  $x$  and  $y$  positions, respectively as:

$$\begin{cases} \ddot{x}_d = K_p(x_d - x) + K_d(\dot{x}_d - \dot{x}) + K_i \int (x_d - x) dt \\ \ddot{y}_d = K_p(y_d - y) + K_d(\dot{y}_d - \dot{y}) + K_i \int (y_d - y) dt \end{cases} \quad (4.30)$$

After calculating these accelerations and substituting them into Equation 4.25 we will get the desired values for roll and pitch angles. Then these desired angles can be used as an input for the attitude controller as given below:

$$U_2 = K_p(\phi_d - \phi) + K_d(\dot{\phi}_d - \dot{\phi}) + K_i \int (\phi_d - \phi) dt \quad (4.31)$$

$$U_3 = K_p(\theta_d - \theta) + K_d(\dot{\theta}_d - \dot{\theta}) + K_i \int (\theta_d - \theta) dt \quad (4.32)$$

The simulation results will be presented and discussed in Chapter 5.

### 4.5.2 PD Controller Synthesis

A Proportional-Derivative (PD) controller is used as observed in Figure (4.8) for each orientation angle.

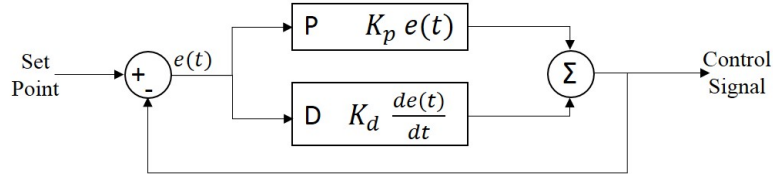


Figure 4.8: Proportional-Derivative (PD) Controller Block Diagram

The input signals for the PD controller introduced are:

$$\begin{cases} U_2 = K_{p2(\phi, \theta, \psi)}(\phi, \theta, \psi) + K_{d2(\phi, \theta, \psi)}(\phi, \theta, \psi) \\ U_3 = K_{p3(\phi, \theta, \psi)}(\phi, \theta, \psi) + K_{d3(\phi, \theta, \psi)}(\phi, \theta, \psi) \\ U_4 = K_{p4(\phi, \theta, \psi)}(\phi, \theta, \psi) + K_{d4(\phi, \theta, \psi)}(\phi, \theta, \psi) \end{cases} \quad (4.33)$$

The simulation results will be presented and discussed in Chapter 5.

### 4.5.3 Control Using Lyapunov Theory

Using Lyapunov control theory, we developed a controller in order to stabilize the attitude of X5 in this thesis. In this controller, the rotational and translational dynamics have been separated as subsystems like it is done in the previous algorithms. The components of restricted state  $X_\alpha$  are roll, pitch and yaw and their rate of change which are the first 6 components of the state vector  $X$  (4.1). These dynamical variables can be described as:

$$f(X_\alpha, U) = \begin{bmatrix} \dot{\phi} \\ a_1\dot{\theta}\dot{\psi} - a_2\dot{\theta} + b_1U_2 \\ \dot{\theta} \\ a_3\dot{\phi}\dot{\psi} + a_4\dot{\phi} + b_2U_3 \\ \dot{\psi} \\ a_5\dot{\phi}\dot{\theta} + b_3U_4 \end{bmatrix} = \begin{bmatrix} x_2 \\ a_1x_4x_6 - a_2x_4 + b_1U_2 \\ x_4 \\ a_3x_2x_6 + a_4x_2 + b_2U_3 \\ x_6 \\ a_5x_2x_4 + b_3U_4 \end{bmatrix} \quad (4.34)$$

where

$$\begin{aligned} a_1 &= \frac{I_y - I_z}{I_x} \\ a_2 &= \frac{J_r \Omega_r}{I_x} & b_1 &= \frac{L}{I_x} \\ a_3 &= \frac{I_z - I_x}{I_y} & b_2 &= \frac{L}{I_y} \\ a_4 &= \frac{J_r \Omega_r}{I_y} & b_3 &= \frac{1}{I_z} \\ a_5 &= \frac{I_x - I_y}{I_z} \end{aligned} \quad (4.35)$$

This controller mainly focuses on the stabilization of the roll, pitch and yaw angles in a specific desired condition which is defined in Equation (4.36).

$$X_{\alpha d} = \begin{bmatrix} x_{1d} & 0 & x_{3d} & 0 & x_{5d} & 0 \end{bmatrix}^T \quad (4.36)$$

To find a proper positive definite Lyapunov function, consider  $V(X_\alpha)$  as given Lyapunov function in Equation (4.37):

$$V(X_\alpha) = \frac{1}{2}[(x_{1d} - x_1)^2 + x_2^2 + (x_{3d} - x_3)^2 + x_4^2 + (x_{5d} - x_5)^2 + x_6^2] \quad (4.37)$$

By taking the time derivative of Lyapunov Equation (4.37), Equation (4.38) can be obtained. Please note that in this derivation we have used the property of X5 being a perfect cross VTOL. Because of this property, moment of inertia in x axis equals to the moment of inertia in y axis ( $I_x = I_y$ ) and  $\Omega_r$  does not appear.

$$\begin{aligned}\dot{V} &= (\nabla V(X_\alpha))^T f(X_\alpha, U) \\ &= e_1 x_2 + b_1 x_2 U_2 + e_3 x_4 + b_2 x_4 U_3 + e_5 x_6 + b_3 x_6 U_4\end{aligned}\tag{4.38}$$

where  $b_1, b_2$  and  $b_3$  are defined in equations A.13 and

$$e_1 = x_{1d} - x_1, \quad e_3 = x_{3d} - x_3, \quad e_5 = x_{5d} - x_5$$

By choosing the input signals as following,

$$U_2 = -e_1 \frac{1}{b_1} - k_1 x_2 \tag{4.39}$$

$$U_3 = -e_3 \frac{1}{b_2} - k_2 x_4 \tag{4.40}$$

$$U_4 = -e_5 \frac{1}{b_3} - k_3 x_6 \tag{4.41}$$

where  $k_1, k_2$  and  $k_3$  are positive constants and by substituting these input signals in Equation 4.38 we obtain:

$$\dot{V} = -(k_1 b_1 x_2^2 + k_2 b_2 x_4^2 + k_3 b_3 x_6^2) \tag{4.42}$$

which simply shows that the equation above is negative semi-definite and by Lyapunov theorem [56] [57] we can claim that the stability of the equilibrium point associated with the hover can be achieved. More detail about Lyapunov based control is presented in Appendix A.3 and the simulation results will be presented and discussed in Chapter 5.

## **CHAPTER 5**

### **SIMULATION RESULTS**

#### **5.1 Introduction**

In this chapter the mathematical model of X5 aerial robot will be used to simulate the autopilot design which includes both open-loop and closed-loop simulations in Matlab/Simulink environment. We have designed PD, PID and Lyapunov control theory based controllers and we have compared the performances of them. In order to control the system using PD/PID technique, one can linearize the system around an equilibrium (trim) point, which is hover in our case, using Simulink/Control Design/Linear Analysis Tool. Then, running the PD/PID controller on linearized model and using PID Tuner we can find controller parameters (gains of controller). Using these gains as initial parameters of controller, one can implement the controller on nonlinear system and modify/tune the parameters with respect to the response and behavior of nonlinear model manually. As another approach the nonlinear system can be linearized at a number of equilibrium points and suitable PID controllers can be designed for each of them. Next, they can be interpolated using the gain scheduling point.

#### **5.2 Open-Loop Simulations**

The open-loop simulation only includes the Mathematical model of X5 and desired RPM of the rotors in order to keep the vehicle in hover with respect to initial condi-

tion. The following Figure will show the open-loop simulation of X5 implemented in Matlab/Simulink.

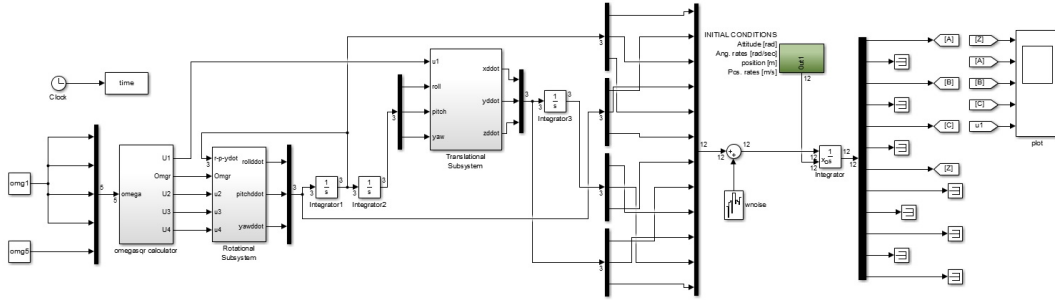


Figure 5.1: Open-Loop Simulation of X5 With Desired Inputs for System to Stay in Hover Position

The desired RPM values was calculated using Equations (4.19) through (4.21) and the simulation result for altitude of the system is shown as Figure (5.2).

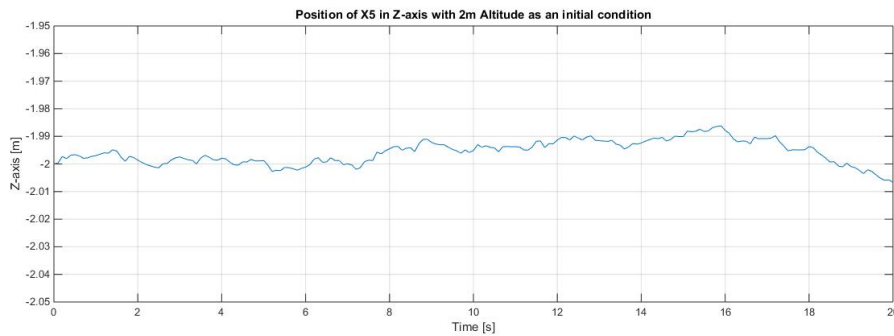


Figure 5.2: The Result of Open-Loop Simulation in z-Axis With 2m Height as an Initial Condition

### 5.3 Closed-Loop Simulations

In this section we used PD, PID and Lyapunov control theory based controllers as closed-loop controllers. The task of each control method, is to stabilize roll, pitch and yaw angles and restitution of the initial error in each angle. Reaching the desired altitude and  $x$  and  $y$  positions and following a desired trajectory is another task studied in this thesis. The overall closed-loop controller is shown in Figure (5.3).



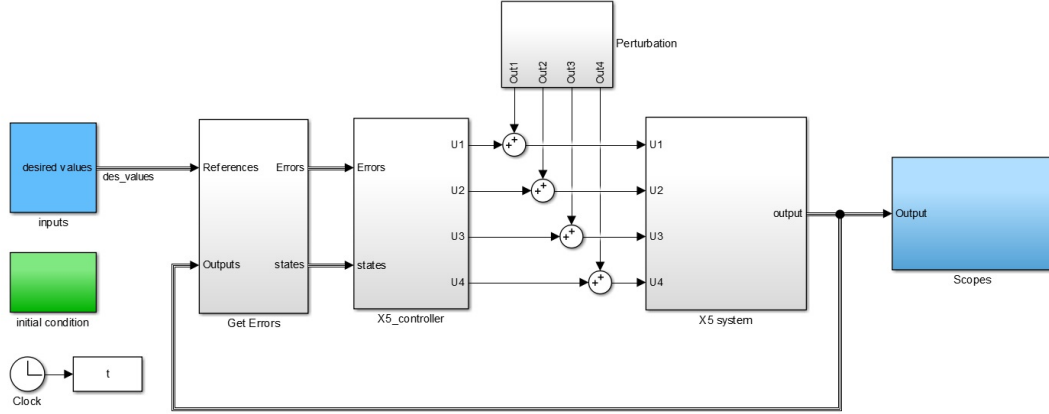


Figure 5.3: The Overall Closed-Loop Simulation of X5 in MATLAB/Simulink

### 5.3.1 PD Controller Simulations

The maximum angular velocity for boom rotors is limited as 1200 rad/sec and the main rotor has a maximum angular velocity of 600 rad/sec. This was done by placing saturation blocks between the controller and motor dynamics.

#### Altitude Control

In order to control the altitude of system using PD technique, one can linearize the system around an equilibrium point which is near hover in the case of X5. Then, running the PD controller on linearized model to obtain the gains of controller. Using these gains as initial condition of PD controller, one can modify the gains with respect to the response and behavior of nonlinear system. After running the numerical application of altitude control design as Equation 4.26, the gains of PD controller can be obtained as shown in Table 5.1. The task of altitude controller is to keep the system in the desired altitude despite the initial condition and disturbance. In the following simulation (see Figure 5.4) we can see the performance of PD controller with respect to the desired values mentioned in Table 5.1.

Table 5.1: The Results of PD Altitude Controller

	Desired Value	$K_p$	$K_d$	Settling Time	Overshoot
Altitude ( $z$ )	2m	4.5	1.5	2.6 sec	4.6%

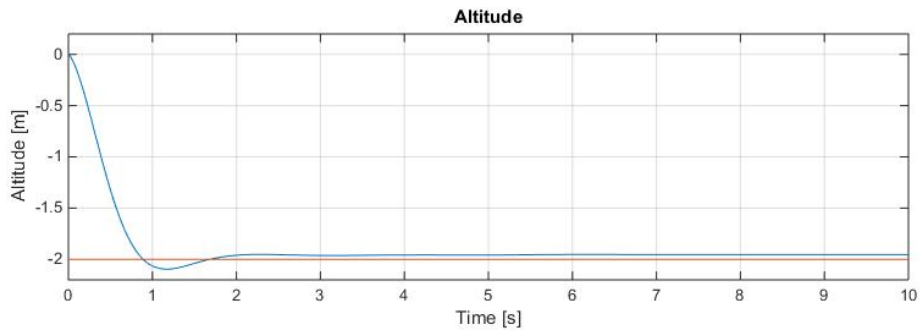


Figure 5.4: Altitude Controller Result in Desired 2m Height Using PD Controller

The simulation result in Figure (5.5) shows the result of the same PD controller with zero initial condition and 2m desired altitude; However, by adding a second order Bessel low-pass filter with 1 rad/sec pass-band edge frequency to smooth the reference we can see that the overshoot of the altitude signal vanished .

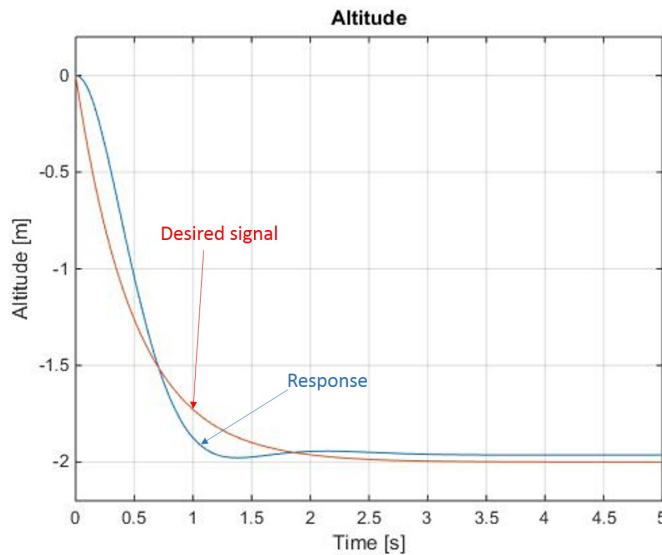


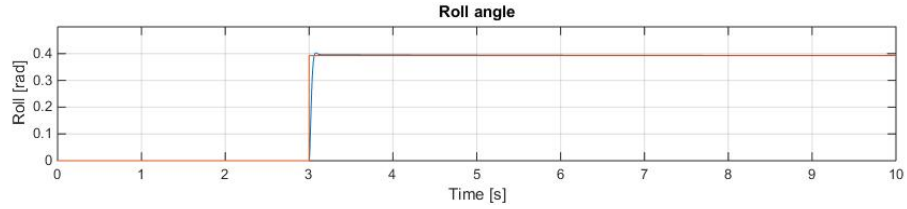
Figure 5.5: Result of Altitude Controller With Zero Initial Condition, 2m Height as Desired Altitude and Added Second Order Filter to the Desired Signal

## Attitude Control

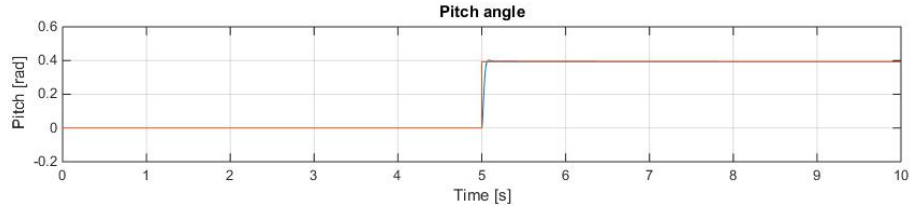
After running the numerical application of attitude control design (See Equations 4.28) on Matlab/Simulink we get the attitude controller result shown in Figure 5.6 and the gains of the controller are shown in Table 5.2.

Table 5.2: The Results of PD Attitude Controller

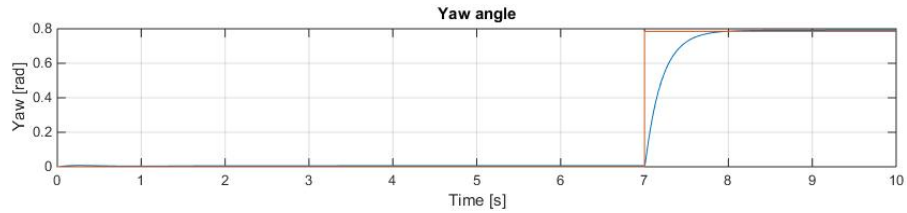
	Desired Value	$K_p$	$K_d$	Settling Time	Overshoot
Attitude ( $\phi$ )	$\pi/8$	0.1	0.2	1 sec	2.3%
Attitude ( $\theta$ )	$\pi/8$	0.1	0.2	1 sec	2.4%
Heading ( $\psi$ )	$\pi/4$	3.9	0.7	1.5 sec	1.8%



(a) Result of Roll Angle



(b) Result of Pitch Angle

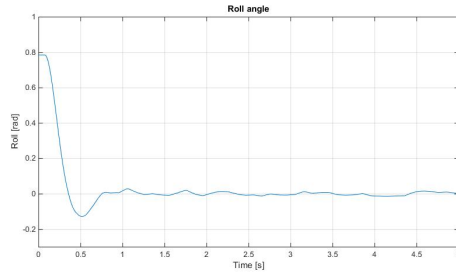


(c) Result of Yaw Angle

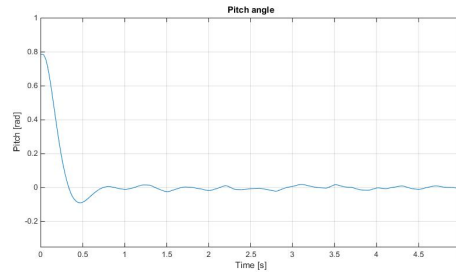
Figure 5.6: The Result of Roll, Pitch and Yaw Angles Using the PD Controller. The Desired Value For Roll and Pitch Was  $\pi/8$  in 3rd sec and 5th sec, Respectively and  $\pi/4$  in the 7th sec For the Yaw Angle

The simulation results have shown that for small disturbances in hover flight, the rate of change of the orientation angles ( $\dot{\phi}$ ,  $\dot{\theta}$  and  $\dot{\psi}$ ) are almost equal to the body angular velocities ( $p$ ,  $q$  and  $r$ ) and the transformation matrix between them can be considered

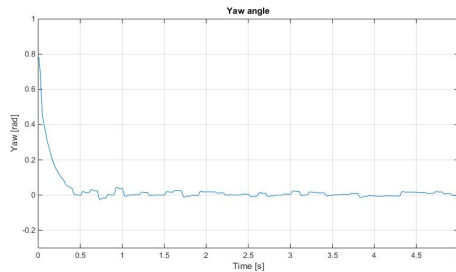
as the unit matrix. Figure 5.7 shows the performance of the PD controller with respect to the initial conditions and added disturbance.  $\pi/4$  is the initial condition of both roll and pitch angles, and  $\pi/8$  for the yaw angle. The performance of the altitude controller can be observed in Figure 5.7d with 5m height as the initial condition.



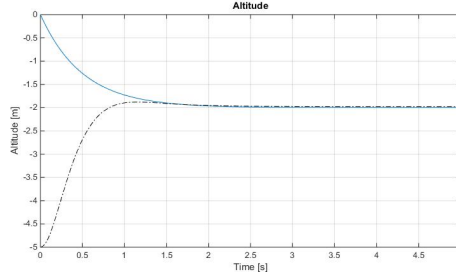
(a) PD Controller Result With the Gains ( $p = 0.8$  and  $D = 0.1$ ) For Roll Angle With  $\pi/4$  as an Initial Condition and Added Noise



(b) PD Controller Result With the Gains ( $p = 0.8$  and  $D = 0.1$ ) For Pitch Angle With  $\pi/4$  as an Initial Condition and Added Noise



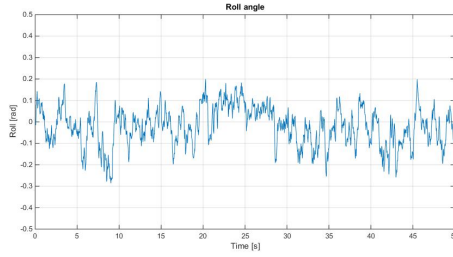
(c) PD Controller Result With the Gains ( $p = 3.9$  and  $D = 0.5$ ) For Yaw Angle With  $\pi/4$  as an Initial Condition and Added Noise



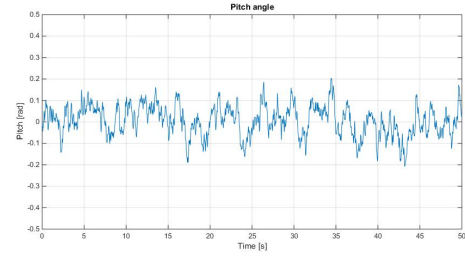
(d) PD Controller Result For Altitude With 5m as an Initial Condition, 2m as Desired Altitude and Added Noise

Figure 5.7: The Result of Roll, Pitch and Yaw Angles Using the PD Controller wrt the Initial Conditions and Disturbance

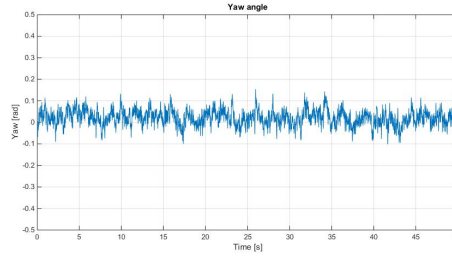
In the simulation results shown in Figure (5.8), the task was to stabilize the roll, pitch and yaw angles under the influence of the added noise. The added disturbance on each angular velocity was the normal Gaussian noise with variance of 2 rad/sec. The gains of the PD controller are  $P = 0.9$  and  $D = 0.5$  for roll and pitch angles and  $P = 3.9$  and  $D = 0.7$  for the yaw angle.



(a) Result of Roll Angle in Hover in Spite the Added Noise



(b) Result of Pitch Angle in Hover in Spite the Added Noise



(c) Result of Yaw Angle in Hover in Spite the Added Noise

Figure 5.8: The Result of Roll, Pitch and Yaw Angles Using PD Controller

## Position Control

In the case of Position control, since we can not control the  $x$  and  $y$  positions directly using input control signals, a Cascade control is used in order to reach the desired position without losing the control of attitude of the system. The block diagram of designed controller for  $y$  position is shown in Figure (5.9).

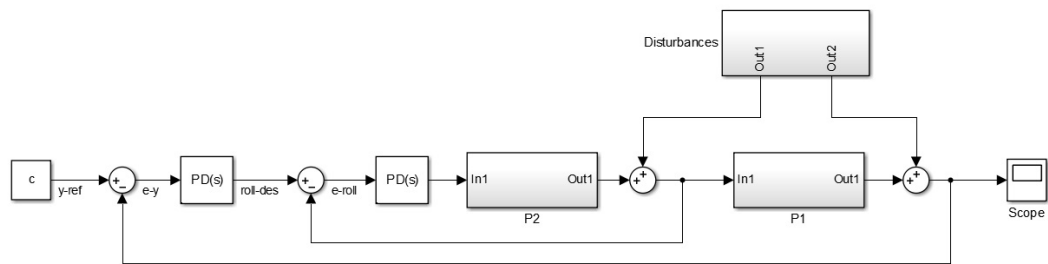


Figure 5.9: Cascade PD Controller Block Diagram for  $y$ -Axis Position Control

The block diagram of the designed controller for  $y$  position is shown in Figure (5.10).

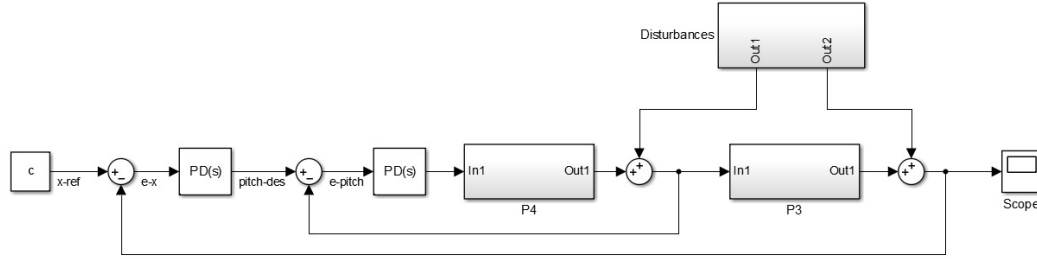


Figure 5.10: Cascade PD Controller Block Diagram For x-Axis Position Control

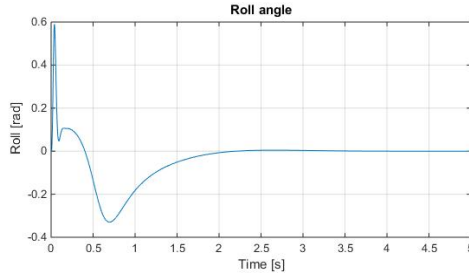
The position controller results are shown in Figure (5.11) and the gains of the controller are shown in Table (5.3).

Table 5.3: The Results of PD Position Controller

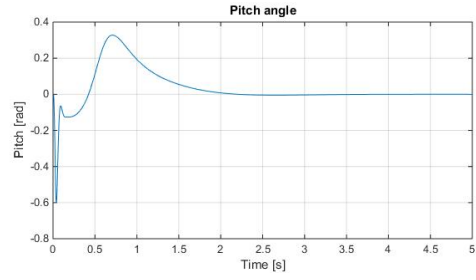
	Desired Value	$K_p$	$K_d$	Settling Time	Overshoot
Altitude (z)	2 m	4.5	1.5	3 sec	4.9%
Attitude ( $\phi$ )	0°	3.7	0.6	2.6 sec	-
Attitude ( $\theta$ )	0°	3.7	0.6	2.6 sec	-
Heading ( $\psi$ )	0°	3.9	0.8	2.8 sec	-
Position (x)	1 m	6.3	3.9	3.1 sec	3.3%
Position (y)	1 m	6.3	3.9	3.2 sec	3.7%

Table 5.4: The Results of PD Trajectory Control

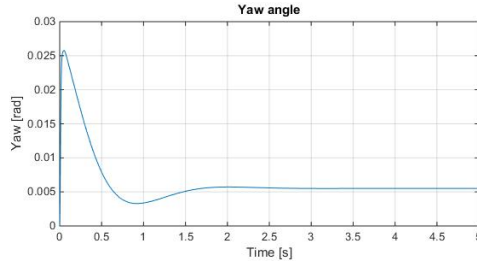
	Desired Value	$K_p$	$K_d$	Settling Time	Overshoot
Altitude (z)	Trajectory	4.5	1.5	2.5 sec	1%
Attitude ( $\phi$ )	0°	0.7	0.5	-	-
Attitude ( $\theta$ )	0°	0.7	0.5	-	-
Heading ( $\psi$ )	0°	3.9	0.8	-	-
Position (x)	Trajectory	3.5	1.8	6 sec	3.36%
Position (y)	Trajectory	3.5	1.8	6 sec	3.34%



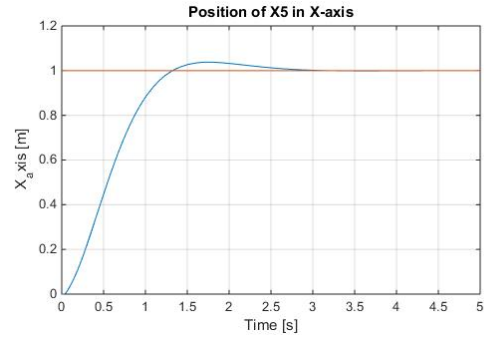
(a) Result of Roll Angle



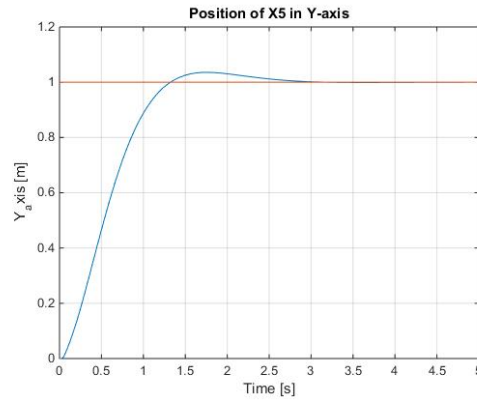
(b) Result of Pitch Angle



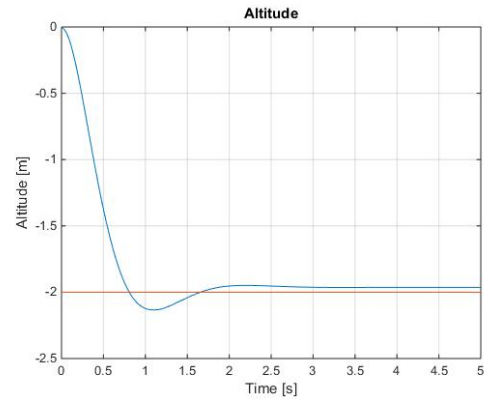
(c) Result of Yaw Angle



(d) Position in x-Axis



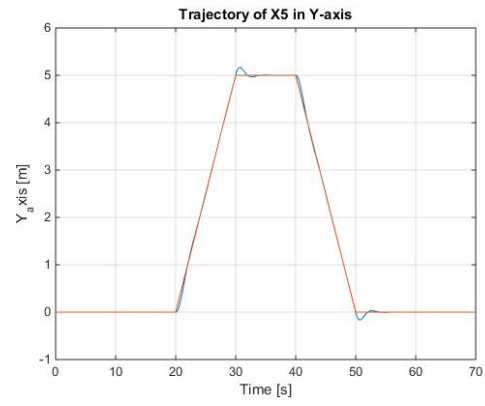
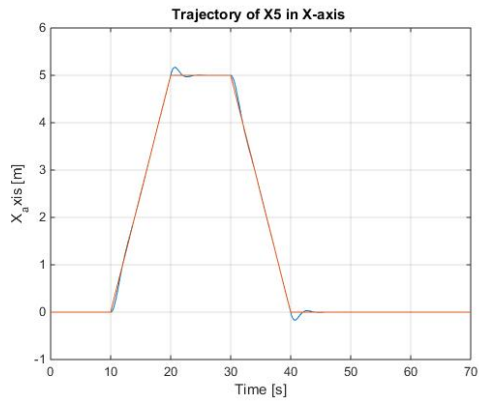
(e) Position in y-Axis



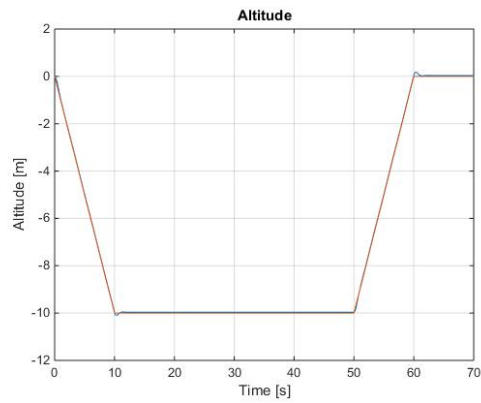
(f) Position in z-Axis

Figure 5.11: The Result of Roll, Pitch, Yaw Angles and x, y, z Position Using PD Controller

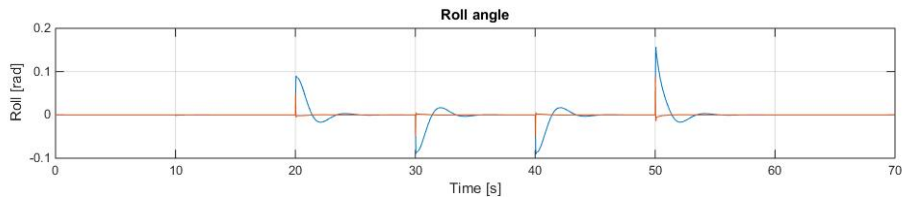
By changing the desired values into two different trajectories we can validate our autopilot and we can see how the designed controller follows the trajectories. In order to increase the accuracy of our controller, the gains of the controller have been modified as seen in Table (5.4). We can see the response of the autopilot to the desired trajectory in Figures (5.12, 5.13). Figures (5.14, 5.15) also show 3D-plot of two different trajectories under the PD controller.



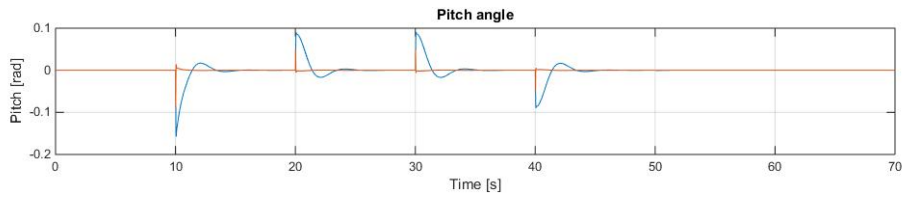
(a) Response of PD Controller to Trajectory in X- Axis (b) Response of PD Controller to Trajectory in Y- Axis



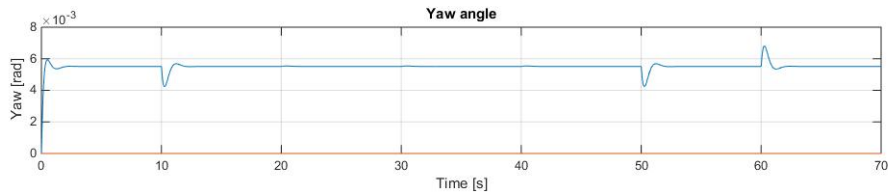
(c) Response of PD Controller to Trajectory in Z- Axis



(d) Roll Angle Response to the Trajectory



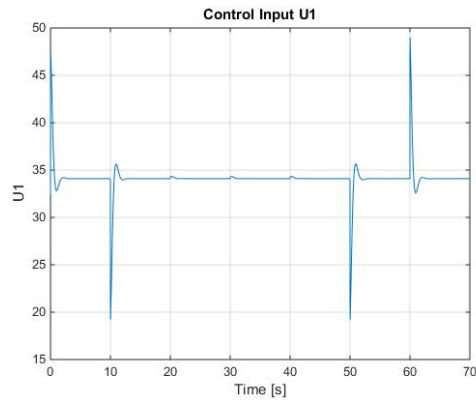
(e) Pitch Angle Response to the Trajectory



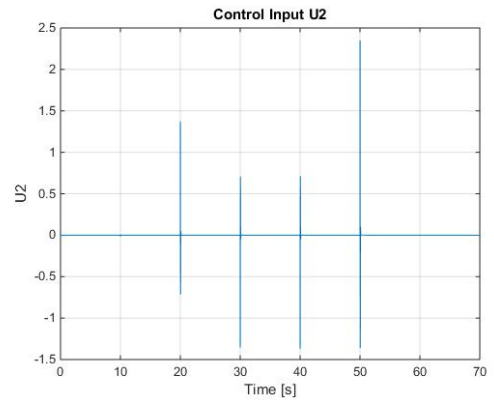
(f) Yaw Angle Response to the Trajectory

Figure 5.12: The Autopilot Response to 1st Trajectory Using PD Controller

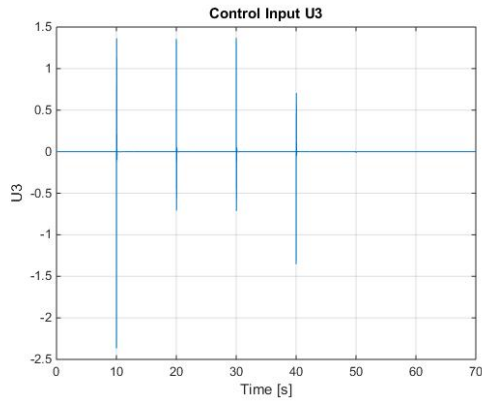




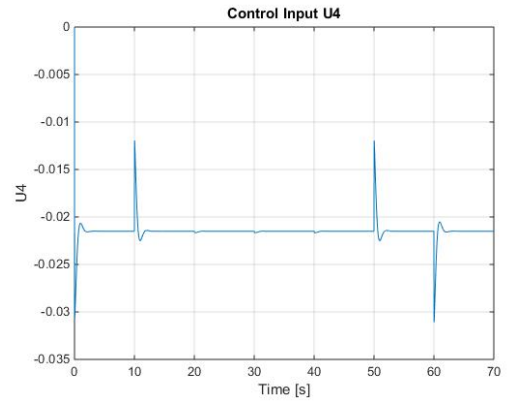
(a) Control Input  $U_1$



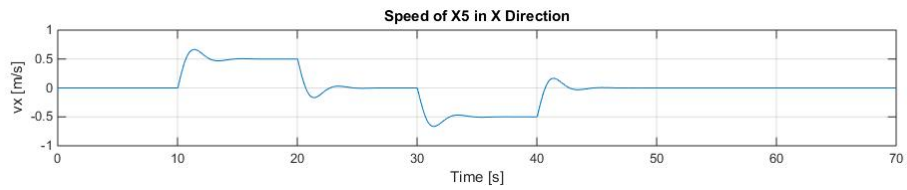
(b) Control Input  $U_2$



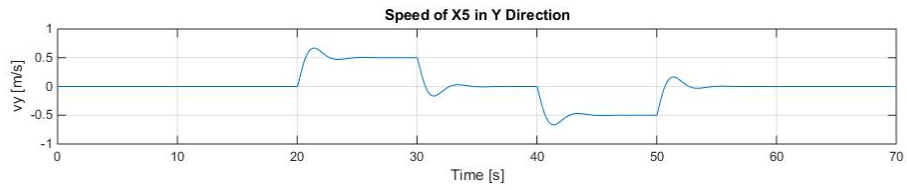
(c) Control Input  $U_3$



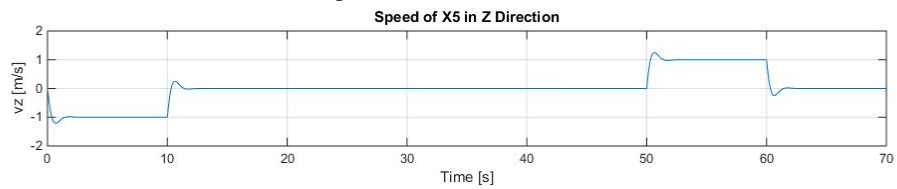
(d) Control Input  $U_4$



(e) Speed of X5 in X Direction



(f) Speed of X5 in Y Direction



(g) Speed of X5 in Z Direction

Figure 5.13: The Autopilot Response to 1st Trajectory Using PD Controller

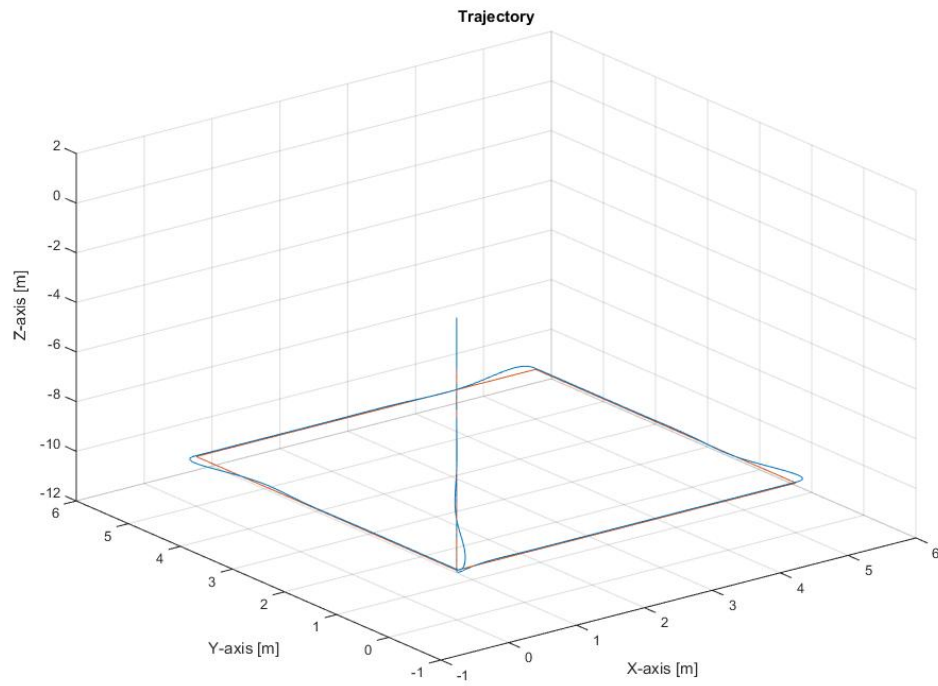


Figure 5.14: 1st Trajectory Response Under PD Controller

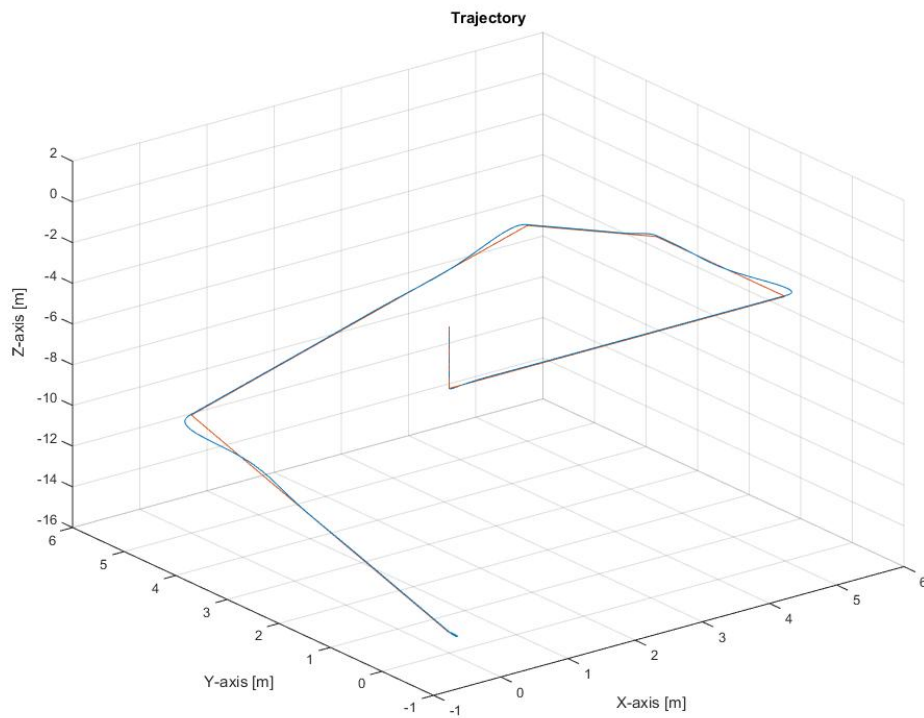


Figure 5.15: 2nd Trajectory Response Under PD Controller

### 5.3.2 PID Controller Simulations

We repeated all steps of simulation to get the autopilot results using the PID controller.

#### Altitude Control

Table 5.5 shows the gains of PID controller used to control the altitude of X5 in 2m of desired height and Figure 5.16 shows the results of the altitude controller with respect to the desired height.

Table 5.5: The Results of PID Altitude Controller

	Desired Value	$K_p$	$K_I$	$K_d$	Settling Time	Overshoot
Altitude ( $z$ )	2m	4.5	0.2	2	2.4 sec	1.55%

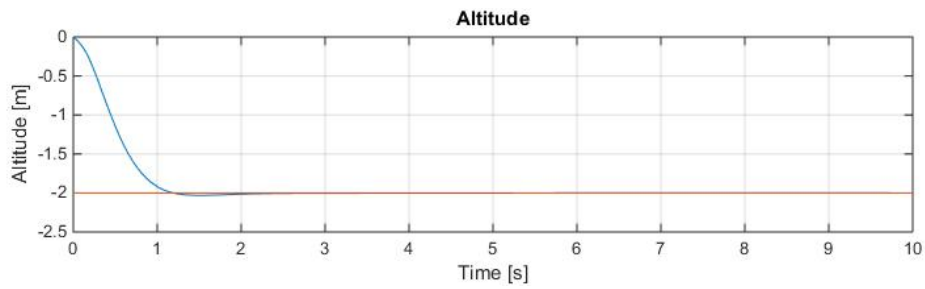


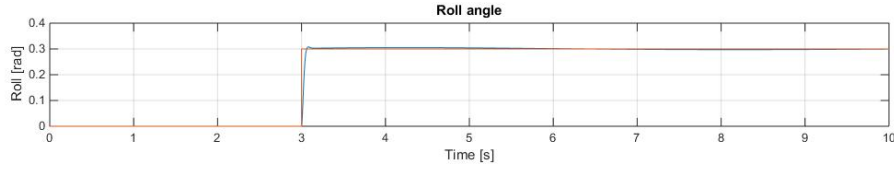
Figure 5.16: Altitude Controller Result in Desired 2m Height Using PID Controller

#### Attitude Control

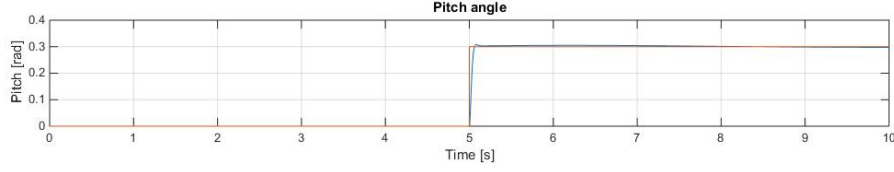
The attitude controller results are shown in Figure (5.17) and the gains of the controller are shown in Table (5.6).

Table 5.6: The Results of PID Attitude Controller

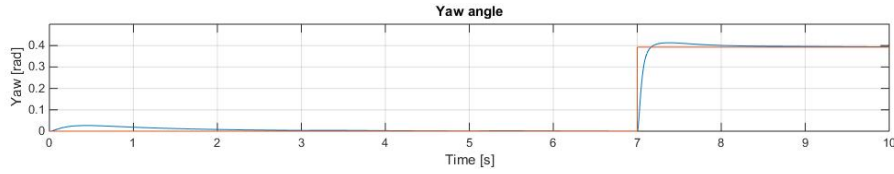
	Desired Value	$K_p$	$K_I$	$K_d$	Settling Time	Overshoot
Attitude ( $\phi$ )	$\pi/8$	0.1	0.2	0.3	0.5 sec	2.5%
Attitude ( $\theta$ )	$\pi/8$	0.1	0.2	0.3	0.5 sec	2.5%
Heading ( $\psi$ )	$\pi/4$	0.7	0.5	0.12	1.1 sec	4.8%



(a) Result of Roll Angle



(b) Result of Pitch Angle



(c) Result of Yaw Angle

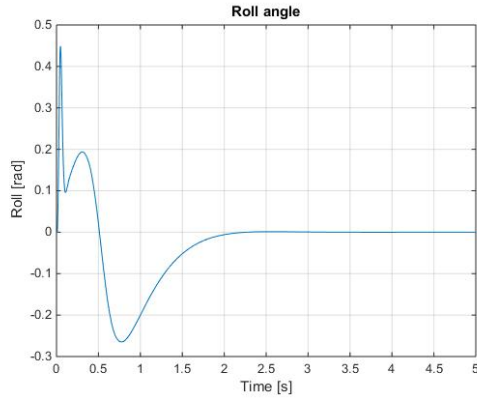
Figure 5.17: The Result of Roll, Pitch and Yaw Angles Using the PID Controller. The Desired Value For Roll and Pitch Was  $\pi/8$  in the 3rd sec and 5th sec, Respectively and  $\pi/4$  in the 7th sec For the Yaw Angle

## Position Control

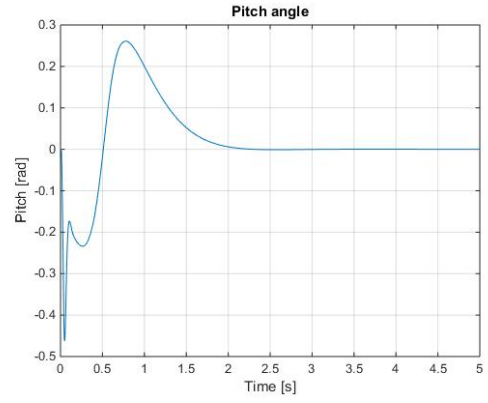
The position control results using the PID controller are shown in Figure (5.18) and the gains of the controller are shown in Table (5.7).

Table 5.7: The Results of Position Control Using PID Controller

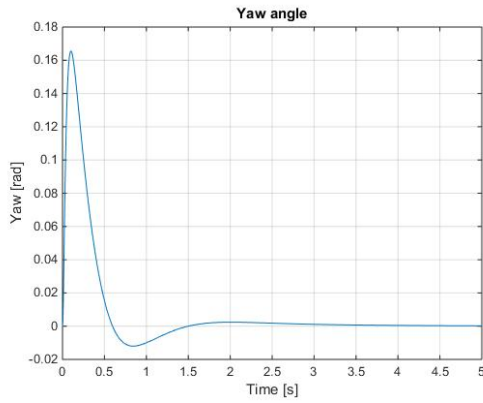
	Desired Value	$K_p$	$K_I$	$K_d$	Settling Time	Overshoot
Altitude (z)	2 m	4.5	0.2	2	2.5 sec	1.5%
Attitude ( $\phi$ )	0°	1	0.5	0.8	2.4 sec	-
Attitude ( $\theta$ )	0°	1	0.5	0.8	2.6 sec	-
Heading ( $\psi$ )	0°	0.7	0.5	0.12	3.1 sec	-
Position (x)	1 m	1.5	0.1	1	2.8 sec	0%
Position (y)	1 m	1.5	0.1	1	2.8 sec	0%



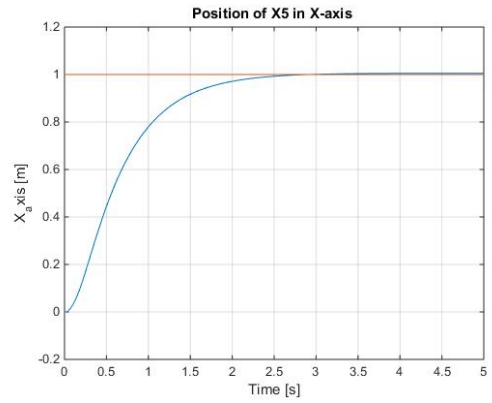
(a) Result of Roll Angle



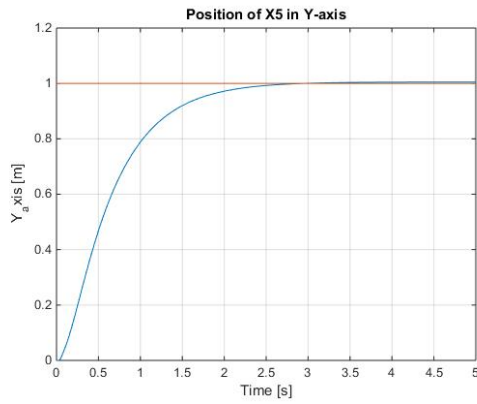
(b) Result of Pitch Angle



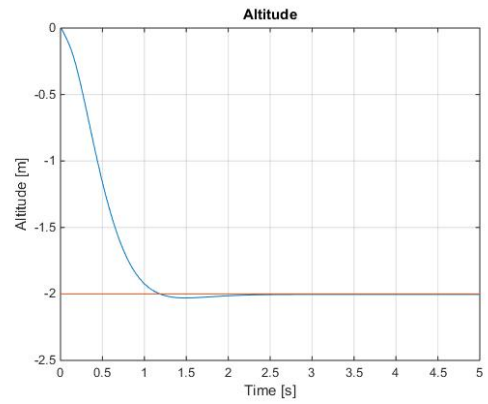
(c) Result of Yaw Angle



(d) Positon in x-axis



(e) Positon in y-Axis



(f) Positon in z-Axis

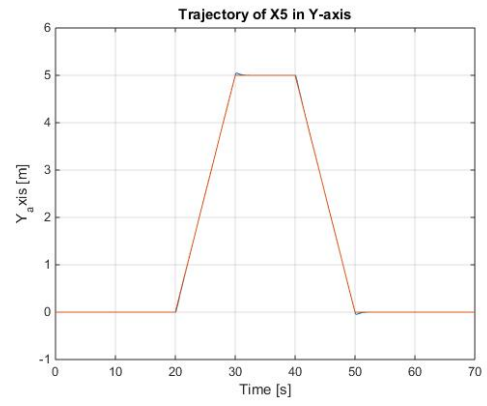
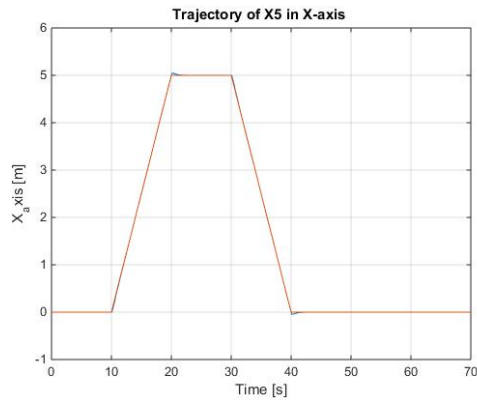
Figure 5.18: The Result of Roll, Pitch, Yaw Angles and x, y, z Position Using PID Controller

By changing the desired values into two different trajectories we can validate our autopilot and we can see how the designed controller follows the trajectories. In order to increase the accuracy of our controller, the gains of the controller have been modified as seen in Table 5.8. The performance of the autopilot for the given trajectory can be

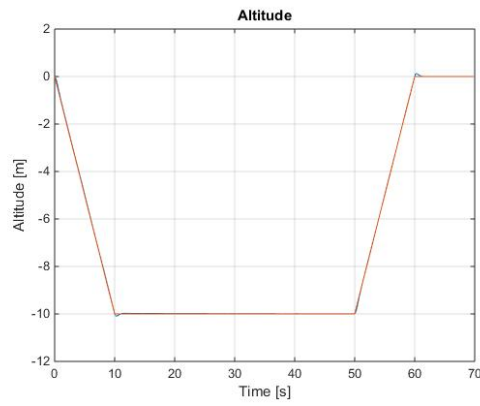
observed in Figures 5.19 and 5.20. Figures 5.21 and 5.22 also show 3D-plot of two different trajectories under the PID controller.

Table 5.8: The Results of PID Trajectory Control

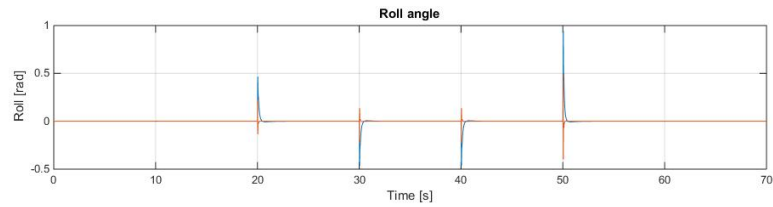
	Desired Value	$K_p$	$K_I$	$K_d$	Settling Time	Overshoot
Altitude (z)	Trajectory	4.5	0.4	1.5	2.5 sec	1%
Attitude ( $\phi$ )	0°	1.1	0.6	0.5	-	-
Attitude ( $\theta$ )	0°	1.1	0.6	0.5	-	-
Heading ( $\psi$ )	0°	0.8	0.55	0.15	-	-
Position (x)	Trajectory	1.7	0.1	1.2	6 sec	3%
Position (y)	Trajectory	1.7	0.1	1.2	6 sec	3%



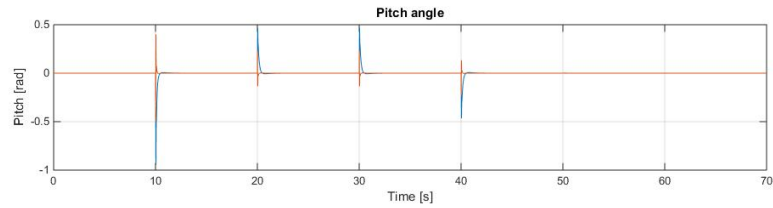
(a) Response of PID Controller to Trajectory in X- Axis (b) Response of PID Controller to Trajectory in Y- Axis



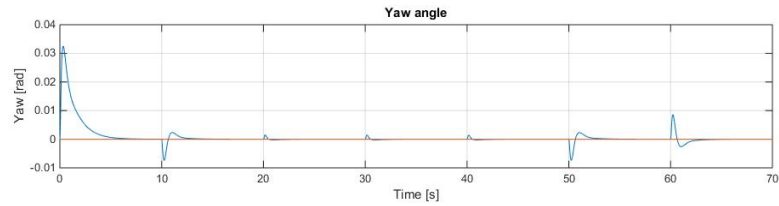
(c) Response of PID Controller to Trajectory in Z- Axis



(d) Roll Angle Response to the Trajectory

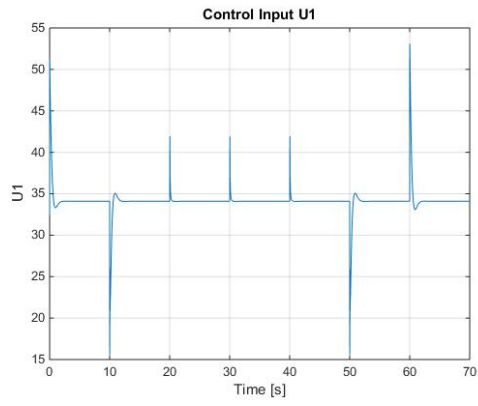


(e) Pitch Angle Response to the Trajectory

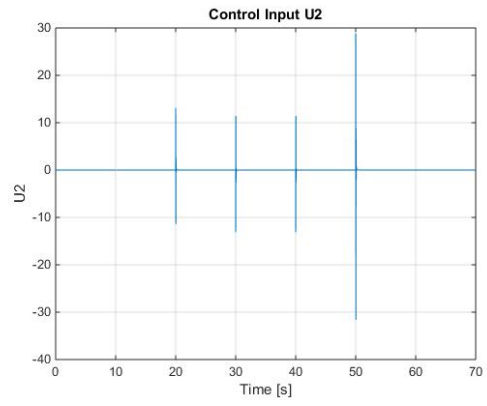


(f) Yaw Angle Response to the Trajectory

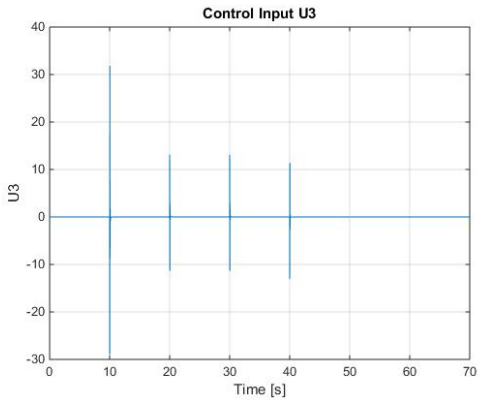
Figure 5.19: The Autopilot Response to 1st Trajectory Using PID Controller



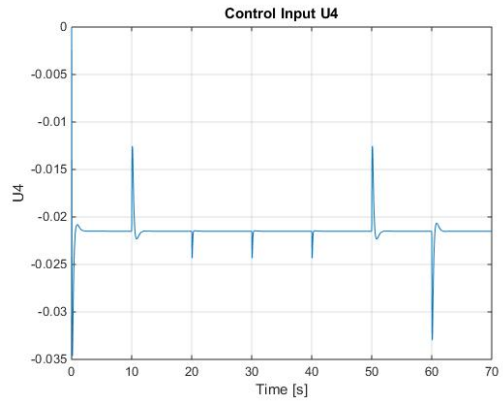
(a) Control Input  $U_1$



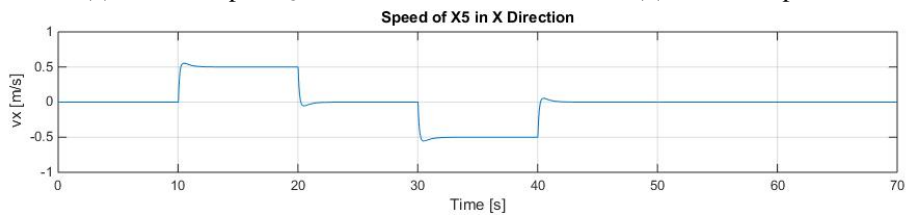
(b) Control Input  $U_2$



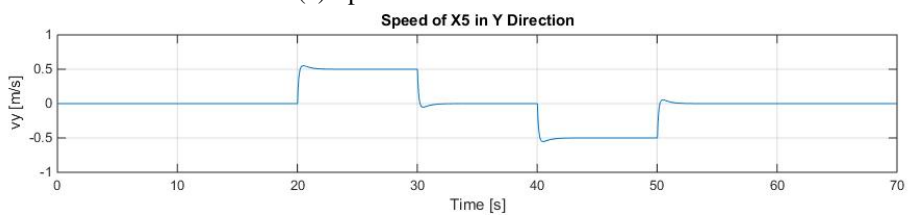
(c) Control Input  $U_3$



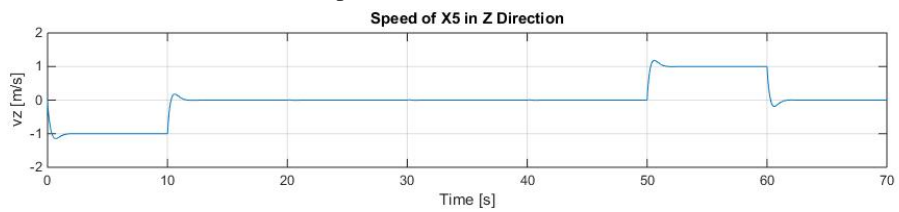
(d) Control Input  $U_4$



(e) Speed of X5 in X Direction



(f) Speed of X5 in Y Direction



(g) Speed of X5 in Z Direction

Figure 5.20: The Autopilot Response to 1st Trajectory Using PID Controller



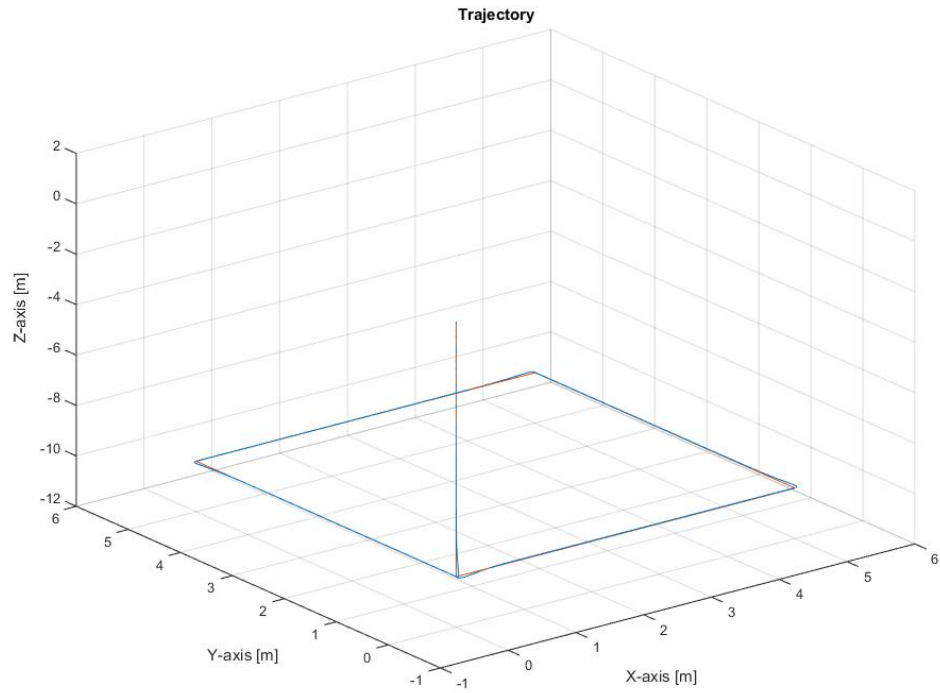


Figure 5.21: 1st Trajectory Response Under PID Controller

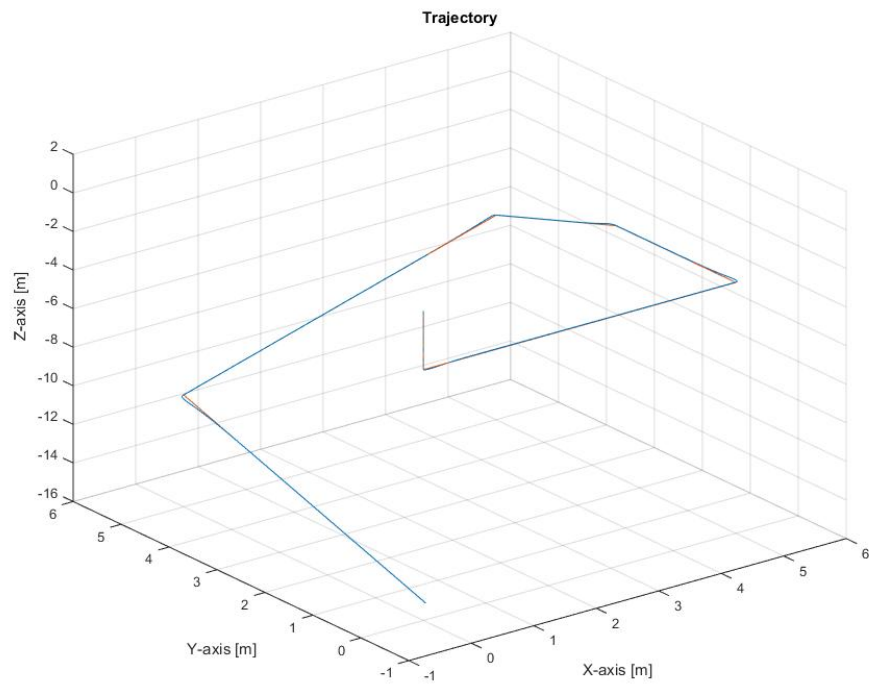


Figure 5.22: 2nd Trajectory Response Under PID Controller

### 5.3.3 Attitude Control Using Lyapunov Theory

The input signals  $U_2$  through  $U_4$  which are responsible for attitude of the system can be controlled using Lyapunov theory as shown in Equations 4.39, 4.40 and 4.41.

The task is to hold attitude angles close to zero (stabilize them) in hover flight under the influence of external disturbances (normal Gaussian noise with 2 rad/sec variance on each angular velocity added to the plant input as shown in Figure 5.3) and also initial errors of attitude angles (roll, pitch and yaw) should be compensate by this controller. After reaching to the desired altitude under PID controller shown in Figure 5.23, the attitude controller which is responsible for hover, tracks the input signals and stabilize the roll, pitch and yaw angles. Table 5.9 shows gains of the controller ( $k_1$ ,  $k_2$  and  $k_3$ ) used to control Lyapunov function and Figure 5.24 show the results of attitude controller for hover flight without noise.

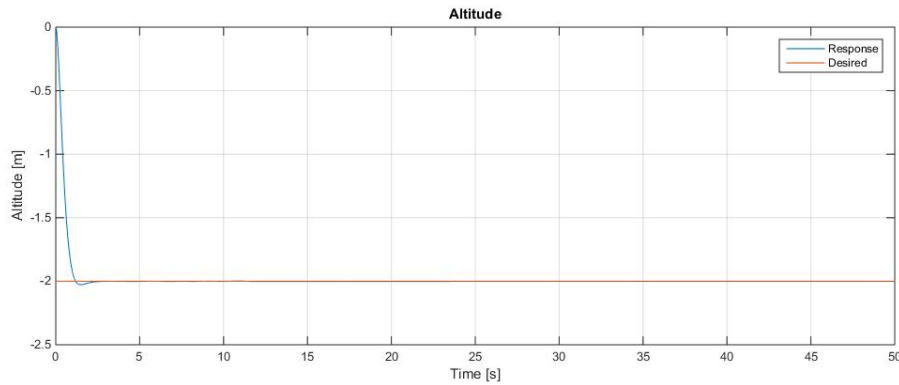
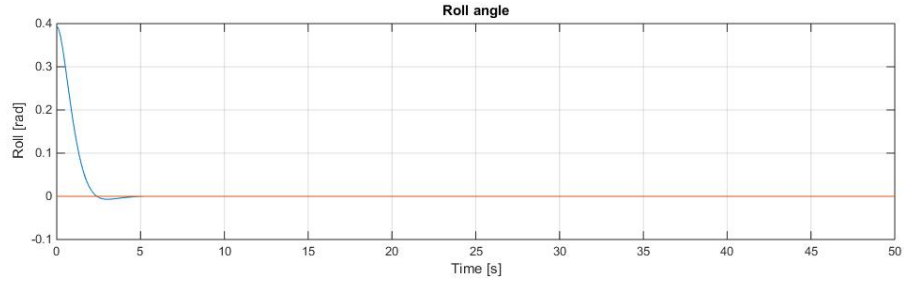


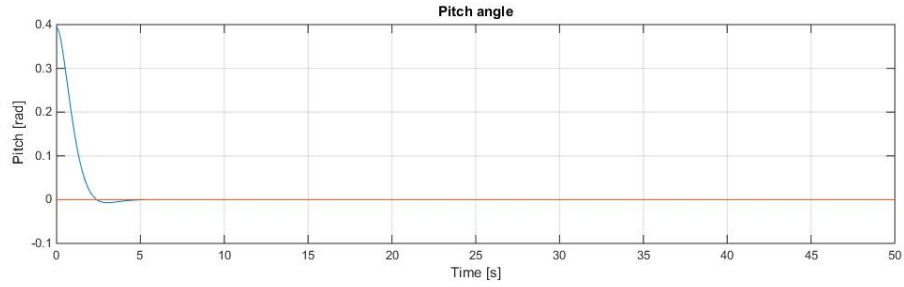
Figure 5.23: Result of Altitude of X5 Under PID Controller for 2m Desired height

Table 5.9: Gains of Control Lyapunov Function

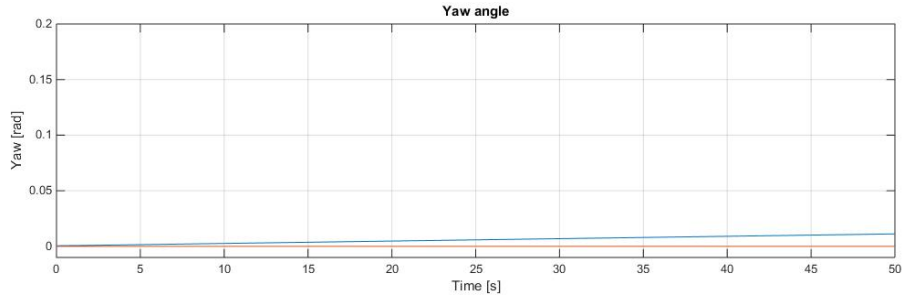
	Desired Value	Gain	Settling Time	Overshoot
Altitude ( $z$ )	2 m	PID	2.5 sec	1%
Attitude ( $\phi$ )	$0^\circ$	$K_1 = 0.02$	5 sec	1.75%
Attitude ( $\theta$ )	$0^\circ$	$K_2 = 0.02$	5 sec	1.75%
Heading ( $\psi$ )	$0^\circ$	$K_3 = 3$	-	-



(a) Result of Roll Angle for  $\pi/8$  as an initial condition



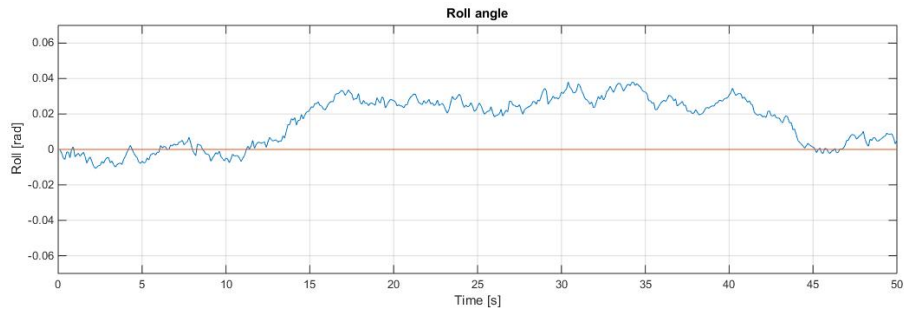
(b) Result of Pitch Angle for  $\pi/8$  as an initial condition



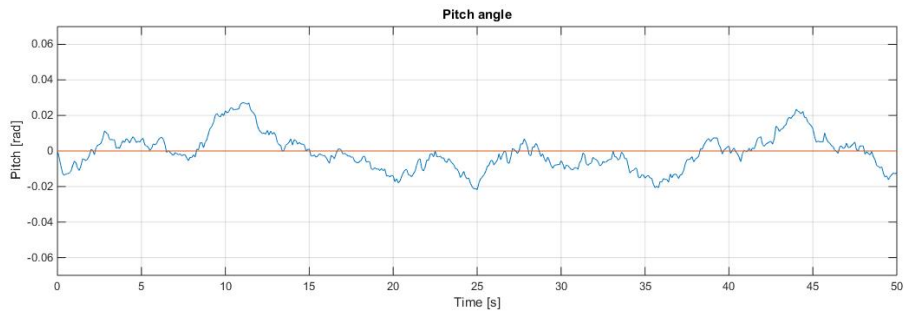
(c) Result of Yaw Angle in Hover

Figure 5.24: Simulation Results of the Attitude Controller Using Lyapunov Theory to Maintain Attitude Angles at Zero Without Noise

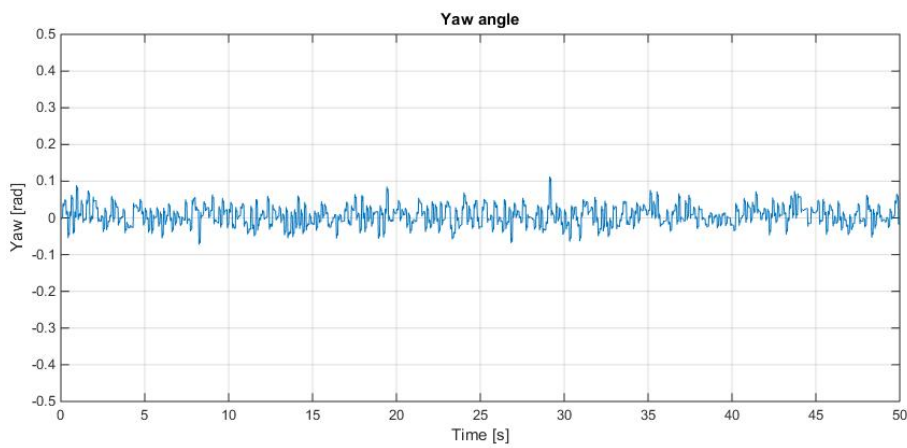
Now, small noises (white Gaussian with zero mean and 2 rad/sec of variance) added on each angular velocity at hover flight and the response of the attitude of the system can be observed in Figure 5.25.



(a) Result of Roll Angle in Hover in Spite the Added Noise



(b) Result of Pitch Angle in Hover in Spite the Added Noise



(c) Result of Yaw Angle in Hover in Spite the Added Noise

Figure 5.25: Simulation Results of the Attitude Controller Using Lyapunov Theory to Maintain Attitude Angles at Zero Under Influence of the Added Noise

### 5.3.4 Results Discussion

#### Altitude Control

The results of PD and PID controllers used for altitude control can be observed in Figure 5.26. As can be seen in the Figure below by adding an integral part to the controller we have almost zero overshoot in response of the system. In addition, decreasing the settling time significantly and increasing the robustness of the response are other benefits of PID controller in comparison with PD controller.

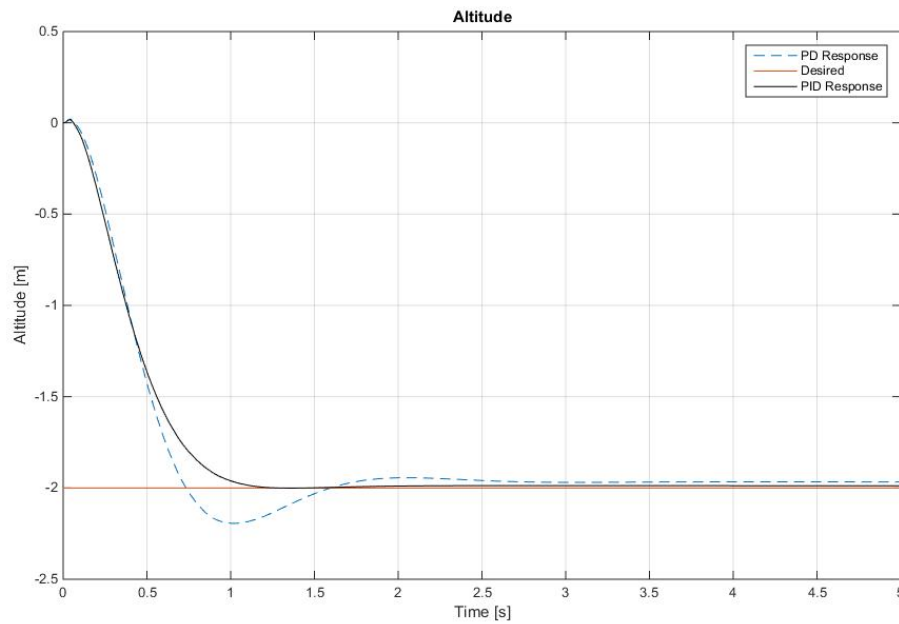
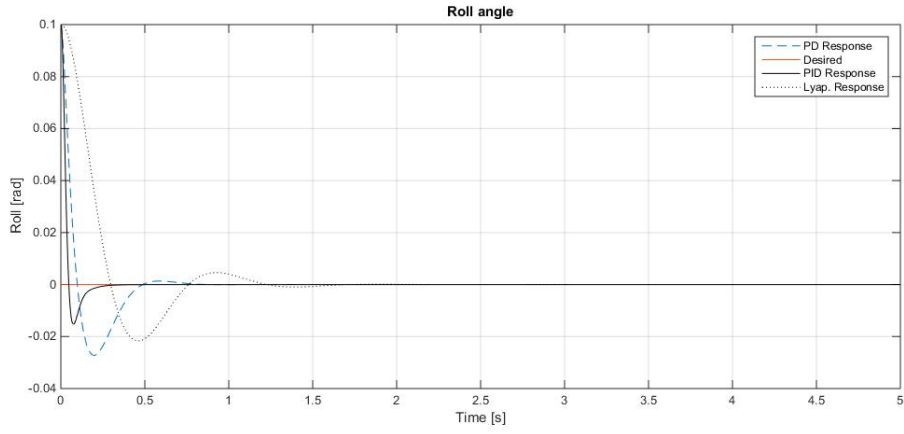


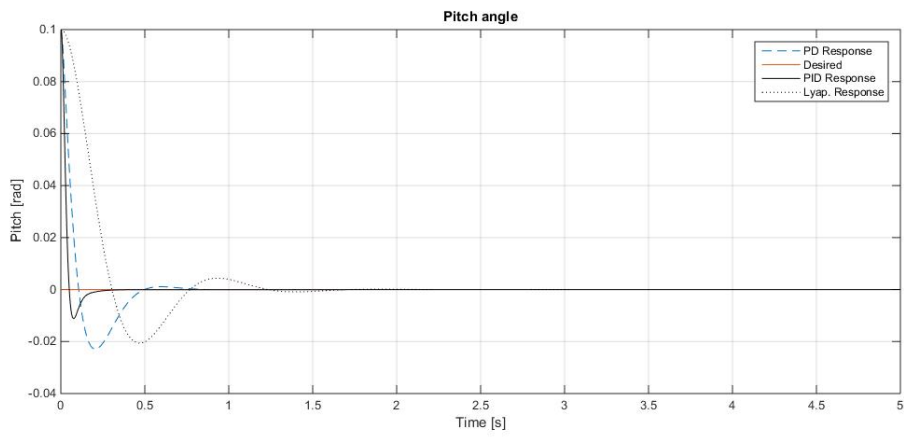
Figure 5.26: Comparison Between Results of Altitude of X5 Under PD and PID Controller for 2m Desired height

#### Attitude Control

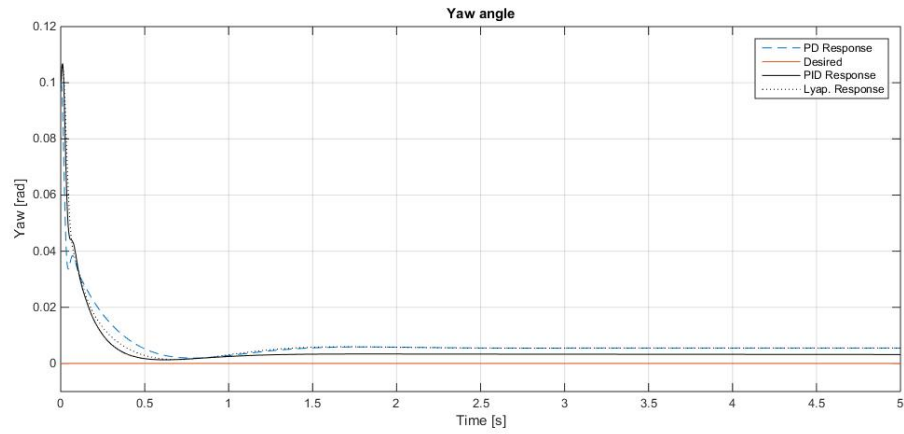
The attitude control results using Lyapunov, PD and PID controllers can be observed in Figure 5.27. This comparison shows that the result of PID controller response faster than the other two controllers. Although the response of the other two controllers are fast enough for system, PID controller has less overshoot in roll and pitch angles and less settling time with compare to the PD and Lyapunov techniques.



(a) Comparison Between Results of Roll Angle



(b) Comparison Between Results of Pitch Angle

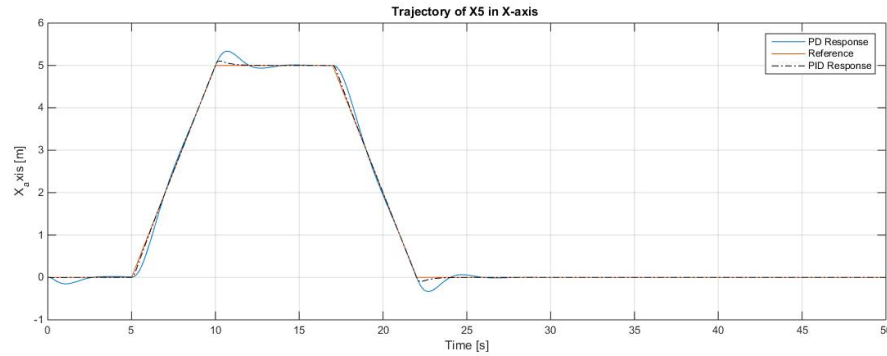


(c) Comparison Between Results of Yaw Angle

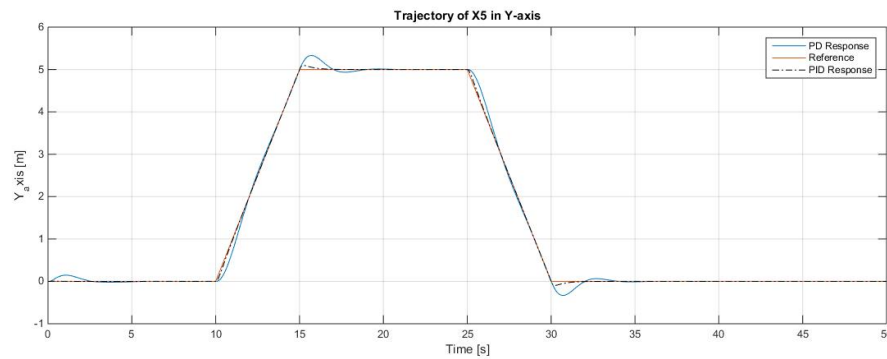
Figure 5.27: Comparison Between Simulation Results of the Attitude Controllers Using PD, PID and Lyapunov controllers to Maintain Attitude Angles at Zero with 0.1 rad as an Initial Condition

## Position Control

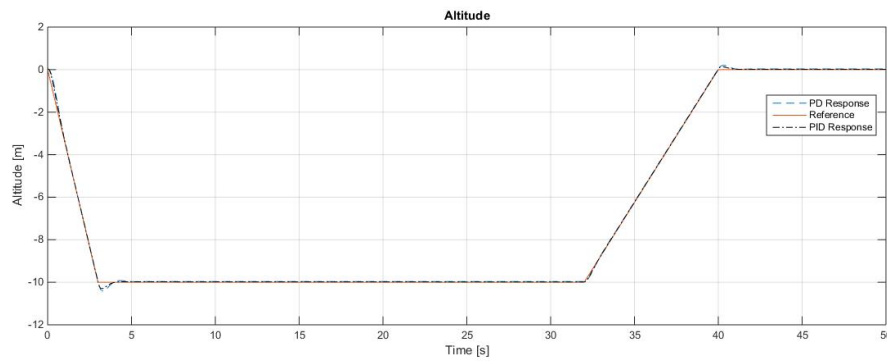
The comparison between the PD and PID controllers response are shown in Figure 5.28. Both controllers designed to follow the trajectory references in x,y and z axes which generate four way-points. The Results show that the PID controller has better response by having less overshoot and settling time.



(a) Comparison Between Responses of the PD and PID controllers to Trajectory in X-Axis



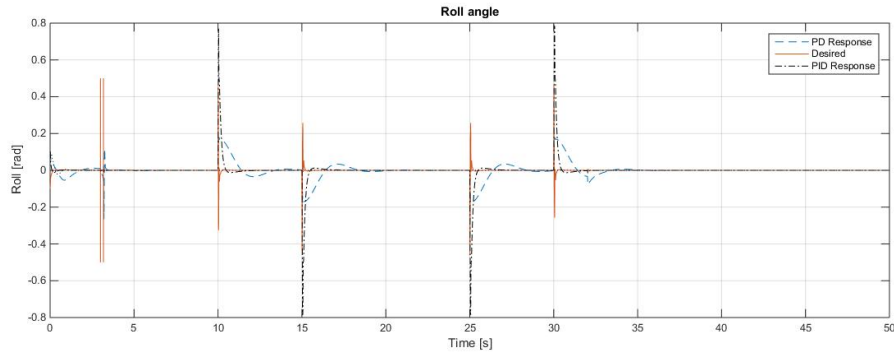
(b) Comparison Between Responses of the PD and PID controllers to Trajectory in Y-Axis



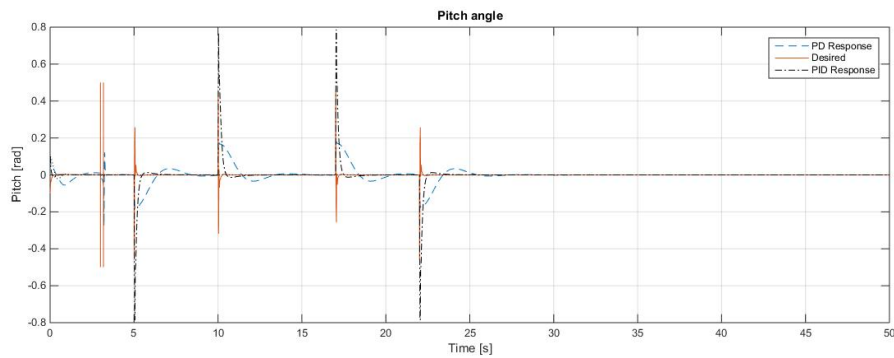
(c) Comparison Between Responses of the PD and PID controllers to Trajectory in Z-Axis

Figure 5.28: Comparison Between Simulation Results of the Trajectory Control Using PD and PID controllers for X, Y and Z axes

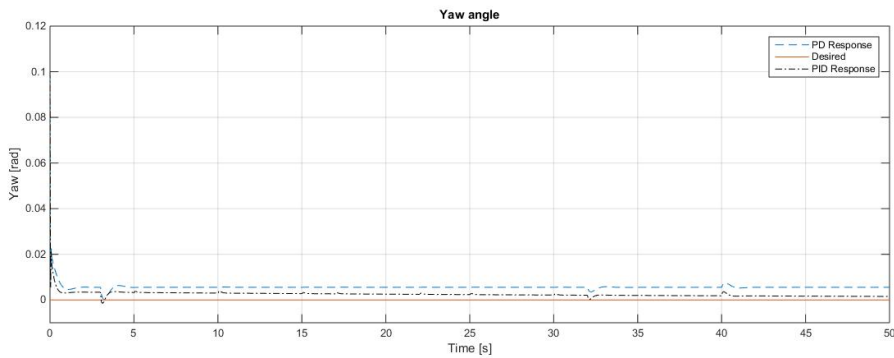
Figure 5.29 shows the response of the designed controllers in roll, pitch and yaw angles. The PID controller has faster response to the trajectory with comparison to the PD controller.



(a) Roll Angle Responses of the PD and PID controllers to the Trajectory



(b) Pitch Angle Responses of the PD and PID controllers to the Trajectory



(c) Yaw Angle Responses of the PD and PID controllers to the Trajectory

Figure 5.29: Comparison Between Simulation Results of the Roll, Pitch and Yaw Angles to the Trajectory Using PD and PID controllers



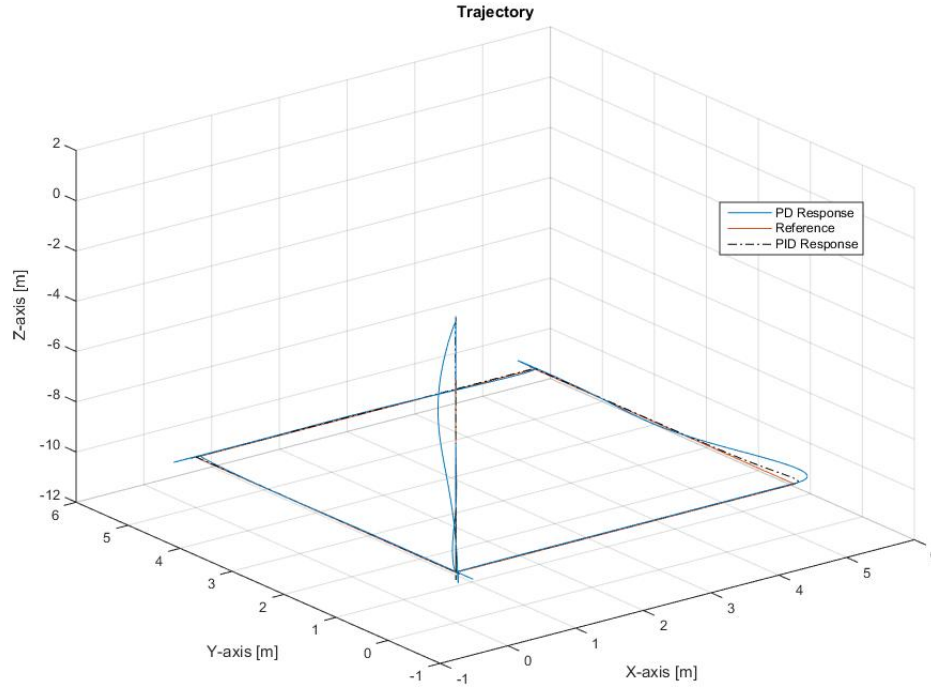


Figure 5.30: Comparison Between Results PD and PID Controller to the Square Trajectory Defined by Four Way-Points

#### 5.4 Some Experimental Results

In this section results of some test-bench flight will be presented. For test-bench flight tests we fixed the vehicle's position which means we cannot get the altitude controller's response during this tests. After a number of attempts we try to modify and tune the attitude controller which is responsible for roll, pitch and yaw angles. Figures 5.31, 5.32 and 5.33 shows the response of the attitude controller to the desired reference signal. The controller's task was to stabilize the roll, pitch yaw angles in fixed altitude. However, since this was the first attempt, we can see from Figures below that although the attitude controller could catch the desired roll angle after a while (see Figure 5.31), the pitch and yaw controllers' responses shown in Figures 5.32 and 5.33 are not satisfactory. These result recorded without tuning the controller.

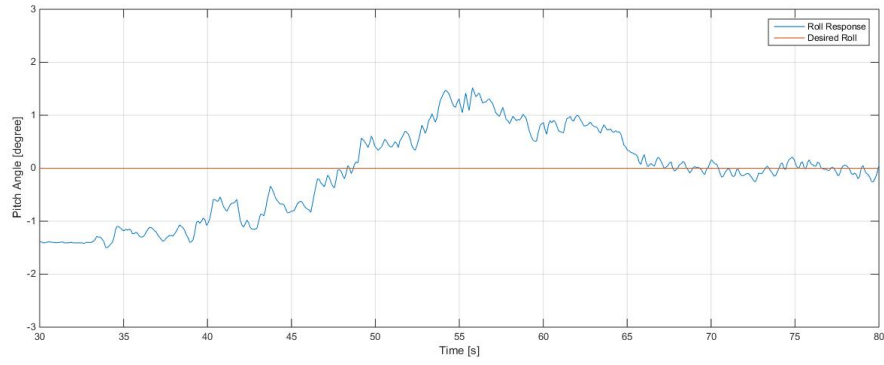


Figure 5.31: Response of the Controller to the Autopilot Desired Signal in Roll Angle

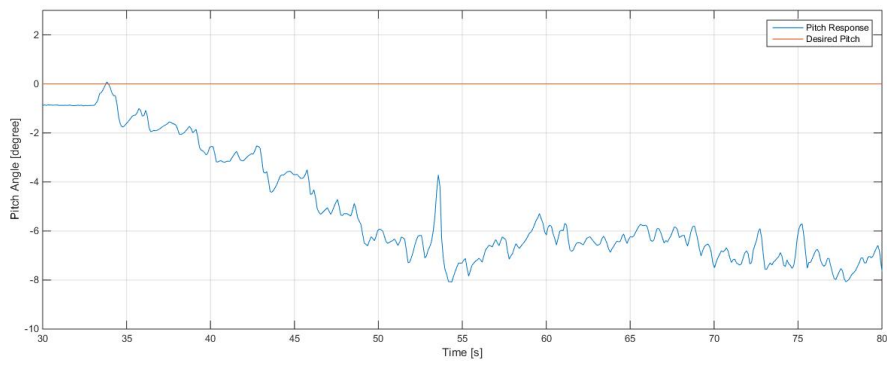


Figure 5.32: Response of the Controller to the Autopilot Desired Signal in Pitch Angle

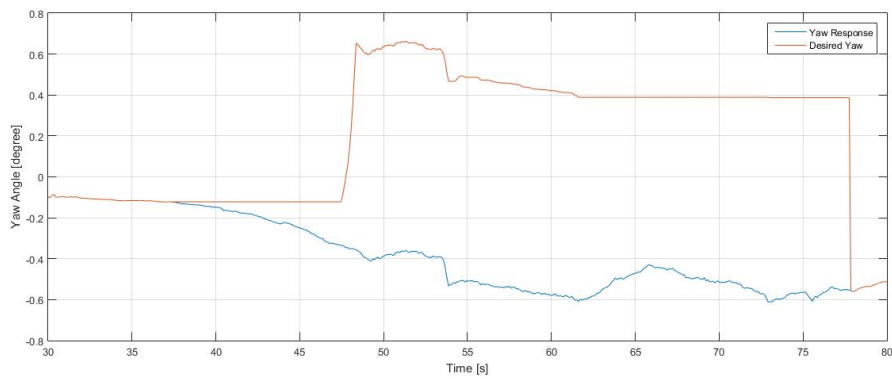


Figure 5.33: Response of the Controller to the Autopilot Desired Signal in Yaw Angle

Figures 5.34, 5.35 and 5.36 show the response of the attitude controller after several attempts and tuning the controller experimentally.

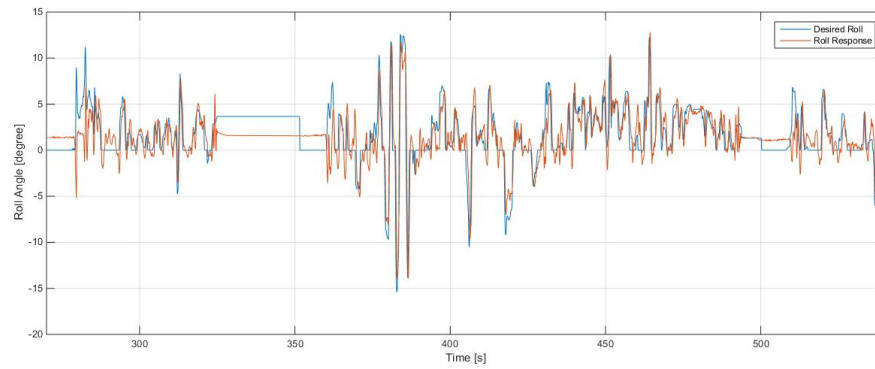


Figure 5.34: Response of the Controller to the Autopilot Desired Signal in Roll Angle

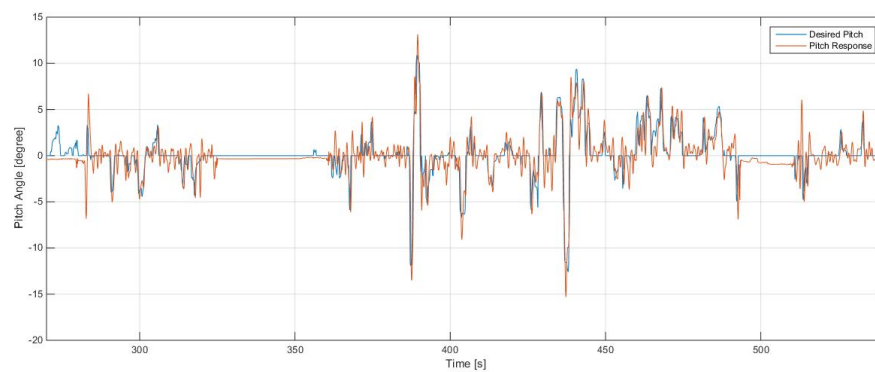


Figure 5.35: Response of the Controller to the Autopilot Desired Signal in Pitch Angle

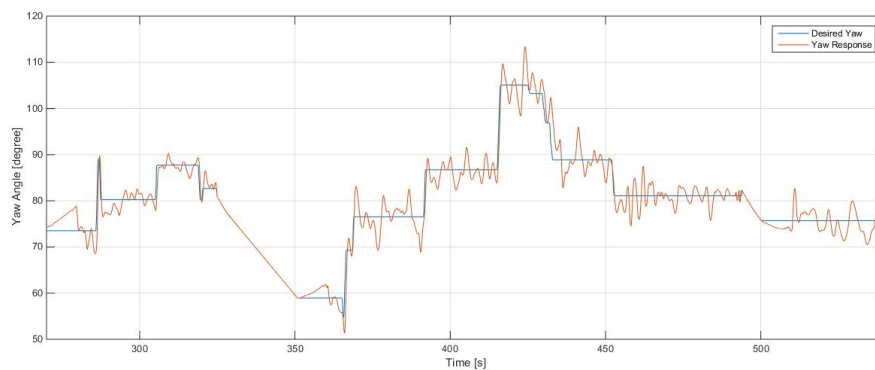


Figure 5.36: Response of the Controller to the Autopilot Desired Signal in Yaw Angle



## **CHAPTER 6**

### **CONCLUSIONS AND FUTURE WORKS**

This chapter is divided into two sections: General conclusion and future works. In general conclusion, the main advantages of X5 aerial robot and the contributions of this study will be discussed. The second section is followed by an outlook on future studies and works, which gives us a larger perspective on future of small-scale aerial robots.

#### **6.1 General Conclusion**

In this study, the goal was to derive a mathematical model for a new type unmanned aerial robot "X5", designing its hardware using CAD, built a prototype model and develop a composite controller in order to control X5 fully including its altitude, attitude, heading and position. Deriving the dynamic model of X5 requires knowledge of Direction Cosine Matrices (DCM) which converts forces from one reference frame to another. The whole mathematical model of X5 was built on basic physics and aerodynamic equations. Moreover, dynamics of both boom-mounted and main rotors were identified using Identification toolbox/MATLAB and experimental data from test-bench for each rotor in order to more accurately understand the BLDC motors, their power electronics and propellers all together at once. The motors and propellers are generate enough force to lift a payload of approximately 5.5 kg. Such a high lift power provides us a fast stabilizing control of X5. The combination of motors and electronic speed controller has a very low time response (i.e., ESCs operate at 100Hz and controller operates at 50Hz).

Developing a simulation based on this model and designing a good controller are one of the most strict requirements of this work. Three controller design techniques were explored from theoretical development to simulation based experiments. The controllers have been implemented and their performances have been compared under different input conditions and trajectories using MATLAB/Simulink.

The physical designed construction of the aerial robot X5 is near completion. In fact some simple flight test have performed on the robot. The whole design and construction process of the robot has been performed in unmanned vehicles laboratory of Electrical and Electronics Engineering Department of METU.

## **6.2 Future Studies**

The first step of future studies can be validation of the mathematical model of X5 using MATLAB/System Identification Toolbox. Using system identification methods in order to built and validate the complete dynamic requires collecting data of experimental results from both hover and motion flight tests for each component. For instance, in order to characterize and validate the model of Inertial Measurement Unit (IMU) one can perform indoor flight tests. Using two digital cameras in certain positions and video processing techniques can help one to track the motions of arms of rotorcraft. Each arm can be painted in a different color which makes the motion tracking more simple. This technique could also help to measure the position of the vehicle in x, y and z axes which is more accurate than GPS measurement in small and limited areas. Another important task of future works can be test the validity of autopilot for specific situations. For instance, this can be done by putting 50 g extra payload on one of the arms which will unbalance the vehicle and monitoring the response of the autopilot for this situation, in which autopilot should be able to keep the vehicle in balance.

The robot has an autopilot card (Pixhawk or PX4 as main control board), one 400KV BLDC motor (T-Motor MN4014-9) as main motor, four 980KV BLDC motors "T-Motor MS2212-13" as boom-mounted motors, one 40Amps ESC used for main motor, four 25Amps ESCs used for boom-mounted motors and a 3DR GPS in order to give the real-time position to the autopilot controller.

Building a X5 multirotor with many sensors implemented is a good educational platform. There is also a room for even more sensors like a internet protocol (IP) camera for visual recognition and surveillance which expands the ability to perform more advanced tasks.





## REFERENCES

- [1] H. Hou, J. Zhuang, H. Xia, G. Wang, and D. Yu, "A simple controller of mini-size quad-rotor vehicle," in *Mechatronics and Automation (ICMA), 2010 International Conference on*, pp. 1701–1706, IEEE, 2010.
- [2] J. Kim, M.-S. Kang, and S. Park, "Accurate modeling and robust hovering control for a quad-rotor vtol aircraft," in *Selected papers from the 2nd International Symposium on UAVs, Reno, Nevada, USA June 8–10, 2009*, pp. 9–26, Springer, 2010.
- [3] L. R. García Carrillo, R. Lozano, C. Pégard, and A. E. Dzúl López, *Quad Rotorcraft Control*. Springer, 2013.
- [4] "Aerial torpedo." <http://apps.npr.org/dailygraphics/assets/quiz-wwi/1-hewitt-sperry.jpg>. Accessed: 2014-11-15.
- [5] "Gyrodyne qh-50 dash." [https://en.wikipedia.org/wiki/Gyrodyne\\_QH-50\\_DASH](https://en.wikipedia.org/wiki/Gyrodyne_QH-50_DASH). Accessed: 2014-10-01.
- [6] "Gyrodyne dash." [https://en.wikipedia.org/wiki/Gyrodyne\\_QH-50\\_DASH](https://en.wikipedia.org/wiki/Gyrodyne_QH-50_DASH). Accessed: 2014-11-15.
- [7] "Westland wisp." [http://www.aviastar.org/helicopters\\_eng/west\\_wisp.php](http://www.aviastar.org/helicopters_eng/west_wisp.php). Accessed: 2014-09-23.
- [8] "Westland wisp." <http://www.gettyimages.com/detail/news-photo/the-westland-wisp-a-radio-controlled-unmanned-miniaturized-3277910>. Accessed: 2014-09-23.
- [9] "Yamaha "rmax". " <http://rmax.yamaha-motor.com.au/history>. Accessed: 2014-09-29.
- [10] "Yamaha "rmax". " <http://www.ainonline.com/aviation-news/2014-05-08/northrop-grumman-yamaha-announce-r-bat-uav>. Accessed: 2014-09-29.
- [11] S. Bouabdallah, *Design and Control of Quadrotors With Application to Autonomous Flying*. PhD thesis, École Polytechnique federale de Lausanne, 2007.
- [12] H. Bendea, F. Chiabrando, F. Giulio Tonolo, and D. Marenchino, "Mapping of archaeological areas using a low-cost uav. the augusta bagienorum test site,"

in *XXI International CIPA Symposium, 01-06 octobre 2007, Athens, Greece*, Citeseer, 2007.

- [13] F. Kendoul, "Survey of advances in guidance, navigation, and control of unmanned rotorcraft systems," *Journal of Field Robotics*, vol. 29, no. 2, pp. 315–378, 2012.
- [14] "Boeing unmanned little bird." <http://www.boeing.com/defense/unmanned-little-bird-h-6u/>. Accessed: 2014-10-01.
- [15] "Yamaha rmax." [http://www.barnardmicrosystems.com/UAV/uav\\_list/yamaha\\_rmax.html](http://www.barnardmicrosystems.com/UAV/uav_list/yamaha_rmax.html). Accessed: 2014-10-01.
- [16] "Viro benzin trainer." <http://www.vario-helicopter.net/products/pod-and-boom/petrol-pod-boom/benzin-trainer/petrol-trainer.html>. Accessed: 2014-10-01.
- [17] "Asctec." <http://www.asctec.de/en/uav-uas-drones-rpas-roav/asctec-pelican/>. Accessed: 2014-10-01.
- [18] "Epson micro-flying robot." <http://thefutureofthings.com/6309-micro-flying-robot/>. Accessed: 2014-10-01.
- [19] R. Lozano, *Unmanned Aerial Vehicles: Embedded Control*. John Wiley & Sons, 2013.
- [20] J. Watkinson in *Art of the Helicopter* (J. Watkinson, ed.), Oxford: Butterworth-Heinemann, 2004.
- [21] J. Paulos and M. Yim, "Flight performance of a swashplateless micro air vehicle," in *Robotics and Automation (ICRA), 2015 IEEE International Conference on*, pp. 5284–5289, IEEE, 2015.
- [22] S. Bouabdallah, R. Siegwart, and G. Caprari, "Design and control of an indoor coaxial helicopter," in *Intelligent Robots and Systems, 2006 IEEE/RSJ International Conference on*, pp. 2930–2935, IEEE, 2006.
- [23] "'gyroplane n:01'." <http://fukosvytuokle.blogspot.com.tr/2013/01/louis-charles-breguet-1880-1955.html>. Accessed: 2014-09-25.
- [24] "Gyroplane n:01." <http://fukosvytuokle.blogspot.com.tr/2013/01/louis-charles-breguet-1880-1955.html>. Accessed: 2014-10-01.

- [25] P. Pounds, R. Mahony, P. Hynes, and J. M. Roberts, "Design of a four-rotor aerial robot," in *Proceedings of the 2002 Australasian Conference on Robotics and Automation (ACRA 2002)*, pp. 145–150, Australian Robotics & Automation Association, 2002.
- [26] S. Bouabdallah, P. Murrieri, and R. Siegwart, "Design and control of an indoor micro quadrotor," in *Robotics and Automation, 2004. Proceedings. ICRA'04. 2004 IEEE International Conference on*, vol. 5, pp. 4393–4398, IEEE, 2004.
- [27] A. L. Salih, M. Moghavvemi, H. A. Mohamed, and K. S. Gaeid, "Modelling and pid controller design for a quadrotor unmanned air vehicle," in *Automation Quality and Testing Robotics (AQTR), 2010 IEEE International Conference on*, vol. 1, pp. 1–5, IEEE, 2010.
- [28] "X4 mini-scale quadrotor." <https://grabcad.com/library/quadrotor-estructure-v2>. Accessed: 2014-10-01.
- [29] N. Guenard, T. Hamel, and V. Moreau, "Dynamic modeling and intuitive control strategy for an" x4-flyer"," in *Control and Automation, 2005. ICCA'05. International Conference on*, vol. 1, pp. 141–146, IEEE, 2005.
- [30] A. Pretorius and E. Boje, "Design and modelling of a quadrotor helicopter with variable pitch rotors for aggressive manoeuvres," in *World Congress*, vol. 19, pp. 12208–12213, 2014.
- [31] J. du Plessis and P. E. Pounds, "Rotor flapping for a triangular quadrotor," *Australasian Conference on Robotics and Automation*, 2014.
- [32] S. Driessens, P. E. Pounds, *et al.*, "Towards a more efficient quadrotor configuration," in *Intelligent Robots and Systems (IROS), 2013 IEEE/RSJ International Conference on*, pp. 1386–1392, IEEE, 2013.
- [33] "Hovermast." <http://www.skysapience.com/>. Accessed: 2015-02-15.
- [34] "Hovermast-120." <http://www.skysapience.com/products/hovermast-120>. Accessed: 2015-02-15.
- [35] P. E. Pounds, R. E. Mahony, and P. I. Corke, "Design of a static thruster for microair vehicle rotorcraft," *Journal of Aerospace Engineering*, vol. 22, no. 1, pp. 85–94, 2009.
- [36] "Xh-17 "flying crane"." <http://www2.ita.br/~bmattos/mundo/exp/flycrane.htm>. Accessed: 2015-01-15.
- [37] M. E. Noudeh and M. K. Leblebicioğlu, "Design and modelling of x5 aerial robot," *TOK-2015 National Conference*, 2015.
- [38] R. M. Murray, Z. Li, S. S. Sastry, and S. S. Sastry, *A Mathematical Introduction to Robotic Manipulation*. CRC press, 1994.

- [39] J.-L. Boiffier, *The Dynamics of Flight: The Equations*. Wiley, 1998.
- [40] J. Leishman, *Principles of Helicopter Aerodynamics*. Cambridge Aerospace Series, Cambridge University Press, 2002.
- [41] J. M. Seddon and S. Newman, *Basic Helicopter Aerodynamics*, vol. 40. John Wiley & Sons, 2011.
- [42] G. Fay, “Derivation of the aerodynamic forces for the mesicopter simulation,” *Stanford University. Stanford, CA*, 2001.
- [43] K. C. Kim, “Analytical calculations of helicopter torque coefficient ( $c_q$ ) and thrust coefficient ( $c_t$ ) values for the helicopter performance (HELPE) model.” <http://www.dtic.mil/dtic/tr/fulltext/u2/a365512.pdf>. Accessed: 2013.
- [44] M. K. Habib, W. G. A. Abdelaal, M. S. Saad, *et al.*, “Dynamic modeling and control of a quadrotor using linear and nonlinear approaches,” 2014.
- [45] A. Nagaty, S. Saeedi, C. Thibault, M. Seto, and H. Li, “Control and navigation framework for quadrotor helicopters,” *Journal of Intelligent & Robotic Systems*, vol. 70, no. 1-4, pp. 1–12, 2013.
- [46] Ø. Magnussen and K. E. Skjønhaug, “Modeling, design and experimental study for a quadcopter system construction,” 2011.
- [47] “3dr radio telemetry v2.” <http://copter.ardupilot.com/wiki/common-optional-hardware/common-telemetry-landingpage/common-3dr-radio-version-2/>. Accessed: 2014-09-15.
- [48] “Pixhawk autopilot.” <https://pixhawk.org/modules/pixhawk>. Accessed: 2014-10-13.
- [49] “High-side measurement current shunt monitor.” <http://www.ti.com/lit/ds/sbos181d/sbos181d.pdf>. Accessed: 2015-03-23.
- [50] T. Söderström and P. Stoica, “Instrumental variable methods for system identification,” *Circuits, Systems and Signal Processing*, vol. 21, no. 1, pp. 1–9, 2002.
- [51] A. Halder and W. Agarwal, “Determination of inertial characteristics of a high wing unmanned air vehicle,” *IE(I) Journal-AS*, vol. 89, no. 1, pp. 1–8, 2002.
- [52] F. Çakici, *Modeling, Stability Analysis and Control System Design of a Small-Sized Tiltrotor UAV*. PhD thesis, MIDDLE EAST TECHNICAL UNIVERSITY, 2009.
- [53] “Pixhawk configuration.” [http://ark-lab.blogspot.com.tr/2014\\_12\\_01\\_archive.html](http://ark-lab.blogspot.com.tr/2014_12_01_archive.html). Accessed: 2014-11-15.

- [54] A. L. Salih, M. Moghavvemi, H. A. Mohamed, and K. S. Gaeid, "Flight pid controller design for a uav quadrotor," *Scientific Research and Essays*, vol. 5, no. 23, pp. 3660–3667, 2010.
- [55] D. E. Seborg, D. A. Mellichamp, T. F. Edgar, and F. J. Doyle III, *Process Dynamics and Control*. John Wiley & Sons, 2010.
- [56] H. K. Khalil and J. Grizzle, *Nonlinear Systems*, vol. 3. Prentice hall New Jersey, 1996.
- [57] I. Fantoni and R. Lozano, *Non-linear Control for Underactuated Mechanical Systems*. Springer Science & Business Media, 2001.
- [58] R. W. Beard, "Quadrotor dynamics and control," *Brigham Young University*, 2008.
- [59] J. L. Massera, "Contributions to stability theory," *Annals of Mathematics*, pp. 182–206, 1956.
- [60] J. Kurzweil, "On the inversion of lyapunov's second theorem on stability of motion," *Ann. Math. Soc. Transl. Ser.*, vol. 24, no. 2, pp. 19–77, 1956.
- [61] R. A. Freeman and P. V. Kokotovic, *Robust Nonlinear Control Design: State-Space and Lyapunov Techniques*. Springer Science & Business Media, 2008.



## APPENDIX A

### MODELLING

#### A.1 Rotation Matrix R

Using a right-hand oriented coordinate system we have the followings:

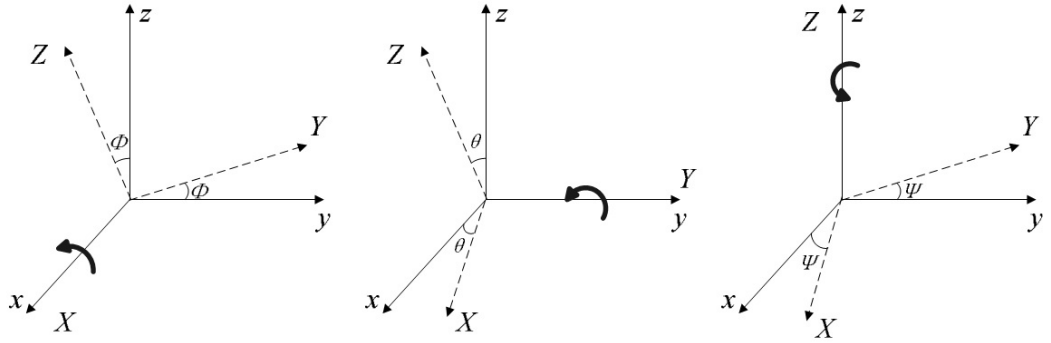


Figure A.1: Euler Angle Diagram

- $R(x, \phi)$  rotation around  $x$  axis.
- $R(y, \theta)$  rotation around  $y$  axis.
- $R(z, \psi)$  rotation around  $z$  axis.

$$R(x, \phi) = \begin{bmatrix} 1 & 0 & 0 \\ 0 & \cos\phi & \sin\phi \\ 0 & -\sin\phi & \cos\phi \end{bmatrix} \quad (\text{A.1})$$

$$R(y, \theta) = \begin{bmatrix} \cos\theta & 0 & -\sin\theta \\ 0 & 1 & 0 \\ \sin\theta & 0 & \cos\theta \end{bmatrix} \quad (\text{A.2})$$

$$R(z, \psi) = \begin{bmatrix} \cos\psi & \sin\psi & 0 \\ -\sin\psi & \cos\psi & 0 \\ 0 & 0 & 1 \end{bmatrix} \quad (\text{A.3})$$

and finally the rotation matrix  $R$  2.2 is the product of these three rotations:

$$R(\phi, \theta, \psi) = R(x, \phi)R(y, \theta)R(z, \psi) \quad (\text{A.4})$$

### Angular Rates

The angular rates  $\omega = [p \ q \ r]^T$  which measured with gyroscopes are different than time variation of Euler-angles  $\eta = [\phi \ \theta \ \psi]^T$  and in order to convert one to another one should use a transformation. The transformation is derived as follows [58]:

$$\begin{bmatrix} p \\ q \\ r \end{bmatrix} = R(\dot{\phi}) \begin{bmatrix} \dot{\phi} \\ 0 \\ 0 \end{bmatrix} + R(\phi)R(\dot{\theta}) \begin{bmatrix} 0 \\ \dot{\theta} \\ 0 \end{bmatrix} + R(\phi)R(\theta)R(\dot{\psi}) \begin{bmatrix} 0 \\ 0 \\ \dot{\psi} \end{bmatrix} \quad (\text{A.5})$$

where  $R(\dot{\phi}) = R(\dot{\theta}) = R(\dot{\psi}) = I$ ,

$$\begin{aligned} \begin{bmatrix} p \\ q \\ r \end{bmatrix} &= \begin{bmatrix} \dot{\phi} \\ 0 \\ 0 \end{bmatrix} + \begin{bmatrix} 1 & 0 & 0 \\ 0 & \cos\phi & \sin\phi \\ 0 & -\sin\phi & \cos\phi \end{bmatrix} \begin{bmatrix} 0 \\ \dot{\theta} \\ 0 \end{bmatrix} + \begin{bmatrix} 1 & 0 & 0 \\ 0 & \cos\phi & \sin\phi \\ 0 & -\sin\phi & \cos\phi \end{bmatrix} \begin{bmatrix} \cos\theta & 0 & -\sin\theta \\ 0 & 1 & 0 \\ \sin\theta & 0 & \cos\theta \end{bmatrix} \begin{bmatrix} 0 \\ 0 \\ \dot{\psi} \end{bmatrix} \\ &= \begin{bmatrix} 1 & 0 & -\sin\theta \\ 0 & \cos\phi & \sin\phi\cos\theta \\ 0 & -\sin\phi & \cos\phi\cos\theta \end{bmatrix} \begin{bmatrix} \dot{\phi} \\ \dot{\theta} \\ \dot{\psi} \end{bmatrix} \end{aligned} \quad (\text{A.6})$$



hence the transformation between angular body rates and Euler-rates defined as below:

$$R_r = \begin{bmatrix} 1 & 0 & -\sin\theta \\ 0 & \cos\phi & \sin\phi\cos\theta \\ 0 & -\sin\phi & \cos\phi\cos\theta \end{bmatrix} \quad (\text{A.7})$$

where  $R_r^{-1} \neq R_r^T$

$$R_r^{-1} = \begin{bmatrix} 1 & \sin\phi\tan\theta & \cos\phi\tan\theta \\ 0 & \cos\phi & -\sin\phi \\ 0 & \sin\phi\sec\theta & \cos\phi\sec\theta \end{bmatrix} \quad (\text{A.8})$$

## A.2 Mathematical Derivations

### A.2.1 Aerodynamic Forces and Moments

$$\begin{cases} C_{tb} = \sigma a \left[ \theta_0 \left( \frac{1}{6} + \frac{1}{4}\mu^2 \right) - \frac{\theta_{tw}}{8} (1 + \mu^2) - \frac{\lambda}{4} \right] \\ C_{tm} = \sigma a \left[ \theta_0 \left( \frac{1}{6} + \frac{1}{4}\mu^2 \right) - \frac{\theta_{tw}}{8} (1 + \mu^2) - \frac{\lambda}{4} \right] \end{cases} \quad (\text{A.9})$$

$$\begin{cases} C_{Hb} = \frac{\sigma}{4} \left[ \overline{C_d}\mu - a\lambda\mu \left( \theta_0 - \frac{\theta_{tw}}{2} \right) \right] \\ C_{Hm} = \frac{\sigma}{4} \left[ \overline{C_d}\mu - a\lambda\mu \left( \theta_0 - \frac{\theta_{tw}}{2} \right) \right] \end{cases} \quad (\text{A.10})$$

$$\begin{cases} C_{Qb} = \sigma \left[ \frac{1}{8} (1 + \mu^2) \overline{C_d} + a\lambda \left( \frac{1}{6}\theta_0 - \frac{1}{8}\theta_{tw} - \frac{1}{4}\lambda \right) \right] \\ C_{Qm} = \sigma \left[ \frac{1}{8} (1 + \mu^2) \overline{C_d} + a\lambda \left( \frac{1}{6}\theta_0 - \frac{1}{8}\theta_{tw} - \frac{1}{4}\lambda \right) \right] \end{cases} \quad (\text{A.11})$$

$$I = \begin{bmatrix} I_x & 0 & 0 \\ 0 & I_y & 0 \\ 0 & 0 & I_z \end{bmatrix} \quad (\text{A.12})$$

### A.3 Control Lyapunov Functions

A control Lyapunov function (clf) for a system of the form

$$\dot{x} = f(x, u) \quad (\text{A.13})$$

is a positive definite, radially unbounded function  $V(x)$  such that

$$x \neq 0 \quad \Rightarrow \quad \inf_{u \in U} \nabla V(x) \cdot f(x, u) < 0 \quad (\text{A.14})$$

where  $U$  is a convex set of admissible values of the control variable  $u$ . In other words, a clf is simply a candidate Lyapunov function whose derivative can be made negative *pointwise* by the choice of control values. Clearly, if  $f$  is continuous and there exists a continuous state feedback for Equation A.13 such that the point  $x = 0$  becomes a globally asymptotically stable equilibrium of the closed-loop system, then by standard converse Lyapunov theorems [59, 60] there must exist a clf for the system A.13. If  $f$  is affine in the control variable, then the existence of a clf for A.13 is also sufficient for stabilizability via continuous state feedback.

To summarize, just as the existence of a Lyapunov function is necessary and sufficient for the stability of a system without inputs, the existence of a clf is necessary and sufficient for the stabilizability of a system with a control input [61].

Dynamic model of X5 describing the roll, pitch and yaw rotations contains then, three terms which are the gyroscopic effect resulting from the rigid body rotation, the gyroscopic effect resulting from the propeller rotation coupled with the body rotation and finally the actuators action:

$$\begin{cases} I_x \ddot{\phi} = \dot{\theta} \dot{\psi} (I_y - I_z) - J_r \Omega_r \dot{\theta} + \tau_x \\ I_y \ddot{\theta} = \dot{\phi} \dot{\psi} (I_z - I_x) - J_r \Omega_r \dot{\phi} + \tau_y \\ I_z \ddot{\psi} = \dot{\phi} \dot{\theta} (I_x - I_y) + \tau_z \end{cases} \quad (\text{A.15})$$

where

$$\begin{cases} \tau_x = L(-T_2 + T_4) \\ \tau_y = L(T_1 - T_3) \\ \tau_z = L(\sum_{i=1}^4 Q_i) - Q_5 \end{cases} \quad (\text{A.16})$$

It makes a direct use of Lyapunov control theory to stabilize the attitude of X5. From Equations A.15 and 4.2 we obtain:

$$f(X_\alpha, U) = \begin{bmatrix} x_2 \\ a_1 x_4 x_6 - a_2 x_4 + b_1 U_2 \\ x_4 \\ a_3 x_2 x_6 + a_4 x_2 + b_2 U_3 \\ x_6 \\ a_5 x_2 x_4 + b_3 U_4 \end{bmatrix} \quad (\text{A.17})$$

The angular rotations subsystem has as state the restriction  $X_\alpha$  of  $X$  to the first 6 components which concerns roll, pitch, yaw angles and their time derivatives. The dynamics of these variables are described by  $f(X_\alpha, U)$ . This section mainly considers the stabilization of the angles in a particular configuration  $X_{\alpha d} = (x_{1d}, 0, x_{3d}, 0, x_{5d}, 0)^T$ . Let us consider the Lyapunov function  $V(X_\alpha)$  which is positive defined around the desired position  $X_{\alpha d}$ :

$$V(X_\alpha) = \frac{1}{2}[(x_{1d} - x_1)^2 + x_2^2 + (x_{3d} - x_3)^2 + x_4^2 + (x_{5d} - x_5)^2 + x_6^2]$$

The time derivative of equation above,  $\dot{V} = (\nabla V)^T f_\alpha$ , in the case of a perfect cross VTOL ( $I_x = I_y$ ) is drastically reduced to the following equation, where  $\Omega_r$  does not appear.

$$\begin{aligned} \dot{V} &= (\nabla V(X_\alpha))^T f(X_\alpha, U) \\ &= e_1 x_2 + b_1 x_2 U_2 + e_3 x_4 + b_2 x_4 U_3 + e_5 x_6 + b_3 x_6 U_4 \end{aligned}$$

By simply choosing

$$\begin{aligned}
U_2 &= -(x_{1d} - x_1) \frac{1}{b_1} - k_1 x_2 \\
U_3 &= -(x_{3d} - x_3) \frac{1}{b_2} - k_2 x_4 \\
U_4 &= -(x_{5d} - x_5) \frac{1}{b_3} - k_3 x_6
\end{aligned}$$

with  $k_1$ ,  $k_2$  and  $k_3$  positive constants, we obtain for Equation 4.38:

$$\dot{V} = -x_2^2 \frac{L}{Ix} k_1 - x_4^2 \frac{L}{Iy} k_2 - x_6^2 \frac{1}{Iz} k_3$$

which is only negative semi-definite. By Lyapunov theorem [59], the simple stability for equilibrium is now ensured. By LaSalle invariance theorem, we can ensure also that starting from a level curve of the Lyapunov function defined in Equation 4.37, where  $V(X_\alpha)$  is constant, the the state evolution is constrained inside the region bounded by the level curve. This is very useful when trying to avoid a particular configuration; it is simply necessary to start with a level curve not containing these points and apply the previous defined controls. We can also ensure the asymptotic stability by applying LaSalle theorem because the maximum invariance set of rotations' subsystem under control signals as shown in Equations 4.39 through 4.41 contained in the set  $S = \left\{ X_\alpha^S \in R^6 : \dot{V}|_{X_\alpha^S} = 0 \right\}$  is restricted only to the equilibrium point. By the latter consideration we can ensure an asymptotical stability starting from a point in a set around the equilibrium. To ensure the global stability it is sufficient that the  $\lim_{|X_\alpha| \rightarrow \infty} V(X_\alpha) = \infty$ , which is our case.